# Structure and function of the GluN1–GluN2B NMDA receptor

By

Chia-Hsueh Lee

A DISSERTATION

Presented to the Neuroscience Graduate Program and

the Oregon Health & Science University

School of Medicine

in partial fulfillment of the requirements for the degree of

Doctor of Philosophy

January 2015

School of Medicine

Oregon Health & Science University

---

CERTIFICATE OF APPROVAL

---

This is to certify that the Ph.D. dissertation of

CHIA-HSUEH LEE

has been approved on January 27, 2015

---

Advisor, Eric Gouaux, Ph.D.

---

Member and Chair, John Adelman, Ph.D.

---

Member, Mark Mayer, Ph.D.

---

Member, Francis Valiyaveetil, Ph.D.

---

Member, Gary Westbrook, M.D.

# Table of Contents

Acknowledgements ..... 4

List of figures ..... 5

List of tables ..... 7

## Chapter 1

Introduction ..... 8

The molecular design of the glutamate receptor family ..... 10

Key features of the NMDA receptor ..... 11

Endogenous agonists for the NMDA receptor ..... 12

Ion selectivity of the NMDA receptor ..... 13

Magnesium block of the NMDA receptor ..... 14

Expression and subunit patterns of the NMDA receptor ..... 15

Subunit content and NMDA receptor properties ..... 16

Biophysical characteristics ..... 16

Response to endogenous modulators ..... 18

NMDA receptors and diseases ..... 20

The pharmacology of NMDA receptors ..... 21

Ligands targeting the amino-terminal domain ..... 21

Ligands targeting the interface between ATD and LBD ..... 22

Ligands targeting the ligand-binding domain ..... 23

Ligands targeting the transmembrane domain ..... 24

Structural information of the NMDA receptor ..... 25

Subunit orientation of the NMDA receptor ..... 28

Specific aims of this thesis ..... 29

Figures and legends ..... 31

## Chapter 2

Amino terminal domains of the NMDA receptor are organized as local heterodimers ... 36

Abstract ..... 37

Introduction ..... 38
Methods ..... 40
Receptor expression ..... 40
Site-directed mutagenesis ..... 41
Western blotting ..... 41
Results and discussion ..... 43
Crosslinking between NMDA receptor ATDs in the R1–R1 interface ..... 43
Crosslinking partners in the R1-R1 interface ..... 45
GluN1 and GluN2A ATD heterodimer ..... 46
GluN1 and GluN2B ATD heterodimer ..... 46
Conclusion ..... 48
Figures and legends ..... 52

## Chapter 3

NMDA receptor structures reveal subunit arrangement and pore architecture ..... 59
Abstract ..... 60
Introduction ..... 61
Methods ..... 64
Receptor constructs ..... 64
Expression and purification ..... 64
Crystallization and cryoprotection ..... 65
Structure determination ..... 66
Two-electrode voltage clamp electrophysiology and western blotting ..... 68
Ligand binding assays ..... 69
Results and discussion ..... 70
Architecture and symmetry ..... 70
Arrangement of amino-terminal domains ..... 71
Ligand binding domain layer ..... 73
ATD–LBD interactions and allosteric coupling ..... 75
Transmembrane domain ..... 77
Ion channel gate and central vestibule ..... 79

Coupling of ligand binding and transmembrane domains ..... 81
Conclusion ..... 81
Supplementary discussion: model quality ..... 83
GluN1–GluN2B structure 1 at 3.7 Å resolution ..... 83
GluN1–GluN2B structure 2 at 3.9 Å resolution ..... 84
Figures and legends ..... 86
Tables ..... 116

## Chapter 4

Concluding remarks ..... 122
Comparison of the available NMDA receptor structure ..... 123
Implications for the gating mechanism ..... 125
Subunit non-equivalence ..... 125
Dynamics of the extracellular domains ..... 127
Putative $Ca^{2+}$ modulation sites on the NMDA receptor ..... 129
Perspectives ..... 130
Figures and legends ..... 133
References ..... 137

# Acknowledgements

I would like to take this opportunity to express my greatest appreciation to my mentor Eric Gouaux for his incredible support and encouragement. With his immense knowledge and enthusiasm, Eric guided me along the right path and helped me to overcome all the difficulties. I especially thank Jennifer, April, Wei, Ricarda, Dan, Juan, Xianqiang, Kevin, Lei and Katharina. This work would not have been possible without them. It is such a fortune to join the Gouaux lab and work together with many admirable scientists, from whom I received tremendous help.

My sincere gratitude also go to my thesis committee: Dr. Gary Westbrook, Dr. John Adelman, Dr. Francis I. Valiyaveetil, and Dr. Mark L. Mayer for their suggestions and insightful criticisms. I thank members of the lab for their comments on the thesis, and Lori for assistance with the figures.

I cannot finish without thanking my family and friends for their warm supports.

# List of figures

## Chapter 1

Figure 1.1: Modular architecture of the iGluR subunit. ..... 31

Figure 1.2: Ligands targeting the NMDA receptor. ..... 32

Figure 1.3: Structure of GluN1–GluN2A LBD heterodimer. ..... 33

Figure 1.4: Comparison of iGluR ATDs ..... 34

Figure 1.5: Architecture of the homomeric rat GluA2 receptor. ..... 35

## Chapter 2

Figure 2.1: ATD residues studied in this work. ..... 52

Figure 2.2: ATD cysteine mutants in the R1–R1 interface crosslink spontaneously. ..... 53

Figure 2.3: Crosslinking suggests heterodimer formation in the NMDA receptor ATD. 55

Figure 2.4: Crosslinking partners in the GluN1 ATD R1–R1 interface. ..... 56

Figure 2.5: GluN2B ATD forms a heterodimer with GluN1 ATD. ..... 57

## Chapter 3

Figure 3.1: Summary of Xenopus laevis NMDA crystallization constructs. ..... 86

Figure 3.2: Electrophysiology and western blot analysis of the NMDA receptors. ..... 88

Figure 3.3: $2F_o$-$F_c$ electron density maps of the GluN1–GluN2B NMDA structure. ..... 90

Figure 3.4: Analysis of spontaneous crosslinking of single cysteine point mutants. ..... 92

Figure 3.5: Architecture, symmetry and domain organization of the NMDA receptor. ... 94

Figure 3.6: ATD arrangement, cation binding sites and conformational mobility. ..... 95

Figure 3.7: Structural analyses and electron density maps of the ATD heterodimer. ..... 97

Figure 3.8: LBD layer forms a ring-like structure. ..... 99

Figure 3.9: LBD ligand electron densities and conformations. ..... 101

Figure 3.10: The ATDs participate in extensive contacts with the LBD layer. ..... 103

Figure 3.11: Transmembrane domain architecture, symmetry and coupling to LBD. ... 105

Figure 3.12: Structural analyses of the transmembrane domain of NMDA receptor. .... 107

Figure 3.13: Comparison of LBD layers and LBD–TMD linkers between structures. .. 109

Figure 3.14: Schematic of the NMDA receptor. ..... 111

Figure 3.15: Completeness of the structural models. ..... 115

## Chapter 4

Figure 4.1: Key ATD residues studied in chapter 2 map to the structure in chapter 3... 133

Figure 4.2: Subunit non-equivalence of the NMDA receptor. ..... 134

Figure 4.3: ATD and LBD dynamics of the NMDA receptor. ..... 135

# List of tables

Table 1: Constructs and mutations. ..... 116

Table 2: Crystallographic and structure refinement statistics. ..... 118

Table 3: ATDs and LBDs r.m.s.d. ..... 120

# Chapter 1

## Introduction

Neurons, information-processing units of the human brain, are polarized cells that have a soma, tentacle-like dendrites and a typically tubular axon. For information transfer, the axon of a neuron create contacts with the soma or dendrites of another neuron. Ramón y Cajal provided the first evidence that neurons are discrete entities that are connected not by actual confluences but by specialized sites of contact, which were later termed "synapses" by Charles Sherrington and Michael Foster [*1*]. Synaptic transmission therefore could be thought of as the communication between neurons that is essential for brain development and function. Two types of synapses are used by neurons to transfer an electrical signal. At an electrical synapse, electrical signals are transmitted directly from a presynaptic cell to a postsynaptic cell through gap junctions. At a chemical synapse, however, the electrical signal is converted into a chemical signal in the axon terminal of the presynaptic neuron. In 1921, Otto Loewi experimentally demonstrated that the axon terminal releases chemical substances [*2*], also known as neurotransmitters, which could be recognized by the postsynaptic neuron and lead to a regeneration of the electrical signal in the postsynaptic neuron. In the mammalian nervous system, most neurons communicate through chemical synapses. I am interested in understanding the molecular mechanism of chemical synaptic transmission in excitatory neurons or, more specifically, in glutamatergic neurons.

Glutamate is the major excitatory neurotransmitter in the mammalian central nervous system [*3*]. At the surface of the postsynaptic neuron there are integral membrane proteins that can recognize glutamate. These glutamate receptors are divided into two families: metabotropic receptors and ionotropic receptors. The metabotropic glutamate receptors are G-protein coupled receptors, typically producing slow responses in postsynaptic neurons.

The ionotropic glutamate receptors (iGluRs) are ligand-gated ion channels and mediate fast synaptic excitatory effects of glutamate. The cloning of cDNAs encoding iGluR subunits was first reported in 1989 [for review, see *4*] and at present eighteen genes of mammalian iGluRs have been identified. Based on pharmacological and electrophysiological data, these subunits have been classified into four subfamilies: α-amino-3-hydroxy-5-methyl-4-isoxazolepropionic acid (AMPA) receptors, kainate receptors, delta receptors, and *N*-methyl-D-aspartate (NMDA) receptors. There are four AMPA receptor subunits (GluA1–A4), five kainate receptor subunits (GluK1–K5), two delta receptor subunits (GluD1–D2), and six NMDA receptor subunits (GluN1, GluN2A–2D, and GluN3A–3B).

This dissertation focuses on the relationships between molecular structure and physiological function of the NMDA receptor, which is a pivotal molecule at chemical synapses and is required for neurodevelopment, synaptic plasticity, learning and memory formation [*5*–*7*]. In the first chapter, I will briefly summarize the background information of the NMDA receptor and reveal voids in the knowledge of the NMDA receptor that my thesis attempts to fill.

## The molecular design of the glutamate receptor family

All eukaryotic iGluRs share a similar architecture and contain four subunits. Each subunit has a "modular" design that, in turn, harbors four domains: an amino-terminal domain (ATD), a ligand-binding domain (LBD), a transmembrane domain (TMD) and a carboxyl-terminal domain (CTD) (Fig. 1.1) [*5*, *6*]. The ATDs of iGluR subunits participate in subunit assembly during receptor biogenesis and in modulation that shapes the diverse

biophysical properties of each iGluR type [*8*, *9*]. The ATD has sequence homology to the bacterial periplasmic leucine/isoleucine/valine binding protein [*10*]. The LBD constitutes binding pockets for full agonists, partial agonists, and antagonists. The LBD is structurally related to the bacterial lysine/arginine/ornithine binding protein [*11*, *12*]. The pore-forming TMD has three transmembrane helices (M1, M3, and M4) and a re-entrant loop (M2) facing inside the cell. The TMD of iGluR subunits is reminiscent of the pore of the potassium channel but the orientation is inverted [*13–15*]. The CTD includes sites for posttranslational modifications and also forms binding sites for intracellular proteins, including scaffold proteins important for receptor trafficking (e.g., PSD-95) and signaling proteins (e.g., calmodulin) [*6*]. The CTD does not have sequence similarity to known proteins and is the most diverse domain among the iGluR subunits in terms of its amino acid sequence and length.

## Key features of the NMDA receptor

In the early 1960s, Curtis and Watkins were the first to demonstrate that NMDA leads to the depolarization of motor neurons and could facilitate the ventral root reflex responses in frogs and cats [*16*, *17*]. After comparing the structure and response of NMDA to those of L-glutamic acid analogues, Johnston *et al.* proposed that NMDA specifically activates a subgroup of excitatory amino acid receptors [*18*], an idea that was supported by the development of selective antagonists on NMDA-sensitive receptors [*19*].

The NMDA receptor represents a unique member of the glutamate receptor family. In contrast to all other glutamate receptors, the NMDA receptor possesses several distinct

properties. First, the activation of the NMDA receptor requires the simultaneous presence of two chemically distinct agonists. Second, the receptor has relatively high calcium permeability. Third, the receptor is blocked by magnesium ions under physiological conditions. These features govern the key role of the NMDA receptor in brain function and each will be discussed in greater detail in following subsections.

## Endogenous agonists for the NMDA receptor

The NMDA receptor is a hetero-tetrameric assembly that comprises two GluN1 subunits and two non-GluN1 subunits [*6*]. In the receptor complex, the two non-GluN1 subunits could be comprised of two identical or different GluN2 subunits, or one GluN2 together with one GluN3 subunit.

This obligate heteromeric nature distinguishes NMDA receptors from most other iGluRs. Whereas all non-NMDA receptors can be activated by the neurotransmitter glutamate alone, the activation of the NMDA receptor requires an additional ligand. In 1987, Johnson and Ascher observed that glycine significantly "potentiates" NMDA receptor currents [*20*]. Afterward, Kleckner and Dingledine showed that glycine is in fact an absolute necessity for the receptor activation [*21*]. A two-site model better described the NMDA dose-response curve from steady-state analyses, implying that there may be two glutamate-binding sites on the receptor [*22*]. Antagonist kinetics measured by Benveniste and Mayer [*23*], and activation kinetics measured by Clements and Westbrook [*24*] both led to the conclusion that one hippocampal NMDA receptor has two glycine-binding sites and two-glutamate binding sites. After the cloning of the GluN1 and GluN2 subunits, site-

directed mutagenesis experiments suggested that glycine binds to the GluN1 subunit [*25*] and glutamate binds to the GluN2 subunit [*26*] (Fig. 1.2a).

The role of the co-agonist glycine in synaptic transmission is not fully understood. Initially glycine was thought to be the endogenous synaptic co-agonist, but recent studies challenged this paradigm. D-serine, which also binds to the glycine site, was proposed to be the dominant co-agonist for NMDA receptors in synapses, while glycine may act mainly at extrasynaptic NMDA receptors [*27*, *28*].

## Ion selectivity of the NMDA receptor

The NMDA receptor is permeable to cations such as sodium ($Na^+$) and potassium ($K^+$). In native neurons, the reversal potential of NMDA receptor-mediated currents is close to 0 mV, suggesting that the receptor has an almost equal preference for $Na^+$ and $K^+$ [*29*]. One hallmark of the NMDA receptor is that it is also permeable to calcium ($Ca^{2+}$). By simultaneously measuring currents of NMDA receptors and changes in $Ca^{2+}$ concentration using $Ca^{2+}$ dye, MacDermott *et al.* provided convincing evidence that the activation of the NMDA receptor allows $Ca^{2+}$ influx through its pore and results in an increase of the intracellular $Ca^{2+}$ concentration [*30*]. The relative calcium permeability ($P_{Ca}/P_{Na\ or\ Cs}$) is about 4-11, much higher than for other non-NMDA receptors in the iGluR family [*31–34*]. $Ca^{2+}$ contributes to about 10-19% of the total ion influx through the NMDA receptor [*34*, *35*]. As an important secondary messenger, $Ca^{2+}$ impacts many cellular processes [*36*]. The activation of NMDA receptors and the subsequent ion flux are therefore coupled to numerous downstream cellular pathways in neurons.

**Magnesium block of the NMDA receptor**

Unlike other ligand-gated ion channels, the function of the NMDA receptor *in vivo* is also sensitive to the membrane potential. Thirty years ago, Nowak *et al.* and Mayer *et al.* independently found that this voltage dependence is not from conformational changes associated with voltage-sensing domains, as in the case of voltage-gated ion channels, but from the pore block effect of extracellular magnesium ($Mg^{2+}$) [*37*, *38*] (Fig. 1.2a). The physiological concentration of extracellular $Mg^{2+}$ is not trivial and estimated to be about 1 mM [*39*, *40*]. The binding of $Mg^{2+}$ to the pore at negative membrane potentials prevents ion flux through the NMDA receptor and effectively 'silences' the receptor, even if glycine (or D-serine) and glutamate are bound. The $Mg^{2+}$ site is located deep in the pore, as estimated by electrical distance measurements [*32*, *41*], and the movement of bound $Mg^{2+}$ is influenced by permeant ions like $Na^+$ and $K^+$ [*42–44*]. These two properties give rise to the pronounced voltage dependence of $Mg^{2+}$ block. The block can be relieved by depolarizing the membrane potential. Therefore, NMDA receptor-mediated currents *in vivo* require not only the release of neurotransmitters from the presynaptic neurons but also the membrane depolarization of postsynaptic neurons. The NMDA receptor thus acts as a coincidence detector, monitoring the simultaneous activity in the synapse.

The structural bases of ion selectivity and $Mg^{2+}$ block in the NMDA receptor were largely unknown. From site-directed mutagenesis studies, Asn residues in the M2 segments play important roles in $Ca^{2+}$ permeability and $Mg^{2+}$ block [*45*, *46*]. However, it is difficult to dissect whether these cations are coordinated with the main-chain carbonyls of Asn residues, like $K^+$ channels [*47*], or coordinated with side-chain oxygen atoms. It is also unclear that how many ion binding sites are there in the selectivity filter. A physical

structure of the intact receptor determined at atomic resolution will help to illuminate how permeant and blocking ions interact with the ion channel pore.

## Expression and subunit patterns of the NMDA receptor

NMDA receptors are widely expressed in the central nervous system. In most areas the GluN1 subunit is constantly expressed from the embryonic period to adulthood. The expression of GluN2 subunits, on the other hand, is tightly regulated during development [*48–50*]. Monyer *et al.* discovered that GluN2 subunit mRNAs display distinct expression patterns in the developing rat brain [*49*]. The expression of the GluN2A subunit increases progressively after birth and eventually becomes the most abundant type of GluN2 subunit in the adult rat. The GluN2A subunit is almost ubiquitously expressed in the adult central nervous system. The GluN2B subunit is the major GluN2 subunit in the embryonic brain. Its expression reaches a peak at postnatal day seven but also maintains a significant level in the forebrain later on. Together with GluN2A, these two subunits become the predominant GluN2 subunits in the adult brain. The GluN2C subunit is expressed after postnatal day ten and mainly in certain areas such as the cerebellum and the olfactory bulb. The GluN2D subunit is expressed early in the embryonic stage but its expression decreases during development and eventually it is expressed at only a low level in the mature brain. The expression of the GluN3A and GluN3B subunits is also spatially and temporally restricted [*51*, *52*]. Whereas the expression of the GluN3A subunit peaks during the early postnatal period, mainly in the forebrain and hindbrain, and then reduces to a lower level,

the expression of the GluN3B subunit increases progressively with brain development, and eventually maintains at a high level in the adult neocortex, hippocampus, and cerebellum.

NMDA receptors that have two identical GluN2 subunits are called di-heteromeric NMDA receptors and whereas receptors with three distinct subunits are called tri-heteromeric NMDA receptors. Traditionally, studies have been focused on the di-heteromeric NMDA receptors, but recent evidence suggested that tri-heteromeric GluN1–GluN2A–GluN2B NMDA receptors may be the predominant type of receptor in the synapses, especially in the hippocampus [*53–55*].

The GluN3 subunit, like GluN1 subunit, binds glycine and D-serine [*56, 57*]. *In vitro*, GluN1 and GluN3 subunits can form a di-heteromeric receptor that can be activated solely by glycine [*56*]. In that sense, the GluN1–GluN3 receptors are not glutamate receptors but excitatory "glycine" receptors. However, whether GluN1–GluN3 receptors are expressed *in vivo* remains an open question. Tri-heteromeric GluN1–GluN2–GluN3 receptors exist both *in vitro* and *in vivo* [*51, 52*] but the physiological role of the GluN3-containing tri-heteromeric NMDA receptor is unclear.

## Subunit content and NMDA receptor properties

### Biophysical characteristics

The subunit composition of the NMDA receptor determines the gating and permeation properties and pharmacology of the receptor. There are eight splice isoforms of the GluN1 subunit (GluN1-1a to GluN1-4a, GluN1-1b to GluN1-4b) [*6, 7*]. The GluN1-b isoforms contain exon 5, which encodes an additional twenty-one amino acid residues in the ATD.

The presence of exon 5 accelerates the glutamate deactivation rate and the recovery rate from desensitization. It also slightly enhances glycine potency, reduces glutamate potency, and increases the open probability of the NMDA receptor [*58*, *59*]. In addition, exon 5 reduces the proton and polyamine sensitivity of the NMDA receptor [*60*, *61*]. With respect to the GluN2 subunit, GluN2A- or GluN2B-containing di-heteromeric receptors display higher open probabilities, faster glutamate deactivation rates, larger single-channel conductance, higher $Ca^{2+}$ permeabilities, and higher sensitivities of $Mg^{2+}$ block than GluN2C- or GluN2D-containing receptors. GluN2A- or GluN2B-containing receptors also have lower glycine and glutamate potency [*7*, *62*, *63*].

Interestingly, the subtype-dependent properties are controlled mainly by two distal regions. The ATD and ATD–LBD linker are responsible for the gating and pharmacological properties. Gielen *et al.* and Yuan *et al.* conducted detailed electro-physiological analyses on ATD chimera constructs and showed that engineering the GluN2A ATD and ATD–LBD linker on a GluN2D subunit will transform the gating of the GluN2D-containing receptor into a "GluN2A-like" receptor [*64*, *65*]. Similar experiments were also performed on GluN2B and GluN2C subunits, thus leading to the conclusion that the ATD, together with its linker to the LBD, is an important determinant for fine-tuning the functional properties of the NMDA receptor subtypes. Nevertheless, the structural mechanism of ATD modulation is still elusive.

A single residue in the TMD of GluN2 subunits is responsible for most of the subtype-dependent channel pore properties, including differences in single-channel conductance, calcium ion permeability, and $Mg^{2+}$ block [*66*]. This residue in the M3 helix of the TMD is a serine in the GluN2A or GluN2B subunits but a leucine in the GluN2C or GluN2D

subunits. A mutation of serine to leucine converts the ion permeation properties of the GluN2A-containing receptor into that of the GluN2D-containing receptor. As for $Mg^{2+}$ block, in addition to the single residue in the M3 helix, M1 and M4 helices in the TMD are also involved in subtype-dependent block [*67*].

**Response to endogenous modulators**

NMDA receptor subtypes differ in their sensitivity toward endogenous allosteric modulators. Westbrook and Mayer pointed out that NMDA receptors in hippocampal neurons are antagonized by zinc ($Zn^{2+}$), a highly concentrated ion in the synaptic vesicles [*68*]. $Zn^{2+}$ also attenuates the activity of the NMDA receptor in cortical neurons [*69*]. The GluN2A-containing receptor is very sensitive to $Zn^{2+}$ with an $IC_{50}$ of voltage-independent zinc inhibition of ~10 nM [*70*]. In contrast, the GluN2B-containing receptor has an $IC_{50}$ in the low micromolar range and the GluN2C- or GluN2D-containing receptor is even less sensitive to $Zn^{2+}$ [*71*]. $Zn^{2+}$ binds to the ATD in the GluN2A and GluN2B subunits, resulting in a voltage-independent inhibition of NMDA receptors (Fig. 1.2a) [*70*, *71*]. Histidine and acidic residues within the cleft of the ATD are potential binding sites of $Zn^{2+}$ [*72–74*]. Two additional histidine residues in the loop after β strand 1 of the GluN2A ATD were proposed to provide a more optimal metal coordination environment for $Zn^{2+}$ compared to that of the GluN2B ATD [*74*], giving rise to the almost hundred-fold difference in zinc sensitivity between GluN2A and GluN2B subunits.

The pH of the extracellular environment also regulates the activity of the NMDA receptor. GluN2B- or GluN2D-containing receptors have the highest proton sensitivity

with a $pH_{IC50}$ around 7.4. GluN2A-containing receptors have a $pH_{IC50}$ of 7 and GluN2C-containing receptors exhibit the lowest sensitivity with a $pH_{IC50}$ of 6.2 [*61, 64, 75*], indicating that, under physiological conditions, a significant number of NMDA receptors are under tonic proton inhibition.

Polyamines such as spermine potentiate GluN2B-containing receptors but not other NMDA receptor subtypes [*76*]. The binding site for polyamines is believed to be located partially within the ATD. Numerous site-directed mutagenesis experiments identified residues scattered throughout both the GluN1 and GluN2B ATDs that modulate spermine potentiation [*77–79*]. Direct binding of spermine to the GluN1 or GluN2 ATD can be measured by using $^{14}C$-radiolabeled spermine [*80*]. Furthermore, deletions of either the GluN1 or GluN2 ATD eliminated spermine potentiation [*81*]. It was proposed that spermine binds to the dimer interface formed by the lower lobes of the GluN1–GluN2B ATD (Fig. 1.2a) [*81*]. In this model, the region of β strands 6-8 in the lower lobe of the GluN2B ATD forms part of the spermine binding site and the region of β strands 6-8 in the GluN1 ATD complements the binding site. By contrast, another study suggested the upper lobe of the GluN1 ATD is also involved in binding of spermine [*82*].

Extracellular $Mg^{2+}$, in addition to its blocking effect, selectively potentiates GluN2B-containing receptors [*83*]. Interestingly, when exon 5 is present in the GluN1 subunit, the potentiation effects of polyamines and $Mg^{2+}$ are prevented [*61, 83*]. Lysophospholipids including lysophosphatidylinositol, lysophosphatidylcholine and lysophosphatidyl-ethanolamine, exert a larger inhibitory effect on GluN2B containing-receptors than on GluN2A- or GluN2C-containing receptors [*84*]. The neurosteroid pregnenolone sulphate

is a positive modulator for GluN2A- or GluN2B-containing receptors but a negative modulator for GluN2C- or GluN2D-containing receptors [*85*].

Ultimately, it may require multiple structures of different NMDA receptor subtypes to fully understand how the subunit composition contributes to the biogenesis and biophysical properties of the receptor. For example, are there structural features that preclude the incorporation of three GluN1 subunits into one mature receptor? Are there specific interactions in between the ATDs and LBDs of GluN2A and GluN2B subunits that favor the formation of tri-heteromeric GluN1–GluN2A–GluN2B NMDA receptors over di-heteromeric receptors? Nevertheless, any structure of an intact NMDA receptor will be a huge step forward in understanding how the subunit stoichiometry is established and how subunit contents shape the receptor properties.

## NMDA receptors and diseases

Malfunction of NMDA receptors has been implicated in a wide range of developmental disorders, neurological diseases and psychiatric conditions, from autism, Parkinson's disease to cognitive impairment [*7, 86, 87*]. Hyperactive NMDA receptors cause excessive $Ca^{2+}$ influx through the channels, resulting in the alteration of $Ca^{2+}$ homeostasis and cell damage. This excitotoxicity is thought to underpin neuronal death during cerebral ischemia. The hypoactivity of NMDA receptors can also be pathological. The reduced activity of the NMDA receptor in GABAergic neurons has been linked to schizophrenia and depression [*88, 89*]. Mutations in the GluN2 LBD [*90*] and the TMD [*90–92*] are associated with mental retardation and epilepsy. Autoimmune responses

against the GluN1 subunit, probably on the ATD, underlie anti-NMDA receptor encephalitis [*93*]. In agreement with a prominent role for the NMDA receptor in brain function, the receptor is a target of drugs for the treatments of Alzheimer's disease, depression, schizophrenia and traumatic brain injury [*7*].

## The pharmacology of NMDA receptors

The large extracellular domains of NMDA receptors provide multiple regulatory sites that recognize small molecules. Potential sites for ligand binding at NMDA receptors include the cleft of the GluN2 ATD, the GluN1–GluN2 ATD interface, the ATD–LBD interface, canonical ligand pockets in the LBDs, and the GluN1–GluN2 LBD interface. Moreover, the TMD may also form binding sites for ion channel pore blockers or modulators (Fig. 1.2b). The discussion in this section is focused on synthetic compounds for NMDA receptors. Many of these compounds not only have been proven to be invaluable research tools but also offer new therapeutic prospects.

### Ligands targeting the amino-terminal domain

The relatively low sequence similarity between the ATDs of GluN2 subtypes provides ATD ligands an opportunity to discriminate between GluN2 subtypes. Ifenprodil is the first discovered synthetic compound that displays high selectivity among NMDA receptor subtypes. Keith Williams found that ifenprodil shows more than 400-fold preferred inhibition of GluN1–GluN2B receptors over GluN1–GluN2A receptors [*94*]. Even after more than twenty years, ifenprodil and related phenylethanolamine derivatives are still the

most specific and widely accepted subtype-selective antagonists for NMDA receptors. Initially several residues on the GluN1 ATD were found to form part of the ifenprodil binding site [*79*]. It was subsequently suggested that the cleft of the GluN2B is the putative ifenprodil binding site and a binding mechanism similar to that of zinc binding to the GluN2A ATD was proposed [*95*]. The crystal structure of the isolated GluN1–GluN2B ATD ultimately revealed the atomic details of the ifenprodil site [*96*], which is located in the GluN1–GluN2B ATD dimer interface (Fig. 1.2b). Consistently, ifenprodil stabilizes the isolated GluN1-GluN2B ATD dimer and lowers the dimer dissociation constant more than twenty-fold [*96*].

**Ligands targeting the interface between ATD and LBD**

Recently, a novel class of pyrrolidinone compounds has been identified as allosteric potentiators specific to GluN2C-containing NMDA receptors [*97*]. One of the pyrrolidinone compounds, PYD-106, has a $EC_{50}$ of about 15 μM for GluN2C-containing NMDA receptors but only shows a mild inhibitory effect on GluN2A-, GluN2B-, and GluN2D-containing receptors at concentrations as high as 100 μM [*97*, *98*]. Intriguingly, PYD-106 has a small effect on the $EC_{50}$ of glutamate and glycine but doubles the channel open probability. Based on experiments using chimeric constructs and site-directed mutagenesis, the binding pocket for PYD-related compounds was suggested to be located in the GluN2C ATD and the upper lobes of the LBD [*98*] (Fig. 1.2b). It is the first class of allosteric modulators proposed to bind to the ATD–LBD interface of NMDA receptors. The mechanism by which modulator binding to the ATD–LBD interface can influence

movements of the TMD layer without having a remarkable effect on the $EC_{50}$ of LBD agonists is unknown.

**Ligands targeting the ligand-binding domain**

The ligand-binding pocket of the LBD is the canonical site for agonists and competitive antagonists [*6*]. Not until recently have the intradimer interface [*99–101*] and the lower lobes of the LBD [*102, 103*] been identified as potential sites for allosteric ligands. UBP-512 is a positive modulator for GluN2A-containing NMDA receptors but a negative modulator for GluN2C- or GluN2D-containing NMDA receptors. The deletion of the ATD does not affect UBP-512 modulation and the binding of UBP-512 does not compete with GluN1 or GluN2 agonists, so it is hypothesized that UBP-512 binds to the intradimer interface of the LBD [*99*] (Fig. 1.2b). UBP-710, which is structurally related to UBP-512, potentiates both GluN2A- and GluN2B-containing NMDA receptors [*99*]. Another interesting molecule that may bind to a similar location is TCN-201, which displays a strong selectivity toward GluN2A-containing NMDA receptors with an $IC_{50}$ of 0.32 μM. On the other hand, TCN-201 does not inhibit GluN2B-, GluN2C-, or GluN2D-containing NMDA receptors at concentrations below 10 μM. The binding of TCN-201 reduces GluN1 agonist potency but not GluN2 agonist potency [*101*].

QNZ46 and DQP-1105 are allosteric inhibitors preferring GluN2C- or GluN2D- over GluN2A- and GluN2B-containing receptors, although the selectivity is only about 50-fold. These two molecules appear to bind to domain 2 of the GluN2 LBD (Fig. 1.2b) and share a similar mechanism for inhibition [*102, 103*].

**Ligands targeting the transmembrane domain**

The aqueous pathway in the TMD provides binding sites for ion channel blockers, such as PCP or MK-801 [*104–106*] (Fig. 1.2b). The binding of blockers directly prevents ion flux but sometimes also modifies the gating properties of the receptor. For example, MK-801 can accelerate the unbinding of glutamate and thus shift the population of receptors to a closed state [*107*]. Amantadine doubles the channel closing rate, resulting in the stabilization of closed states [*108*]. By contrast, 9-aminoacridine blocks the receptor but traps the receptor in an open state [*109*]. The binding regions for many channel blockers seem to overlap. Certain asparagine residues in the selective filter segment of the GluN1 and GluN2 were shown to be important for the action of many pore blockers including PCP, MK-801, amantadine, and memantine [*110–113*]. NMDA receptor pore blockers have the potential to lead to novel therapeutic treatments. Memantine is an FDA-approved drug which can alleviate cognitive deficits in patients with Alzheimer's disease [*114*]. Memantine prevents ion flux through NMDA receptors by binding either to a superficial site or a deep site in the pore [*112*]. Ketamine, a low affinity pore blocker, is an acute antidepressant and may be useful in patients suffering from major depressive disorder, especially for those resistant to traditional antidepressants, such as selective serotonin reuptake inhibitors [*115*, *116*].

Besides pore blockers, there are only a handful of compounds that may target the TMD. CIQ, a positive modulator selective for GluN2C- or GluN2D-containing NMDA receptors, was suggested to interact directly with residues in the M1 transmembrane helix [*117*, *118*]. Residues in the pre-M1 helix also influence the CIQ potentiation. An endogenous neurosteroid, pregnanolone sulphate (3α5βS), inhibits NMDA receptors in a

use-dependent manner by promoting a desensitized state of the receptor [*119–121*]. Pregnanolone sulphate is speculated to bind to the TMD, although a direct experimental proof is necessary to support this hypothesis [*122*]

Due to the higher amino acid sequence diversity in the extracellular domains of the NMDA receptor, ligands targeting ATDs and LBDs are more likely to be subunit-specific, thus may providing better therapeutic benefits and less side effects. Nevertheless, little is known about the nature of interfaces between ATDs and LBDs or interfaces between LBD dimers. A structure of an intact NMDA receptor will be important in unraveling the interactions between these domains and therefore contribute to the structure-based drug design. Furthermore, many small molecules discussed in this sub-section were discovered by screening from compound libraries. Comprehensive structural information of the NMDA receptor in complex with these ligands will reveal the structural mechanisms of these ligands and facilitate the optimization of lead compounds.

## Structural information of the NMDA receptor

A breakthrough in our understanding of the three-dimensional structures of iGluRs came when the first crystal structures of the GluA2 AMPA receptor LBD were determined by Armstrong *et al.* in 1998 [*123*]. The LBD has a bi-lobed, clamshell-like structure consisting of domains 1 and 2 (also known as D1 and D2) where the binding of agonist promotes domain closure. The GluN1 LBD structure shares a similar fold with the GluA2 LBD [*124*]. Comparing the apo GluN1 LBD structure with the structures in complex with glycine or 5,7-dichlorokynurenic acid (DCKA) revealed the conformational changes

accompanying agonist and antagonist binding [*124*, *125*]. The trend of changes resembles that of GluA2 LBD [*126*]. In the apo state, the LBD is in an open-cleft conformation. The binding of competitive antagonists stabilizes an "apo-like" open-cleft conformation whereas the binding of agonists reduces the separation of domains 1 and 2, resulting in a closed-cleft conformation. This domain closure is believed to generate tensions on the LBD–TMD linkers and subsequently "pull open" the pore [*6*, *127*]. A similar conclusion was reached for the GluN2 subunit after comparing the agonist and antagonist-bound structures of the GluN2A LBD [*128*, *129*]. The crystal structure of the GluN1–GluN2A LBD dimer solved by Furukawa *et al.* uncovered that the GluN1 and GluN2 LBDs form a heterodimer in a back-to-back fashion (Fig. 1.3). The dimeric interaction is mediated by contacts not only between domain 1 of the LBDs but also by between domain 1 and domain 2. The structure suggested that the NMDA receptor tetramer is made of two copies of GluN1–GluN2 heterodimers in the LBD layer, rather than one GluN1 LBD homodimer pairing with one GluN2 LBD homodimer [*128*].

In the ATD layer, the GluN2B subunit possess an overall similar shape to AMPA or kainate receptor ATDs [*74*, *130–132*]. In all cases, the ATD is a bi-lobed structure consisting of R1 and R2 domains. However, compared with non-NMDA receptor ATDs, the R2 domain of the GluN2B ATD is rotated by about 50°, which in turn generates a "twisted" conformation (Fig. 1.4a). Although the existence of an open-cleft conformation of the GluN2 ATD was suggested by functional data [*64*], both the zinc-free and the zinc-bound structures of the GluN2B ATD adopt the same close-cleft conformation [*74*]. The functional significance of the open-cleft conformation, if present at all, remains to be elucidated.

Five years ago, structural information for the GluN1 ATD was nonexistent. It was also unclear whether the ATDs of the NMDA receptor form local homo- or heterodimers. I therefore used a biochemical approach to study the dimeric interaction of ATDs in the intact NMDA receptor (**chapter 2**). By introducing disulfide crosslinks, I provided evidence for the heterodimeric nature of ATDs in the NMDA receptor and proposed that the R1–R1 interfaces, but not the R2–R2 interfaces, play a major role in mediating dimerization [*133*]. Consistent with my crosslinking experiments on the full-length receptor, subsequent crystal structures of the isolated GluN1–GluN2B ATD dimer indicated that the GluN1 and GluN2B ATDs are organized as heterodimeric entities [*96*]. Like the GluN2 ATD, the GluN1 ATD shows a similar rotation in the R2 domain [*96, 134*]. Because of the unique conformation of NMDA receptor ATDs, the GluN1 ATD interacts with the GluN2B ATD through R1–R1 domains and R1 (of GluN1)–R2 (of GluN2B) domains, quite different from the interactions in AMPA [*130, 131*] or kainate receptor ATDs [*132, 135*] (Fig. 1.4b).

At the time I started my thesis work, there was also no high-resolution structure available for the TMD of NMDA receptors, let alone the full-length heteromeric receptor. The structure of the M2 re-entrant loop, the pore lining region, and the extracellular vestibule have been probed by the accessibility of substituted cysteines, providing two main conclusions. First, the M2 loop of the GluN1 and GluN2 subunit have similar layouts but the position of the loop may be asymmetrical [*136*]. Second, the extracellular vestibule is formed by part of the pre-M1 helix, and M3 and M4 helices [*137*]. A better description of the NMDA receptor pore could be achieved by making a homology model based on the crystal structure of the full-length GluA2 AMPA receptor, which displays most of the

channel pore architecture of the GluA2 receptor (Fig. 1.5) [*138*]. Sobolevsky *et al.* showed that M1 and M4 helices of GluA2 receptor reside on the exterior of the TMD. The M2 segment forms a pore helix and selectivity filter, although the structure of the M2 segment was not clearly resolved. The M3 helix is in the center of the TMD and, together with the selectivity filter, lines the aqueous pathway of the pore. Due to the relatively high amino acid sequence similarity, it is reasonable to assume the TMD of the NMDA receptor has a similar arrangement. Nevertheless, the heteromeric nature of the full-length NMDA receptor likely causes a divergence in the TMD layer and also in the extracellular domain organization. Therefore, a full-length structure is necessary to understand the molecular underpinnings of channel gating.

## Subunit orientation of the NMDA receptor

From experiments on truncated and tandem constructs, Schorge and Colquhoun suggested that the NMDA receptor has a GluN1–GluN1–GluN2–GluN2 orientation of the subunits [*139*]. Expressing construct combinations that allow an alternating arrangement of subunits (*i.e.* 1–2–1–2 orientation) only results in either non-functional receptors or rapid-rundown receptors. Moreover, atomic force microscopy imaging on NMDA receptors complexed with antibodies also suggested a 1–1–2–2 orientation [*140*].

On the other hand, the full-length GluA2 structure revealed the existence of two "non-equivalent" pairs of subunits, A–C and B–D, in the AMPA receptor and the conformationally distinct A–C and B–D subunits arranged in an alternating fashion (Fig. 1.5). Based on this observation and cysteine-directed crosslinking experiments on the LBD

of the NMDA receptor, a dimer-of-heterodimer model with a GluN1–GluN2-GluN1–GluN2 orientation was proposed for the NMDA receptor [*138*]. A subsequent study using luminescence resonance energy transfer microscopy [*141*] or electrophysiological and crosslinking experiments on the LBD–TMD linker [*142*, *143*] provided further evidence for the 1–2–1–2 paradigm. Ultimately, an atomic resolution structure of the full-length NMDA receptor would distinguish between 1–1–2–2 and 1–2–1–2 models.

## Specific aims of this thesis

In contrast to the abundance of functional and biochemical data, the structural understanding of NMDA receptors at the atomic level is still limited. Furthermore, despite extensive literature on the function and mechanism of NMDA receptors, fundamental questions remain. For example, how are the ATD and LBD domains arranged in a full-length NMDA receptor? What is the subunit orientation? What is the structural basis of the allosteric modulation by the ATD? How do the GluN1 and GluN2 subunits participate in gating? What is the structure of the ion channel pore and where do pore blockers bind? To provide insights into the structural design and molecular principle of the gating mechanism, and also to establish a framework for design of future therapeutic agents, a full-length NMDA receptor structure at atomic resolution is mandatory. My major aim was to determine the first high-resolution structure of the NMDA receptor by x-ray crystallography (**chapter 3**).

In chapter 2, I will describe the introduction of single cysteines into the putative dimeric interfaces of ATDs, which reveals the relationship of GluN1 and GluN2 ATDs. In

chapter 3, I will outline the experimental approach and present the crystal structures of the GluN1–GluN2B receptors.

## Figures and legends

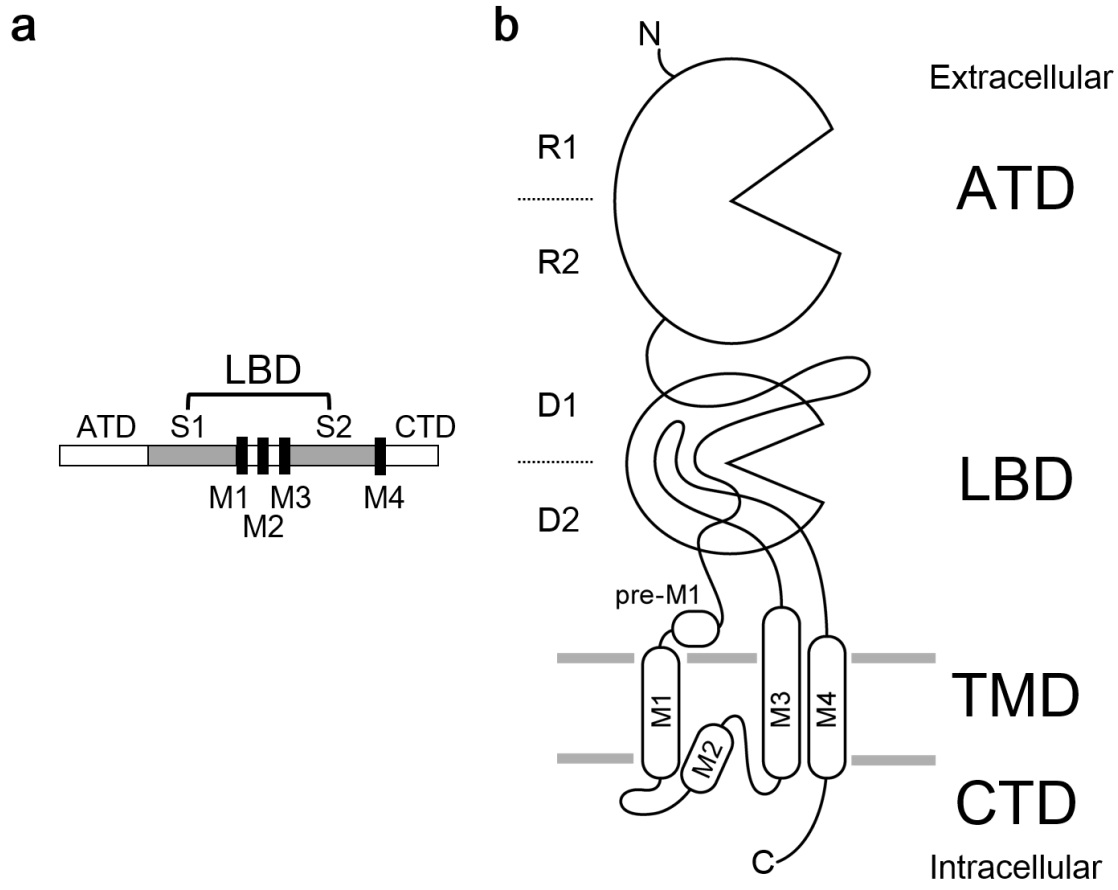


**Figure 1.1: Modular architecture of the iGluR subunit.**

**a**, Linear representation of the polypeptide chain of an iGluR subunit. The S1 segment is defined as the sequence between the ATD and the M1 helix. The S2 segment is defined as the sequence between the M3 and M4 helices. **b**, Schematic illustration of domain structure. The ATD consists of R1 and R2 lobes. The LBD consists of D1 and D2 lobes.

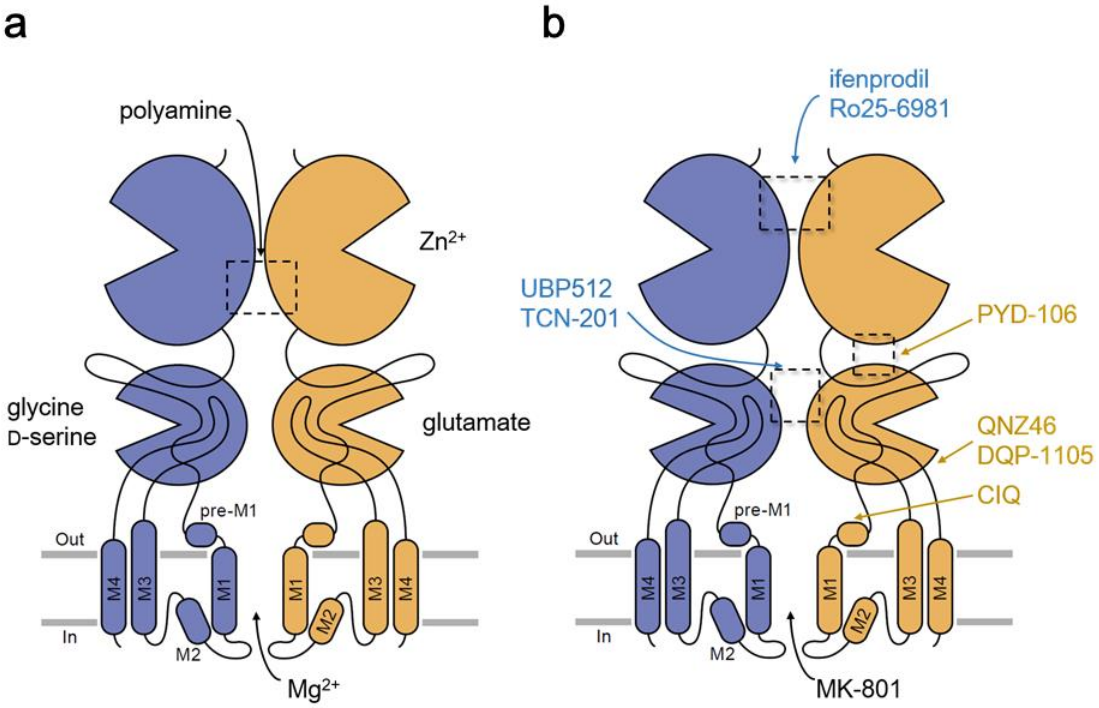


**Figure 1.2: Ligands targeting the NMDA receptor.**

**a**,**b**, Selected endogenous ligands (**a)** and synthetic compounds (**b)** that bind to the NMDA receptor. Only two subunits are shown. Dashed boxes highlight the interfaces between domains. GluN1 is in blue and GluN2 is in orange. Note that the ligands shown here display various degrees of subunit selectivity (see main text).

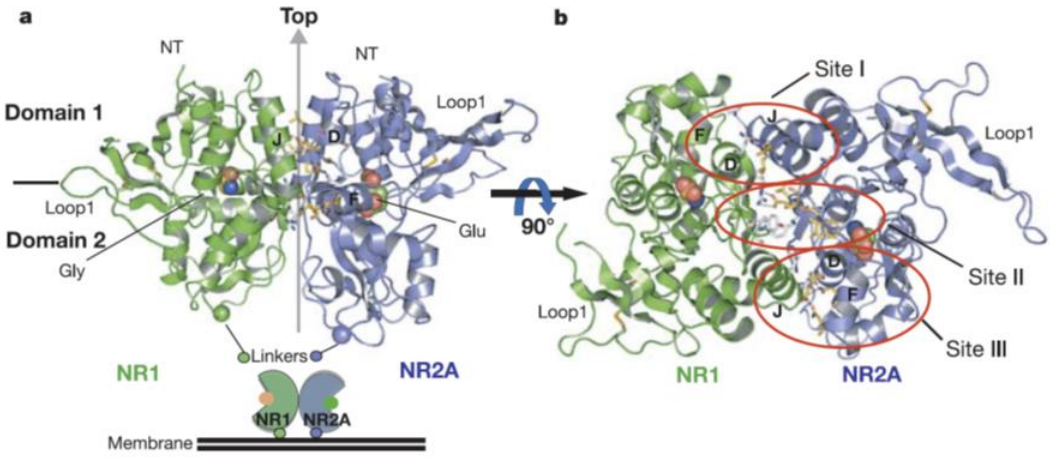


**Figure 1.3: Structure of the GluN1–GluN2A LBD heterodimer.**

**a**, Side view of the GluN2–GluN2A LBD heterodimer in complex with glycine and glutamate (PDB code: 2A5T). The GluN1 and GluN2A LBDs are colored green and blue, respectively. **b**, Top view of the structure. The interface between GluN1 and GluN2A is highlighted with red circles. Figure adapted from Furukawa *et al.* [*128*].

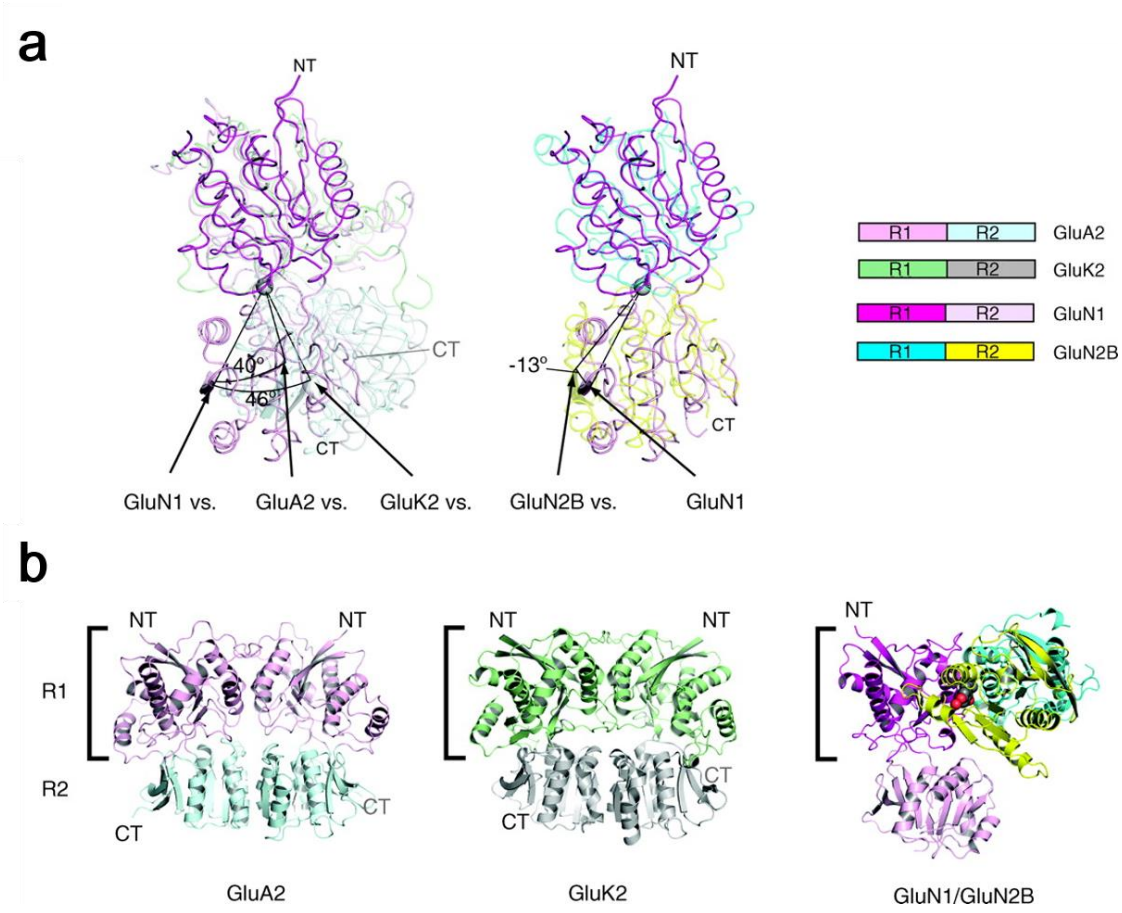


**Figure 1.4: Comparison of iGluR ATDs**

**a**, Structures of iGluR ATD monomers are superposed on the R1 lobes. The superposition shows that the both GluN1 and GluN2B ATDs are significantly 'twisted' compared to those from non-NMDA receptors (PDB codes: 3H5V, 3H6G, 3QEK and 3JPY for GluA2, GluK2, GluN1 and GluN2B, respectively). **b,** Structures of ATD dimers. The structures are aligned so that the R1 domains are in a similar orientation. (PDB codes: 3H5V for the GluA2 ATD homodimer; 3H6G for the GluK2 ATD homodimer; 3QEL for the GluN1-GluN2B ATD heterodimer). Figure adapted from Hiro Furukawa [*8*].

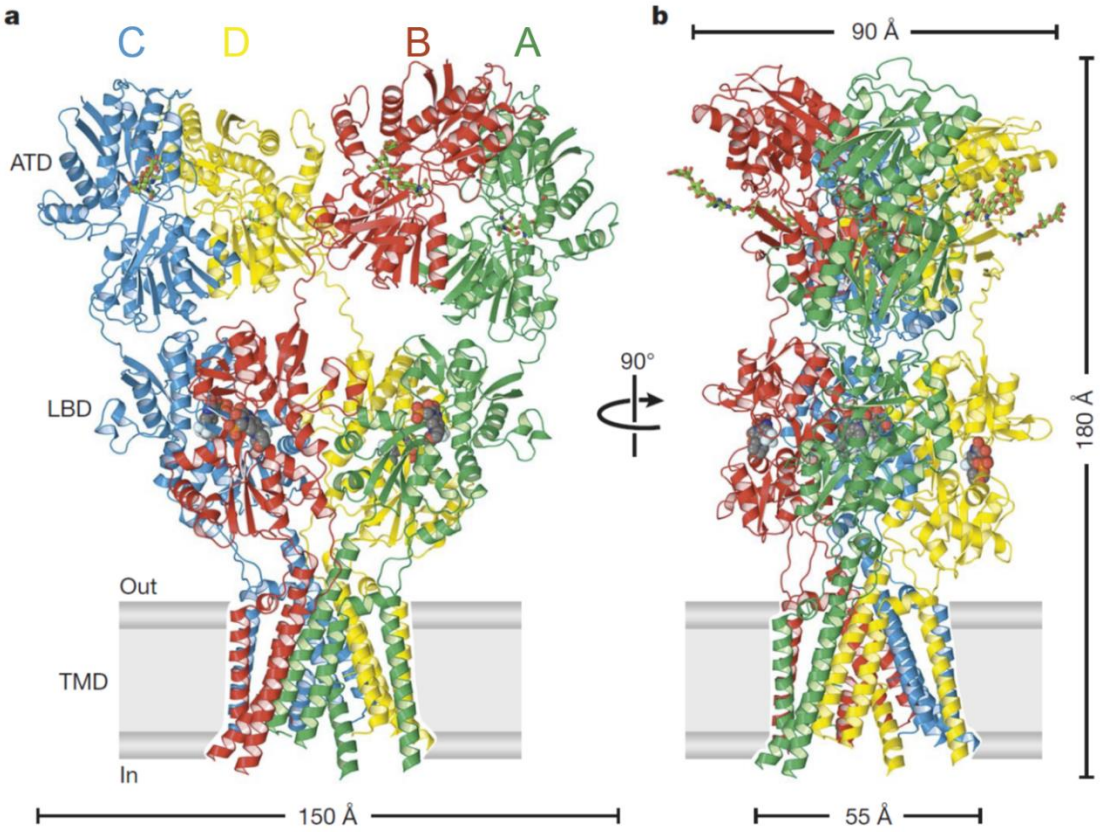


**Figure 1.5: Architecture of the homomeric rat GluA2 receptor.**

**a**, View of the receptor parallel to the membrane. Each subunit is in a different color. The competitive antagonists are in space-filling representation. **b**, View of the complex rotated by ~90° around the overall twofold axis of the receptor. Figure adapted from Sobolevsky *et al.* [*138*].

# Chapter 2

## Amino terminal domains of the NMDA receptor are organized as local heterodimers

The content of chapter two is published in a modified form:

Lee CH, Gouaux E, Amino terminal domains of the NMDA receptor are organized as local heterodimers. *PLoS One*. 6, e19180 (2011).

## Abstract

The *N*-methyl-D-aspartate (NMDA) receptor, an obligate heterotetrameric assembly organized as a dimer-of-dimers, is typically composed of two glycine-binding GluN1 subunits and two glutamate-binding GluN2 subunits. Despite the crucial role that the NMDA receptor plays in the nervous system, the specific arrangement of subunits within the dimer-of-dimers assemblage is not conclusively known. Here we studied the organization of the amino terminal domain (ATD) of the rat GluN1–GluN2A and GluN1–GluN2B NMDA receptors by cysteine-directed, disulfide bond-mediated crosslinking. We found that GluN1 ATDs and GluN2 ATDs spontaneously formed disulfide bond-mediated dimers after introducing cysteines into the R1 interface of GluN2A or GluN2B ATD. The formation of dimers could be prevented by knocking out endogenous cysteines located near the R1 interface of the GluN1 ATD. These results indicate that GluN1 and GluN2 ATDs form local heterodimers through the interactions in the R1–R1 interface and further demonstrate a dimer-of-heterodimers arrangement in GluN1–GluN2A and GluN1–GluN2B NMDA receptors.

## Introduction

The *N*-methyl-D-aspartate (NMDA) receptor, one subgroup of the ionotropic glutamate receptor family, plays an essential role in neurophysiological functions as well as in neuronal disorders [*5*, *144*]. NMDA receptors are obligate heteromers consisting of two essential GluN1 (NR1) subunits with two GluN2 (NR2) or GluN3 (NR3) subunits [*145*]. Eight splice-variant isoforms of GluN1, four isoforms of GluN2 (GluN2A–D), and two isoforms of GluN3 subunits (GluN3A–B) have been identified [*5*, *144*]. Each subunit shares a modular domain architecture: an amino terminal domain (ATD) followed by a ligand-binding domain (LBD), a transmembrane domain and a carboxyl terminal domain. Although there is a consensus that the NMDA receptor forms a hetero-tetramer with subunits arranged as a dimer-of-dimers [*139*], the subunit arrangement within a dimer and the organization of the two dimers are under debate. Two possible arrangements have been proposed. On the one hand, experiments utilizing fluorescence resonance energy transfer (FRET) measurements with fluorophore-tagged subunits and cysteine knockout mutants of the GluN1 subunit were interpreted in terms of a dimer-of-homodimers [*146*, *147*]. On the other hand, the crystal structure of a GluN1–GluN2A LBD heterodimer, FRET measurements with fluorophore-tagged LBDs, and studies on GluN3 subunits are consistent with a dimer-of-heterodimers configuration [*128*, *141*, *148*].

To probe the arrangement of NMDA receptor subunits within a dimer, and to resolve the controversy of homodimer versus heterodimer, we studied the association of subunits at the level of the ATD using cysteine-directed chemical crosslinking. The current model for the NMDA receptor ATDs have been derived from studies on metabotropic glutamate receptors [*149*], on non-NMDA ionotropic glutamate receptors including the GluA2

AMPA receptor and the GluK2 kainate receptor ATDs [*130–132*, *138*], and on the GluN2B ATD [*74*]. The structures of GluA2 and GluK2 ATDs revealed that the ATD forms a homodimer through the interaction between the R1–R1 domain and R2–R2 domain interfaces of ATDs [*130–132*, *138*]. Do NMDA receptor ATDs form architecturally similar local dimers? If the NMDA receptor ATD is indeed a dimer, there are a number of important questions. First, is the dimer a GluN1–GluN1 or GluN2–GluN2 homodimer or is it a GluN1–GluN2 heterodimer? Second, by what interactions does the dimerization occur? For example, do both the R1–R1 and R2–R2 interfaces contribute to the dimerization or does one predominate? Moreover, because the dimerization of ATDs may be an important initial step along the tetrameric assembly pathway of the NMDA receptor [*150*] and because the ATDs modulate the gating activity of the receptor [*64*, *65*], probing the precise mode of ATD association will help in understanding the principles of NMDA receptor assembly and gating. Here we demonstrate that GluN1 and GluN2 ATDs, in the context of an intact NMDA receptor, form a local heterodimer and that the R1–R1 interface mediates interactions between the ATDs of GluN1 and GluN2 subunits.

## Methods

### Receptor expression

We used the rat GluN1a splice variant construct (accession number NP_058706, hereafter referred to as GluN1) with a deletion from M848 to S938 [*151*], the rat GluN2A construct (NP_036705) with a deletion from I867 to V1464, and the rat GluN2B construct (NP_036706) with a deletion from I868 to V1482 [*152*]. These carboxyl terminal truncations reduce non-specific crosslinking yet when coexpressed they assemble to a functional receptor [*153–157*].

We inserted the sequence of the NMDA receptor into the pCGFP-EU vector [*158*]. After the protein sequence, there is a glycine residue, a thrombin cleavage sequence, four alanine residues, followed by a green fluorescent protein (GFP)-tag at the carboxyl terminus. The alanine residues are a result of the NotI digestion site used for cloning. The constructs were expressed in tsA201 cells (HEK 293T, ATCC CRL-11268) plated in 40 mm dishes at a density of $5\times10^5$ cells/ml the night before the transfection. Cells were transfected with lipofectamine 2000 (Invitrogen) according to the manufacturer's instruction. For expression of a single subunit, 1 µg of DNA per dish was used for transfection; for the co-expression of GluN1 and GluN2 subunits we employed a total of 2 µg of DNA with a GluN1:GluN2 plasmid ratio of 1:1. The DNA concentration was estimated by absorbance at 260 nm (A260). At 5 hours post-transfection, the Opti-MEM medium (Invitrogen) was replaced with fresh medium containing 200 µM of dichlorokynurenic acid and 2-amino-5-phosphonopentanoic acid. Cells were harvested at 24 hours post-transfection. The efficiency of transfection was estimated by GFP-dependent epifluorescence.

## Site-directed mutagenesis

The carboxyl terminal-deleted 'wild type' rat GluN1, GluN2A and GluN2B subunits were used as templates and mutations were introduced into desired positions by QuikChange II site-directed mutagenesis kit (Agilent) and confirmed by DNA sequencing of both strands of the entire NMDA receptor open reading frames. Here, the numbering of amino acid residues starts at the position of the initiation methionine. When referring to other studies, however, the numbering follows the original, cited literatures and, in some cases, the numbering may start at the first residue of the mature protein.

## Western blotting

Transfected tsA201 cells were solubilized in 200 µl of lysis buffer (20 mM Tris pH = 8.0, 150 mM NaCl, 40 mM *n*-dodecyl-β-D-maltoside, 1 mM phenylmethyl-sulfonyl fluoride, and a protease inhibitor cocktail composed of 2 mg/ml leupeptin, 0.8 mM aprotinin, and 2 mM pepstatin A) for 1 hr. These whole-cell extracts were centrifuged for 40 minutes at 40000 rpm at 4℃ and the supernatants were collected. The proteins in the collected supernatants were separated by sodium dodecyl sulfate polyacrylamide gel electrophoresis and approximately 4–6 µg of total protein from whole-cell extracts were loaded onto 4–15% gradient gel per lane. The protein concentration was estimated by absorbance at 280 nm ($A_{280}$) and corrected by the equation: protein concentration (µg/µl) = $(1.55\times A_{280})-(0.76\times A_{260})$ [*159*]. For reducing conditions, a final concentration of 100 mM dithiothreitol (DTT) was added to samples before they were loaded onto the gels. Proteins were then transferred to a nitrocellulose membrane and probed with primary antibodies. The anti-GFP (Invitrogen, A11122), anti-GluN1 (Millipore, MAB1586) and

anti-GluN2A antibody (Invitrogen, 480031) were used at dilutions of 1:5000, 1:500 and 1:1000, respectively. The secondary antibodies (LI-COR IRDye 680, 926-32220 and IRDye 800CW, 926-32211) were used at a dilution of 1:10000. PVDF membranes of 0.45 µm (Millipore) and the ODYSSEY CLx imaging system (LI-COR) were used for western blot analysis. We qualitatively estimated the strength of the bands and thus the degree of crosslinking by visual inspection.

## Results and discussion

On the basis of amino acid sequence alignments and the structures of the GluA2, GluK2 and the GluN2 ATDs [*74*, *130–132*, *138*], we selected several residues in the putative R1–R1 and R2–R2 ATD dimer interfaces (Fig. 2.1) for substitution by cysteine because we speculated that these residues may be near each other in an intact NMDA receptor. We asked if any of the introduced cysteine residues would spontaneously form a disulfide bond under ambient conditions. Formation of disulfide bonds would be inferred by the formation of redox-dependent 'dimer bands' at an appropriate molecular mass on a sodium dodecyl sulfate polyacrylamide gel. We then employed Western blotting with a GFP antibody to illuminate all NMDA receptor subunits, or with subunit specific antibodies to unambiguously define a particular subunit.

## Crosslinking between NMDA receptor ATDs in the R1–R1 interface

In the GluA2 and GluK2 ATD structures, the R1–R1 interface is defined mostly by helices α2 and α3 (or helices B and C) [*130–132*] with several polar and non-polar amino acids participating in the inter-subunit contacts. Among them, a phenylalanine in helix α2, F50 in GluA2 or F58 in GluK2, is conserved through GluA1–A4 to GluK1–K2 and interacts with residues on helix α3 of an adjacent subunit. Moreover, when mutations are introduced into this position, they disrupt the dimerization of the ATDs [*131*]. We therefore mutated the equivalent residue in GluN2A, K80, and its possible interacting partner, to cysteine. When two R1 interface mutants, GluN1 S108C and GluN2A K80C, were coexpressed, a band with higher molecular weight was detected with a mass approximately corresponding to two NMDA receptor subunits (Fig. 2.2a). Coexpression of wild-type (WT)

subunits did not give rise to a similar band. Most importantly, the apparent dimer formed spontaneously without the need of oxidizing reagents or bifunctional crosslinkers. We could abolish the dimer formation by incubation with DTT (Fig. 2.2a and 2.2b). The sensitivity of the dimer to reducing agent suggested that dimerization is likely due to formation of a redox-sensitive disulfide bond.

To determine whether other amino acids that are predicted to reside in a putative R1-R1 interface could also spontaneously give rise to disulfide bond-mediated dimers, we coexpressed a panel of cysteine mutant combinations (Fig. 2.1): GluN1 (H101C)–GluN2A (A108C), GluN1 (H101C)–GluN2A (Q111C), GluN1 (P104C)–GluN2A (A108C) or GluN1 (P104C)–GluN2A (Q111C). Because none of these cysteine mutant combinations gave rise to a dimer band on the Western blot (Fig. 2.2c), we believed that the R1–R1 dimer interface was well defined and only specific cysteine residues allowed for spontaneous disulfide bond formation.

We next asked whether we could detect subunit-subunit interactions at the putative R2–R2 dimer interface, drawing upon the recently determined non-NMDA receptor ATD crystal structures as guides. For example, in the GluK2 ATD, L151C on helix F of the R2 interface forms a crosslinked dimer [*160*]. We thus examined the equivalent residues on the GluN1 and GluN2A ATDs (Fig. 2.1). Intriguingly, no crosslinked dimer was found when coexpressing GluN1 (R174C)–GluN2A (Y180C), GluN1 (R174C)–GluN2A (R181C) (Fig. 2.2b), GluN1 (G173C)–GluN2A (Y180C) or GluN1 (G173C)–GluN2A (R181C) (Fig. 2.2c). We therefore concluded that there are significant differences between the R2–R2 interactions in non-NMDA and NMDA receptors.

## Crosslinking partners in the R1-R1 interface

We were interested in whether the formation of the putative ATD dimer, as defined by the GluN1 S108C and GluN2A K80C crosslinking, required both engineered cysteine residues. We therefore coexpressed wild-type and cysteine mutants of GluN1 and GluN2A subunits. Surprisingly, we found that dimer formation did not depend on the GluN1 S108C mutant, although the presence of a cysteine residue at S108 modestly enhanced dimer formation. In fact, the coexpression of GluN1 wild-type with GluN2A K80C was sufficient for producing crosslinked dimers (Fig. 2.3a). This observation suggested two possibilities: either GluN2A K80C crosslinked with an endogenous cysteine on the GluN1 ATD to form a GluN1–GluN2A heterodimer, or GluN2A K80C crosslinked with another GluN2A subunit to form a GluN2A–GluN2A homodimer. If the former hypothesis was correct, then the GluN1 subunit must be present in the dimer band. On the other hand, if GluN1 cannot be detected in the dimer band, then the dimer band was likely the consequence of a GluN2A–GluN2A homodimer.

To distinguish between these scenarios, we probed the blot with a GluN1 specific antibody and robustly detected the presence of the GluN1 subunit (Fig. 2.3b). Furthermore, when the dimer was formed, depletion of the GluN1 and GluN2A monomer populations were almost equal. These data support the conclusion that the GluN1–GluN2A NMDA receptor ATD is a heterodimer and that the GluN2A K80C mutant can form a disulfide bridge with an unidentified endogenous cysteine residue in the GluN1 subunit.

## GluN1 and GluN2A ATD heterodimer

We next sought to identify the crosslinking partner of GluN2A K80C. In the GluN1 ATD there are three endogenous cysteines: C22, C79 and C308. Among them, C79 and C308 are within or near the R1 interface (Fig. 2.1) and are predicted to form an intra-subunit disulfide bridge based on the GluA2, GluK2 and GluN2B ATD crystal structures [*74*, *130–132*]. Nevertheless, we mutated these residues to alanine and coexpressed them with the GluN2A K80C subunit. Neither the C79A nor the C308A single mutant was sufficient to prevent the dimer formation. However, when both cysteines were eliminated, GluN2A K80C no longer crosslinked with GluN1 (Fig. 2.4a). This suggested that both GluN1 C79 and C308 could serve as a crosslinking partner of GluN2A K80C. The shift of the dimer band in the GluN1 (C79A)–GluN2A (K80C) combination may reflect a different ATD conformation adopted by the dimer crosslinked between GluN1 C308 and GluN2A K80C, leading to a change in mobility. The identification of partner residues on GluN1 ATD confirmed that GluN2A ATD associates with GluN1 ATD. We also showed that both GluN1 and GluN2A were present in the crosslinked dimer by probing with GluN1 and GluN2A antibody (Fig. 2.4b). Taken together our data is consistent with the conclusion that the NMDA receptor ATD forms a heterodimer.

## GluN1 and GluN2B ATD heterodimer

Native NMDA receptors are assemblies of the GluN1 subunit with various GluN2 subunits and the GluN2 ATD is responsible for determining the distinct receptor properties in different subtypes of NMDA receptor [*64*, *65*]. Thus, we asked whether a subunit different from the GluN2A could form a similar disulfide bond-mediated ATD heterodimer

with the GluN1 subunit. If it did, then it would suggest conservation in the R1–R1 heterodimer interface among different subunit combinations. To test this hypothesis, we made the GluN2B K79C mutant and coexpressed it with wild type GluN1. Analyses by Western blotting showed the formation of a putative GluN1–GluN2B dimer band, similar in mobility to that formed by the GluN1–GluN2A subunit combination (Fig. 2.5a). The putative dimer band was redox-sensitive, disappearing in the presence of DTT (Fig. 2.5b) and consistent with the idea that subunits were linked by disulfide bonds. This finding supported the notion that both GluN2A and GluN2B subunits can form a local ATD heterodimer with the GluN1 subunit through contacts in the R1–R1 interface.

## Conclusion

The introduction of cysteine residues is a widely accepted method to probe neighboring molecular contacts of a protein [*161*]. Two cysteine residues will form a crosslink only when they are in close proximity [*161, 162*]. We identified a cysteine mutant of GluN2 ATD that was able to spontaneously crosslink with endogenous cysteines C79 and C308 on GluN1 ATD, uncovering the interaction between heteromeric ATD subunits (Fig. 2.5c). When we mutated residues C79 and C308 to alanine, specific cysteine residues in GluN2 ATD no longer resulted in inter-subunit crosslinks. Importantly, experiments by other groups have shown that GluN1 C79A and C308A mutants coexpressed with GluN2A traffic to the cell membranes, form functional receptors [*146, 163*] and do not affect receptor oligomerization [*148*]. Thus, the reason why we did not observe the formation of disulfide bond-mediated dimers with GluN1 C79A C308A double mutant (Fig. 2.4 and 2.5) is not due to the impairment of subunit expression, trafficking or assembly. By contrast, our data strongly suggest that the GluN1 residues C79 and C308 directly participate in forming inter-subunit disulfide crosslinks. The fact that GluN2A K80C or GluN2B K79C could crosslink with more than one GluN1 residue (Fig. 2.4 and 2.5) suggests that the R1–R1 interface is somewhat dynamic or plastic. This observation opens up the possibility that rearrangements within the R1–R1 interface occur during gating of the NMDA receptor. Compared to GluN1 (WT)–GluN2A (K80C), the band shift in the GluN1 (C79A)–GluN2A (K80C) complex but not in the GluN1 (C308A)–GluN2A (K80C) combination (Fig. 2.4 and 2.5), implies that although both GluN1 C79 and C308 could serve as crosslinking partners, GluN2A K80C preferentially crosslinks with GluN1 C79 when coexpressed with wild type GluN1 (Fig. 2.5d). Based on available structural information [*74*], the NMDA

receptor ATD also adopts a "clamshell" conformation. It has been proposed that NMDA receptor ATD clamshells spontaneously switch back and forth between open/closed-cleft conformation and tune the properties of NMDA receptors [*64*]. The rearrangement of R1–R1 interface may participate in this process and make it possible for the remaining GluN1 cysteine to form disulfide bonds with the engineered cysteine on GluN2 when one of the GluN1 cysteines has been knocked out (Fig. 2.5e).

Although we did not exclude the possibility that the R2–R2 interface is also responsible for dimerization, our results suggest a different role for the R2–R2 interface in the NMDA receptor ATD compared to GluA2 or GluK2 ATD. In non-NMDA receptor ATD, the dimer is held together by extensive contacts between the R2–R2 and R1–R1 interfaces [*130–132*]. Indeed, the GluK2 ATD R2–R2 interface mutant, L151C, forms spontaneous crosslinked dimers [*160*], but similar mutants in GluN1 and GluN2A ATD did not (Fig. 2.2b and 2.2c). The lack of this interaction in the NMDA receptor may be because NMDA receptor ATD adopts a twisted conformation, as shown by the structure of isolated GluN2B ATD [*74*] and by the crosslinking experiments on GluN2A ATD [*164*]. At present, there are no specific ligands for the ATDs of non-NMDA receptors, and the stabilization of R2–R2 interface in GluK2 ATD by crosslinking has minimal effects on channel properties [*160*]. By contrast, the GluN2 ATD is the target for the physiological ligand $Zn^{2+}$ or for pharmacological compounds, which allosterically regulate the function of the receptor [*5*, *144*]. We speculate that the difference in the R2–R2 interface between NMDA and non-NMDA receptor helps explain how ATD ligands modulate the functional properties of NMDA receptors.

The GluN1 ATD has been proposed to mask the retention signal on the GluN2A ATD [*165*], a conclusion that is in line with the heteromeric interaction of their respective ATDs. The rat GluN2A ATD retention signal was proposed to be a cryptic signal spread over a number of residues between amino acids 151 to 282. A homology model based on the GluN2B ATD structures [*74*] indicates that residues 151 to 282 constitute the R2 domain of the GluN2A ATD. We, however, did not observe crosslink formations on the selected residues of the R2 domains.

Our results may also explain why the isolated GluN2B ATD predominately exists as a monomer when the GluN1 ATD was not coexpressed [*74*, *80, 134*]. In fact, the isolated GluN2 ATD could associate with the isolated GluN1 ATD in solution [*80, 134*]. On the other hand, several studies have shown that full-length GluN1 subunits or isolated GluN1 domains, when expressed alone, could form homodimers [*80, 134*, *147*, *148, 166–169*]. This has been used as an argument supporting the dimer-of-homodimers model for NMDA receptors. In the present study, upon expression of the GluN1 subunit alone, we also detected a weak band with a size approximately commensurate with a GluN1 homodimer (Fig. 2.2a). We suggest the appearance of this band likely represents the extent to which GluN1 subunits have a weak propensity to form homodimers. Even though this observation is consistent with homodimerization of the GluN1 subunit, it does not mean that the GluN1 subunits form a homodimer in an intact NMDA receptor. Here we studied the association of ATDs within intact NMDA receptors and we found that ATDs form local heterodimers.

The heteromeric NMDA receptor ATDs are reminiscent of the GluA2 ATDs in the GluA2 full-length structure [*138*]. The full-length structure revealed two “non-equivalent” pairs of subunits, A–C and B–D where the two GluA2 ATD dimers are composed of two

conformationally distinct subunits A–B and C–D. Based on the GluA2 full-length structure, a model of NMDA receptor architecture has been proposed which suggested a dimer-of-heterodimers assembly with a GluN1–GluN2-GluN1–GluN2 orientation [*138*]. Our results are in harmony with this model in regard to the heterodimeric feature of NMDA receptors; however, our results were not restricted to the GluN1–GluN2–GluN1–GluN2 orientation proposed by the model. In the NMDA receptor, ATD heterodimers could also be arranged in a GluN1–GluN1–GluN2–GluN2 manner, although in this case the two ATD heterodimers will be arranged 'in parallel', an arrangement that precludes an overall two-fold axis of symmetry. Further experiments, such as the crosslinking of residues in the inter-heterodimer interface [*138, 160*], are needed to clarify this issue.

## Figures and legends

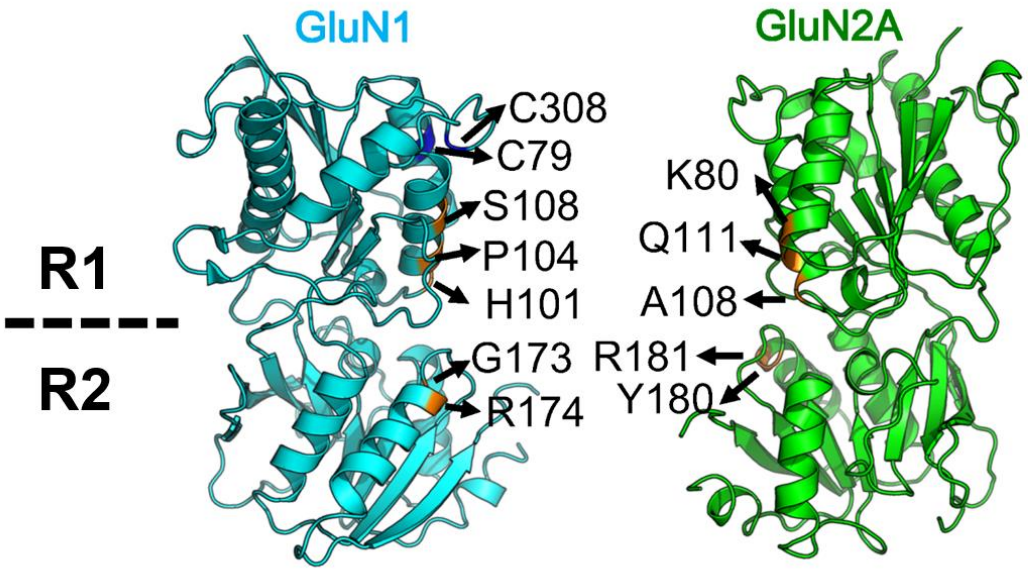


**Figure 2.1: ATD residues studied in this work.**

Here we mapped GluN1 and GluN2A residues onto the GluN2B ATD structure [*74*] based on a multiple amino acid sequence alignment. This figure is for demonstrative purpose to show possible relative locations of these residues and it does not represent an accurate structural model. Endogenous cysteines of the GluN1 ATD are dark blue and the residues studied in this work are orange.

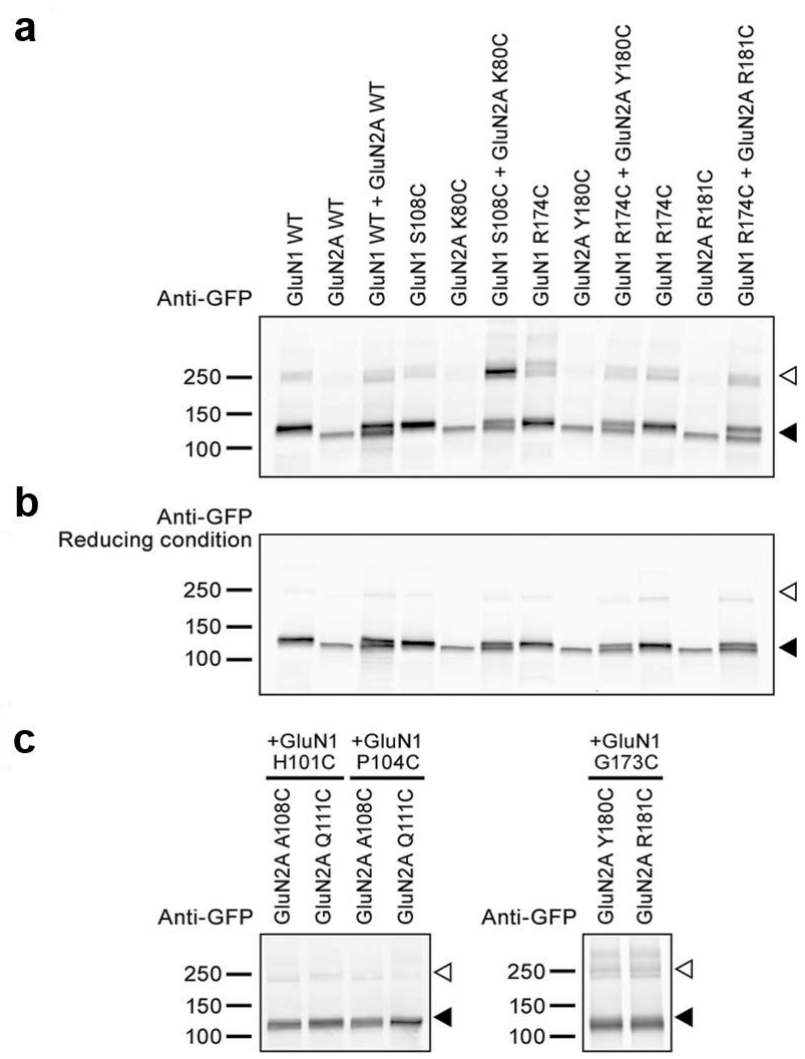


**Figure 2.2: NMDA receptor ATD cysteine mutants in the R1–R1 interface crosslink spontaneously.**

**a–c**, Western blotting analysis of wild type (WT) or cysteine mutants of NMDA receptor probed by GFP antibody. **a** and **c**, Non-reducing conditions. **b**, Reducing conditions. Open arrowhead indicates the crosslinked dimer bands (~250 kDa). Filled arrowhead indicates positions of GluN1 or GluN2A monomer bands. The predicted molecular weights of

GluN1 and GluN2A construct are both ~125 kDa. However, occasionally we could separate two discrete monomer bands in our gels, probably due to differential glycosylation.

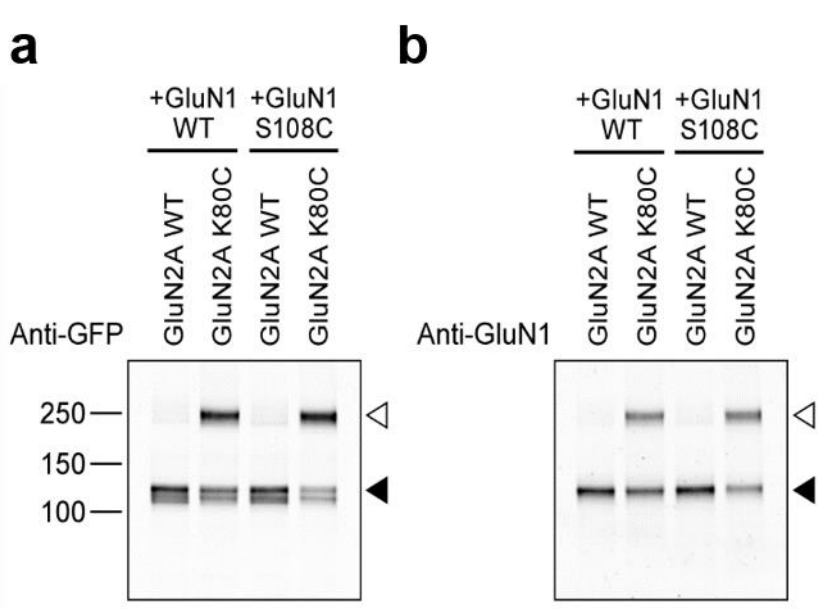


**Figure 2.3: Crosslinking suggests heterodimer formation between GluN1 and GluN2A ATDs.**

**a**, **b**, Western blotting analysis of GluN2A K80C mutant coexpressed with GluN1 WT or GluN1 S108C mutants. **a**, The blot probed by GFP antibody. **b**, The blot probed by GluN1 antibody. Open arrowhead indicates the crosslinked dimer bands. Filled arrowhead indicates positions of GluN1 or GluN2A monomer bands.

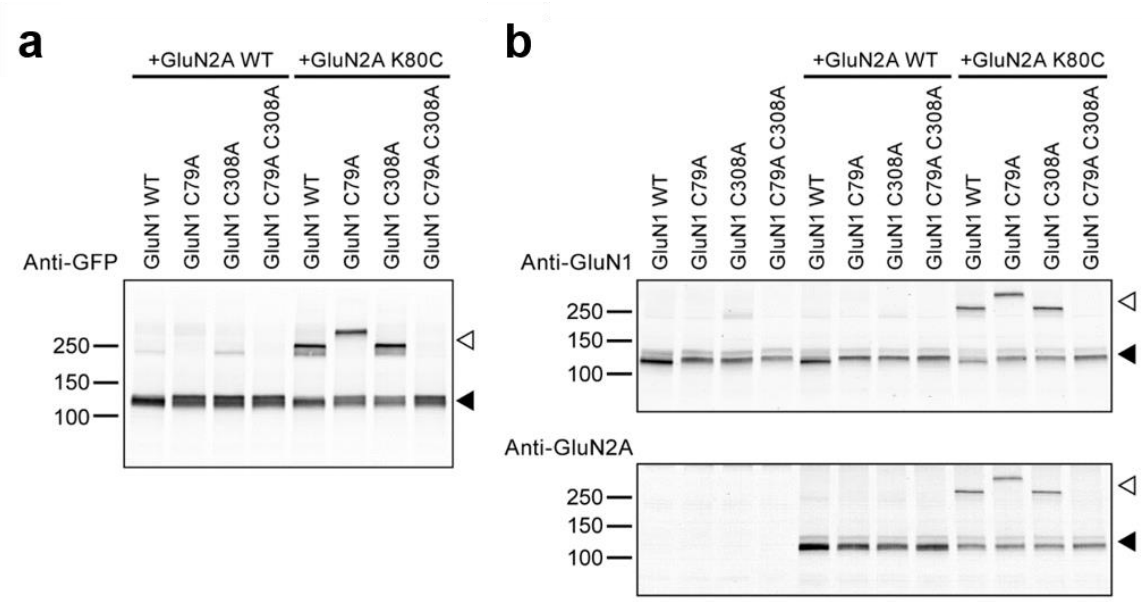


**Figure 2.4: Crosslinking partners in the GluN1 ATD R1–R1 interface.**

**a**, **b**, Western blotting analysis of GluN1 cysteine knockout mutants coexpressed with GluN2A WT or GluN2A cysteine mutants. **a**, The blot probed by GFP antibody. **b**, The blot probed by GluN1 and GluN2A antibody. Open arrowhead indicates the crosslinked dimer bands. Filled arrowhead indicates positions of GluN1 or GluN2A monomer bands.

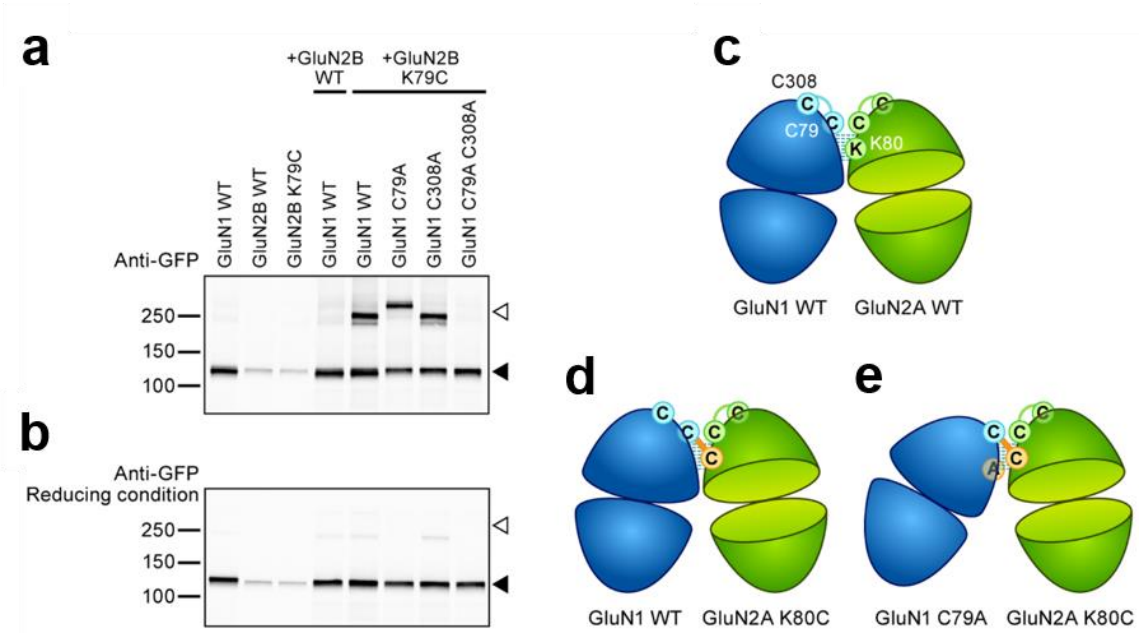


**Figure 2.5: GluN2B ATD forms a heterodimer with GluN1 ATD.**

**a**, **b**, Western blotting analysis of GluN1 cysteine knockout mutants coexpressed with GluN2B WT or GluN2B cysteine mutants probed by a GFP antibody. **a**, Non-reducing conditions. **b**, Reducing conditions. Open arrowhead indicates the cross-linked dimer bands. Filled arrowhead indicates positions of GluN1 or GluN2B monomer bands. The predicted molecular weights of GluN1 and GluN2B construct are both ~125 kDa. **c**, Cartoon model of NMDAR ATD heterodimer. In wild-type subunits, the endogenous cysteines form intra-subunit disulfide bonds. Interactions between the R1–R1 interface are emphasized by thin lines. **d**, **e**, A summary of crosslinking results in the current study. GluN1 C79A and GluN2A K80C residues are colored in orange. The disulfide bond between endogenous cysteines of the GluN1 subunit and engineered cysteines of the GluN2 subunit is represented by thick orange lines. For clarity, in **c**–**e** only GluN2A is

drawn, but our results suggest that GluN2B shares a similar orientation in terms of the ATD heterodimer. The equivalent residue of GluN2A K80 in GluN2B is K79.

# Chapter 3

## NMDA receptor structures reveal subunit arrangement and pore architecture

The content of chapter three is published in a modified form:

Lee CH*, Lü W*, Michel JC, Goehring A, Du J, Song X, Gouaux E. NMDA receptor structures reveal subunit arrangement and pore architecture. *Nature*. 511, 191–197 (2014).

C.H.L. contributed to all aspects of the research; W.L. carried out crystallographic analysis; J.C.M. carried out molecular biology, cell culture, electrophysiology and ligand binding experiments; A.G. performed molecular biology, cell culture, receptor purification and crystallization studies; J.D. and X.S. analyzed the structures.

## Abstract

*N*-methyl-D-aspartate (NMDA) receptors are Hebbian-like coincidence detectors, requiring binding of glycine and glutamate in combination with the relief of voltage-dependent magnesium block to open an ion conductive pore across the membrane bilayer. Despite the importance of the NMDA receptor in the development and function of the brain, a molecular structure of an intact receptor has remained elusive. Here we present X-ray crystal structures of the *Xenopus laevis* GluN1–GluN2B NMDA receptor with the allosteric inhibitor, Ro25-6981, partial agonists and the ion channel blocker, MK-801. Receptor subunits are arranged in a 1–2–1–2 fashion, demonstrating extensive interactions between the amino-terminal and ligand-binding domains. The transmembrane domains harbor a closed-blocked ion channel, a pyramidal central vestibule lined by residues implicated in binding ion channel blockers and magnesium, and a ~twofold symmetric arrangement of ion channel pore loops. These structures provide new insights into the architecture, allosteric coupling and ion channel function of NMDA receptors.

## Introduction

Glutamate is the primary excitatory neurotransmitter in the brain, acting at ionotropic and metabotropic glutamate receptors. Rapid excitation by glutamate, in turn, solely involves action at AMPA, kainate and NMDA ionotropic glutamate receptors [*6*]. The NMDA receptor is central to the development and function of the nervous system and to neurotoxicity [*7*]. As a linchpin of synaptic plasticity, blockade of the NMDA receptor interferes with memory formation and recall [*170*]. Moreover, mutations within the coding regions of NMDA receptor subunit genes are associated with a spectrum of neurological diseases and neuropsychiatric disorders, from schizophrenia to epilepsy [*171*]. Autoimmune responses to the NMDA receptor, and presumed disruption in NMDA receptor organization on neural cell surfaces, probably underlie NMDA receptor encephalitis [*172*]. In keeping with the profound roles of the NMDA receptor in brain function, the receptor is a target of small molecules for the treatment of cognitive impairment, depression, schizophrenia and pain [*7*].

Although AMPA and kainate receptors can be activated solely by glutamate [*173–175*], NMDA receptors are Hebbian-like coincidence detectors, requiring the binding of glycine and glutamate to GluN1 and GluN2 subunits [*20*], respectively, combined with membrane depolarization to relieve magnesium block [*37*, *38*]. Activation of the receptor opens a cation-selective, calcium-permeable channel, thus causing further depolarization of the cell membrane and influx of calcium [*31*]. NMDA receptors are obligatory heterotetrameric assemblies [*151, 152*], usually composed of two glycine-binding GluN1 subunits and two glutamate-binding GluN2A-D subunits, with the GluN1–GluN2A–GluN2B complex as the predominant NMDA receptor at hippocampal synapses [*54*].

Glycine- and D-serine-binding GluN3 subunits are additional subunits, expressed throughout the nervous system, but with roles less well defined in comparison to the GluN1–GluN2 assemblies. A hallmark of NMDA receptors, by contrast with AMPA and kainate receptors, is a wide spectrum of allosteric modulation, from nanomolar concentrations of zinc, to the small molecule ifenprodil, polyamines and protons [*150*] and to voltage-dependent ion channel block by MK-801, ketamine and memantine [*111*].

The GluN1, GluN2 and GluN3 NMDA receptor subunits are related in amino acid sequence and, like AMPA and kainate receptor subunits, possess a modular domain architecture, with amino-terminal domains (ATDs) and ligand-binding domains (LBDs) on the extracellular side of the membrane, a transmembrane domain (TMD) spanning the membrane and defining the ion channel pore, and an intracellular carboxyl-terminal domain (CTD) within the cytoplasm [*6*]. Multiple high-resolution crystal structures of the isolated LBDs from NMDA, AMPA and kainate receptors show that these domains adopt similar clamshell-like structures that are organized in an approximately dimeric, back-to-back fashion [*176–178*]. Although crystal structures of isolated ATDs illustrate that they too possess a clamshell-like structure [*74, 130, 132*], in NMDA receptors not only is the organization of each clamshell lobe distinct from that in AMPA and kainate receptors, but the interactions between subunits are also different [*96*]. The functional properties of the NMDA ion channel pore, which harbors binding sites for magnesium and small molecule blockers, are also distinct from AMPA and kainate receptors [*6*].

Here we report crystal structures of the GluN1–GluN2B NMDA receptor from *Xenopus laevis* in complex with the GluN2B-specific allosteric inhibitor, Ro25-6981 [*179*], the GluN1 and GluN2B partial agonists 1-aminocyclopropane-1-carboxylic acid

(ACPC) [*180*] and trans-1-aminocyclobutane-1,3-dicarboxylic acid (t-ACBD) [*181*], respectively, and the ion channel blocker, MK-801. To enhance the stability of the receptor in detergent micelles and to reduce conformational surface entropy, we replaced the cytoplasmic C terminus of the GluN1 and GluN2B subunits with 11 residues from the GluA2 C terminus [*138*] and we introduced a number of mutations into each subunit, ultimately finding a NMDA receptor complex that preserved binding of full and partial agonists and Ro25-6981, together with small but measurable conductance activated by glycine and glutamate, and with channel block by magnesium. To decrease conformational mobility of the extracellular domains, we substituted GluN2B Lys 216 to Cys (K216C), resulting in spontaneous disulfide bond formation between GluN2B subunits, improving crystal quality yet reducing agonist-induced ion channel activity (Table 1 and Figs 3.1, 3.2, 3.3 and 3.4). We determined crystal structures of the GluN1–GluN2B K216C receptor at resolutions of 3.7 Å (structure 1) and 3.9 Å (structure 2) and refined the structures to reasonable crystallographic residuals and good stereochemistry. In addition, we mapped cation sites in the ATD by exploiting anomalous scattering from a $Tb^{3+}$ derivative and probed the mobility of the ATD and LBD layers by comparing a non K216C crosslinked structure to the higher resolution K216C structures (Table 2).

## Methods

### Receptor constructs

The constructs are detailed in Table 1. Residues 1–834 of *Xenopus laevis* GluN1 (FJ571597.1) and 1–839 of *Xenopus laevis* GluN2B (NM_001110721) were cloned into pEG_BacMam [*182–184*] for analytical-scale transient transfection in adherent cells or for large-scale virus-mediated expression in suspension cells. At the C terminus of both constructs the 3C cleavage site (Leu-Glu-Val-Leu-Phe-Gln-Gly-Pro), enhanced green fluorescent protein and either an octa-histidine tag (at the C terminus of the GluN1 subunit) or StrepII tag (at the C terminus of the GluN2B subunit) were placed for purification and fluorescence-detection size-exclusion chromatography (FSEC) [*158*] and FSEC-thermostability (FSEC-TM) [*185*] analysis.

### Expression and purification

HEK293S GnTI$^{-}$ cells [*186*] were grown in suspension and transduced using P2 BacMam virus at a multiplicity of infection of 1:1 (GluN1:GluN2) and incubated at 37 °C. At 14 h post-transduction, 10 mM sodium butyrate and 2.5 μM MK-801 were added to the cultures and the temperature was shifted to 30 °C. Cells were collected at 60 h post-transduction by centrifugation and disrupted by sonication in a buffer containing 20 mM Tris pH 8.0, 150 mM NaCl and protease inhibitors. Membranes were then collected by centrifugation. Membranes were solubilized in lysis buffer with 20 mM Tris pH 8.0, 150 mM NaCl, protease inhibitors, 1 mM glutamate, 1 mM glycine, 1% MNG-3, and 2 mM cholesteryl hemisuccinate (CHS) for 1.5 h at 4 °C. The soluble fraction was bound to

streptactin resin and eluted with buffer (20 mM Tris pH 8.0, 150 mM NaCl, 0.1% MNG-3, and 2 mM CHS) containing 5 mM desthiobiotin. The receptor was concentrated and digested with 3C protease and endoglycosidase H. Prior to size-exclusion chromatography, the K216C containing receptor was treated with 500 μM copper phenanthroline to enhance cysteine crosslinking. The concentrated GluN1–GluN2B receptor was further purified by size-exclusion chromatography in a buffer composed of 20 mM MES pH 6.5, 400 mM NaCl, 1 mM n-dodecyl β-D-maltoside (DDM) and 0.2 mM CHS. Peak fractions were pooled and concentrated to 2.2 mg $ml^{-1}$ based on absorbance at 280 nm.

**Crystallization and cryoprotection**

Initial crystals of the GluN1–GluN2B NMDA receptor constructs diffracted to ~7 Å resolution. Prior to crystallization, 28 mM DDM, 5 mM ACPC, 1 mM t-ACBD, 1 mM Ro25-6981 and 1 mM MK-801 were added to the GluN1–GluN2B protein, , incubated with a saturating concentration of solid cholesterol for 14–16 h (typically 300 μg cholesterol into ~115 μl protein) [*187*]. Crystals appeared in 16–18% PEG 3350, 200 mM potassium nitrate and 100 mM MES pH 7.1. Crystals were cryoprotected by mother liquor supplemented with 20% glycerol. Crystals used to measure data sets 1 and 2 were obtained with the GluN1 Δ2 and GluN2B Δ2 constructs and by adding 10 mM 6-cyclohexyl-hexyl-β-D-maltoside (Cymal6), together with ACPC, t-ACBD, Ro25-6981 and MK-801 to the protein. Crystals appeared in 19–21% pentaerythritol ethoxylate, 100 mM NaCl, 100 mM $MgCl_2$, and 100 mM HEPES pH 7.5 and were cryoprotected by 12% ethylene glycol. To obtain terbium-complexed crystals, 10 mM Cymal6, 1 mM glutamate, 1 mM glycine, 1 mM Ro25-6981 and 1 mM MK-801 were added to the protein. Crystals appeared in 21–

22% PEG400, 50 µM terbium nitrate and 100 mM MES pH 6.5. Crystals were cryoprotected using a reservoir solution that included PEG400 at 25% and supplemented with 5% ethylene glycol. All crystals were obtained by hanging drop method using 24-well plates at 20 °C.

**Structure determination**

X-ray diffraction data sets were collected at the Advanced Light Source on beamlines 8.2.1 and 5.0.2. Diffraction sets were indexed, integrated, and scaled by XDS [*188*] or HKL2000 [*189*] together with the microdiffraction assembly method [*190*]. The microdiffraction assembly method was first applied to crystallographic studies of G-protein-coupled receptors to minimize the contribution of poorly measured reflections resulting from radiation damage to the crystal. Because diffraction data from NMDA receptor crystals suffered from similar problems, we decided to apply the method to our data, following a protocol similar that previously described. Thus, after the initial scaling of all reflections, each individual reflection that had a correlation threshold below zero was discarded. If $R_{measure}$ was greater than 15 %, the threshold was increased in increments of 1% where all of the observations with a peak profile correlation less than the threshold were subsequently filtered. The filtering procedure was then repeated until $R_{measure}$ was below 15 %. To merge datasets, the additional dataset was filtered and merged to the filtered primary dataset if the $R_{measure}$ was below 15 %. If not, the additional dataset was further filtered with a higher threshold in the correlation. If the threshold went above 40 %, the entire dataset was not be included in the merge step. The best diffraction data for data set 1, as judged by $R_{measure}$, completeness and electron density map quality, were derived

from merging data from three crystals. A single crystal was used for data set 2. The datasets were then processed with diffraction anisotropy server [*191*].

Structure 1 was determined by molecular replacement with Phaser [*192*] using the isolated GluN1–GluN2B ATD in complex with Ro25-6981 (PDB code: 3QEM) [*96*] and the isolated GluN1–GluN2A LBD (PDB code: 2A5T) [*128*] structures as search probes. The molecular replacement solutions were robust with the highest best log likelihood gain and translation function Z-score of 3071.7 and 31.9, respectively. Initial maps were improved by density modification using Parrot [*193*, *194*]. The NCS was automatically determined by Parrot from a partial model containing the entire extracellular domains of GluN1 and GluN2B. The data were truncated to 4 Å resolution and 20 cycles of density modification with solvent flattening, histogram matching, and non-crystallographic symmetry (NCS) averaging were run. The NCS parameters were automatically determined by Parrot from a partial model containing the entire extracellular domains of GluN1 and GluN2B. The radius for NCS mask in Parrot was set to 10 Å. A partial model of the transmembrane domain was manually built into 'omit' style electron density maps. Cycles of manual model building and crystallographic refinement were carried out using the computer graphic program Coot [*195*] and the crystallographic refinement software package Phenix [*196*]. Translation/Libration/Screw groups were determined by phenix.find_tls_groups. Chains A/C were defined as a NCS-related group and chains B/D as the other NCS-related group for torsion-based NCS restraints in Phenix. During the course of model building and refinement, the amino acid sequence and corresponding structure within the ATDs and LBDs were adjusted to the *Xenopus* amino acid sequences. The model was refined to a nominal resolution of 3.7 Å with reasonable R-factors.

Structure 2 derived from data set 2 was solved by molecular replacement using structure 1 as a search probe. Upon inspection of electron density maps, density for the pore loops was visible, along with additional residues in the other TM segments. The final structure 2 was obtained by cycles of manual model building and crystallographic refinement, as described above. Stereochemistry of the model was evaluated by MolProbity [*197*], pore dimensions were estimated using HOLE [*198*] and figures were created using PyMOL [*199*]. Information on the qualities of the structures is provided in the Supplementary discussion (page. 83).

**Two-electrode voltage clamp electrophysiology and western blotting**

Oocytes were injected with RNA (20 ng; 1:1 ratio, GluN1:GluN2B) and stored at 16 °C in the presence of 30 μM DCKA. Recordings were made using a bath solution containing 5 mM HEPES pH 8.0, 100 mM NaCl, 2.8 mM KCl, 10 mM Tricine and 0.3 mM $BaCl_2$. NMDA receptor constructs were activated with a perfusion solution containing 100 μM glycine and 100 μM glutamate with or without 1 mM $MgCl_2$. The holding potential of these recordings is −60 mV. For studies under reducing conditions, oocytes were treated with 5 mM DTT for at least 15 min before recording. For western blots, oocytes were solubilized in lysis buffer (20 mM Tris pH 8.0, 150 mM NaCl, 1% MNG-3, protease inhibitors), and lysates were resolved by SDS–PAGE under non-reducing conditions followed by western blotting analysis using anti-GluN2B antibody.

**Ligand binding assays**

Binding constants were determined by the scintillation proximity assay (SPA) [*200*]. SPA experiments were set up in triplicate wells of a 96-well plate at a final volume of 100 µl in SPA buffer (20 mM Tris pH 8, 150 mM NaCl, 0.01% MNG-3 and 0.02 mM CHS). Affinity-purified (GluN1 Δ2)–(GluN2B Δ2) NMDA receptor (2-5 nM) was incubated with 0.5 mg $ml^{-1}$ of Ysi-Cu (for $^{3}$H-Ro25-6981) or PVT-Cu (for $^{3}$H-L-glutamate and $^{3}$H-glycine binding) SPA beads. Non-specific binding was determined by the addition of 1 mM ifenprodil (for $^{3}$H-Ro25-6981), 1 mM DCKA (for $^{3}$H-glycine), or 1 mM NMDA (for $^{3}$H-glutamate). $^{3}$H-Ro25-6981 binding was performed in the presence of unlabelled 100 µM glutamate and 100 µM glycine.

Inhibition constants were determined by the SPA assay using 5 nM (GluN1 Δ2)–(GluN2B Δ2) NMDA receptor, 0.5 mg $ml^{-1}$ PVT-Cu SPA beads, 200 nM $^{3}$H-glycine or 70 nM $^{3}$H-glutamate, and varying concentrations of ACPC (for competition with $^{3}$H-glycine at the GluN1 LBD) or t-ACBD (for competition with $^{3}$H-glutamate at the GluN2B LBD). Samples were incubated at room temperature for 2 h and then the counts were measured. Data were analyzed using GraphPad Prism using a one-site binding model.

## Results and discussion

## Architecture and symmetry

The structure of the GluN1–GluN2B NMDA receptor resembles a mushroom, with a height of ~150 Å and widths of ~125 × 120 Å (Fig. 3.5a, b). With an overall twofold axis of symmetry, reminiscent of the intact GluA2 AMPA receptor architecture and symmetry [*138*], the receptor domains are organized into three layers with the ATD layer at the top, the LBD layer in the middle and the TMD layer at the bottom. By contrast with the AMPA receptor, the extracellular layers are more compact, with the ATD layer adopting an entirely different structure, interdigitated within the crevices of the LBD layer. The LBD layer caps the extracellular end of the transmembrane domain, with loops from the GluN2B LBDs drooping towards the extracellular leaflet of the membrane bilayer (Fig. 3.5a, b). The TMD hews to an AMPA-like topology and arrangement of helices [*138*], yet with electron density for the M2 segments and pore loops in structure 2, allowing us to define the structure of nearly the entire ion channel pore. Structure 1 and structure 2 are similar, nevertheless, with an overall root mean square deviation on main chain atoms of 0.6 Å. Here we primarily use structure 1 to discuss the ATDs, LBDs and LBD to TMD linkages and structure 2 to describe the TMD.

Subunit arrangement within the GluN1–GluN2B NMDA receptor adheres to the organization of the AMPA receptor [*138*], with the glycine-binding GluN1 subunits occupying the A–C subunit positions and the glutamate-binding GluN2B subunits situated in the B–D subunit sites (Fig. 3.6a). In agreement with crosslinking studies on the GluN1–GluN2A receptor [*138, 142, 143*] and isolated ATDs [*133*] and in agreement with crystal structures of the GluN1–GluN2A LBDs [*128*] and the GluN1–GluN2B ATDs [*96*], the

ATDs and the LBDs are organized as local GluN1–GluN2B heterodimers. Like the AMPA receptor [*138*], there is subunit 'crossover' between ATD and LBD layers such that the subunits of a given ATD heterodimer are connected to subunits in a different LBD heterodimer, thus knitting together the extracellular domain superstructure. The TMDs are further stitched together by the M4 helices interacting nearly exclusively with TM segments from an adjacent subunit. The arrangement of subunits within this NMDA receptor complex illustrates how the subunit non-equivalence first described for the homomeric AMPA receptor [*138*] has been exploited in an obligatory heteromeric assembly.

## Arrangement of amino-terminal domains

The GluN1–GluN2B ATDs are perched above the LBD layer, with the R2 lobes of the GluN2B subunits proximal to each other and near the overall twofold axis of symmetry while the GluN1 ATDs reside at the periphery of the receptor assembly (Fig. 3.6a, b). The ATD heterodimer is shaped like an inverted 'V', in which the open end of the 'V' straddles the GluN1 LBD beneath it, with loops and residues of the GluN1 R2 lobe interacting with its GluN1 LBD and the GluN2B R2 lobe wedged into the interdimer LBD interface. The conformation of an individual ATD heterodimer from the intact receptor structure is slightly contracted compared to the structure of the isolated heterodimer, perhaps because of interactions with the LBD layer or due to lattice contacts (Fig. 3.7a, b and Table 3). There is prominent electron density at the interface between the GluN1 and GluN2B subunits for the allosteric antagonist, Ro25-6981, where it stabilizes the intersubunit interface (Fig. 3.7c) [*96*]. A small interface, formed between the ATD heterodimers, is

centered at the engineered disulfide crosslink at residue 216 of the α5 helix on the GluN2B R2 lobe (Fig. 3.6a).

Zinc acts as an antagonist at nanomolar concentrations on GluN2A-containing receptors and at micromolar concentrations on receptors harboring the GluN2B subunit [*81*]. Because lanthanum also antagonizes the NMDA receptor in a voltage-independent manner [*201*] and lanthanides can bind to zinc sites [*202*], we exploited the anomalous scattering signal of terbium and measured X-ray diffraction data near its f" maximum. Anomalous difference electron density maps show two peaks near the interdomain hinge of the R1–R2 lobes of the GluN2B subunit (Fig. 3.6c and Fig. 3.7d). The Tb2 site overlaps with the previously determined Zn1 site [*74*], whereas the other site (Tb1), near residues Glu 146, Asp 176 and Asp 349, is unique. These data support the notion that ions and small molecules can bind to the ATD clamshells [*203*] in a position to modulate ATD conformation, although future experiments are required to establish the roles of these sites in allosteric regulation of GluN2B-containing NMDA receptors.

The first structure of the NMDA receptor was derived from the low resolution data set 4 (Table 2) and involved a construct lacking the GluN2B K216C mutant. In this crystal form, there are two halves of a receptor in the asymmetric unit and application of crystal symmetry creates two intact receptors, each with a different conformation of the ATDs in which the angles of the ATD domains range from 59° to 84° across the overall twofold axis (Fig. 3.6d). We further observed that helix α5 of the GluN2B R2 lobes face each other, proximal to the overall twofold axis of symmetry. Because we speculated that these structures were indicative of substantial mobility in the ATD layer, we made single cysteine substitutions on the exposed face of helix α5 and screened for redox dependent

crosslinking of GluN2B subunits. Indeed, the K216C mutant, as well as other residues on the face of α5, spontaneously form subunit–subunit crosslinks (Figs 3.1, 3.2 and 3.4), bringing the GluN2B ATDs in close apposition (Fig. 3.7e), diminishing ion channel activity and increasing the resolution to which the crystals diffract. In two electrode voltage clamp experiments, reduction of oocytes using dithiothreitol enhances current responses from the K216C mutant, suggesting that movements of the ATDs allosterically modulate the activity of the ion channel (Fig. 3.2).

## Ligand binding domain layer

The agonist-binding LBDs of the NMDA receptor are organized as a nearly equivalent pair of GluN1–GluN2B heterodimers in which each GluN1–GluN2B heterodimer (Fig. 3.8a, c) closely resembles the water-soluble heterodimers of the isolated GluN1–GluN2A LBDs [*128*] and the homodimeric assemblies of AMPA [*176*] and kainate receptor [*204*] LBDs in non-desensitized conformations. Moreover, the arrangement is similar to that previously observed in the structure of the full-length AMPA receptor (Fig. 3.8b, d) [*138*], although here the electron density for the GluN1 and GluN2B LBDs in chains B and C is weak, perhaps due to an absence of lattice contacts. In comparing this NMDA receptor structure to the antagonist-bound state of the AMPA receptor, the extent to which the local twofold axes of each LBD dimer are angled off of the overall molecular twofold axis of symmetry differ (Fig. 3.8a, b). In addition, inspection of the GluN1–GluN2B and AMPA receptor LBD layers, viewed from the top (Fig. 3.8c, d), shows that there is a relative translation, or shift, of the LBD dimers along the interdimer interface (Fig. 3.8e). Using helix J to align the B–C LBDs, the A–D LBD dimer in the AMPA receptor has undergone

a translational ‘shift’ of ~15 Å relative to the A–D NMDA receptor LBD heterodimer. Although we do not know if these differences in LBD dimer ‘roll’ angle (Fig. 3.8a, b) and translational ‘shift’ (Fig. 3.8e) are due to inherent differences between NMDA and AMPA receptors or to the closed-blocked state of the NMDA receptor versus the competitive antagonist-bound form of the AMPA receptor, or to both factors, this analysis illustrates conformational mobility of the LBD dimers perhaps related to how the LBD couples agonist-binding to the TMD.

Within the LBD layer there are two major interfaces, one within a heterodimer, at the D1–D1 interface of GluN1 and GluN2B subunits, and the second between heterodimers. The intradimer D1–D1 interface is a region of allosteric modulation in NMDA receptors [*101, 205*] and, within one heterodimer, buries ~1,100 $Å^2$ of solvent accessible surface area on each subunit (Fig. 3.8c, f, boxed region). There are two nearly equivalent interdimer interfaces between the heterodimeric LBDs, each burying ~600 $Å^2$ of solvent-accessible surface area, and comprising two loci (Fig. 3.8a, boxed regions). One involves helix G on GluN1 interacting with residues on loop 1 of GluN2B (Fig. 3.8g) and the second includes residues on helix K (GluN2B) making contacts with residues on helix E (GluN1, Fig. 3.8h). Both sets of interactions involve contacts between residues on the D1 and D2 lobes of the GluN1 and GluN2B subunits, providing a direct route by which modulation of the LBD clamshell closure could be translated into rearrangement of the LBD layer. As previously suggested, both the NMDA receptor LBD intradimer interface and the dimer–dimer interface may adopt different conformations depending on the functional state of the receptor.

The initial trigger for the eventual opening of the ion channel gate resides in agonist binding to the LBD clamshells. NMDA receptors require binding by agonists at both the GluN1 and GluN2 sites [*20*], and here we have crystallized the receptor in complex with the partial agonists ACPC [*167*] and t-ACBD [*206*]. Agonist binding results in closure of the LBD clamshell [*126*] and separation of the region proximal to the M3 transmembrane helix [*176*]. Analysis of the GluN1 and GluN2B LBDs demonstrates that each of the two GluN1 and GluN2B clamshells adopt similar conformations (Table 3). Moreover, the degree of closure is similar to that observed for the isolated LBDs (Fig.3.9), except that they are both slightly more open in comparison to the isolated domains, perhaps owing to direct linkage to the ion channel. Separation of the region proximal to the M3 helices is similar between the equivalent residues in the LBD dimers of the full-length receptor and in the glycine/glutamate complex of the isolated GluN1–GluN2A LBDs, yet longer than in an LBD antagonist DCKA/glutamate complex (Fig. 3.9f–h) [*129*]. Thus, by this metric the LBD dimers adopt an agonist-bound, activated conformation.

## ATD–LBD interactions and allosteric coupling

The molecular puzzle of how allosteric inhibitors such as Ro25-6981 and ifenprodil promote closure of the ion channel gate despite the binding of agonists to their cognate LBD dimers must be resolved, at least in part, through communication between the ATD and LBD layers and perturbation of the LBD layer from an active conformation to an inactive state. In the GluN1–GluN2B structure, the ATD heterodimers ‘straddle’ LBD subunits (Fig. 3.10a, b), with the R2 lobe of each GluN1 subunit making extensive contacts with the D1 lobe of the cognate GluN1 LBD and the R2 lobe of the GluN2B subunit

insinuated into the LBD dimer–dimer interface, positioned to make contacts with its cognate GluN2B LBD and with the neighboring GluN1 LBD. Thus we see that the ATDs are judiciously positioned to mediate conformational changes at both LBD intradimer [*101*, *176*, *205*] and interdimer interfaces. Nevertheless, because the intradimer LBD interface is intact, the action of Ro25-6981 and related compounds may not necessarily involve rupture of this interface, and other conformational changes with the LBD layer may be involved in rendering the LBD layer in the apparently inactive conformation observed in the present structures. However, additional studies with robustly active receptor constructs will help to resolve these questions.

In the GluN1 subunit, the ATD α5 helix C terminus, which harbors exon 5 in an alternatively spliced form of the gene [*207*], in combination with the α4–β7 loop, resides close to the LBD dimer interface, near the C terminus of helix J, and in a plausible position to perturb the conformation of the LBD layer (Fig. 3.10c). The GluN2B α4 helix C terminus, along with the loop connecting α4 to β7, a region implicated in regulation of the NMDA receptor by polyamines [*81*], rest on top of the F and G helices of the GluN1 LBD and close to residues in loop 1 of the GluN2B LBD (Fig. 3.10d). Thus, although the linking peptides connecting the ATDs to the LBDs have an important role in the transduction of conformational changes between the two layers [*64*], direct contacts that harness the predicted large-scale motions of the ATDs [*203*] also play a central role in transmitting changes to the transmembrane, ion channel domain.

## Transmembrane domain

NMDA receptors are calcium permeable and toxic to cells upon overexpression and therefore we introduced mutations known in AMPA receptors to increase receptor desensitization [*208*], finding that in the context of the GluN1–GluN2B NMDA receptor, they lead to decreased current amplitudes and enhanced stability of the receptor in detergent micelles. Because native GluN1–GluN2B receptors have a low open probability (Po) [*209*] and the modifications we have introduced further reduce Po, the functional state of the receptor should be an Ro25-6981, partial agonist bound, closed-blocked channel state.

The electron density associated with data set 2/structure 2 allowed us to position the polypeptide main chain for the M1 to M4 helices of all subunits. To trace the polypeptide associated with the pore loop, we exploited the continuous electron density for this region in the GluN2B subunit (chain D) and traced the pore loop of chain B by applying local non-crystallographic symmetry defined by the TMD of the GluN2B subunits. To be specific, we created a copy of the TMD of chain D and superposed this copy on chain B based on M1 to M4 segments. The pore loop of this NCS-related copy was then used to guide the model building of the pore loop in chain B. Similarly, non-crystallographic symmetry of the GluN1 subunits were applied to traced the pore loops of chain A and C (Fig. 3.11a, b). The arrangement of transmembrane helices is like that of the GluA2 AMPA receptor [*138*] (Fig. 3.12a), although in the NMDA receptor we have a more complete representation of the ion channel pore and putative selectivity filter. The pre-M1 region of the NMDA receptor forms a ‘collar’ around the extracellular regions of the M3 helices, residing near the boundary of the extracellular side of the membrane. The M1 helix

descends across the membrane and makes interactions with the pore-lining M3 helix of the same subunit and the M4 helix of a neighbor. Electron density for the cytoplasmic loop connecting M1 to M2 is weak or missing, and thus this region is absent from the structure. We can visualize the M2 pore helix and most of the extended region of the pore loop forming the selectivity filter and its connection to the N terminus of M3.

The conformation of the polypeptide chain throughout the M2 helix and the pore loop are reminiscent of a potassium channel [*47*], although there are differences in the local conformation of the NMDA pore loops, perhaps due to non-glycine residues, SVP, within the canonical GYG motif of potassium channels in the GluN2B subunit (Fig. 3.12b, c) or to the lower resolution of the present structures. For example, the Cα distances between Gly residues (NSGIG) of the two GluN1 subunits, and between Pro residues (NNSVP) of the two GluN2B subunits are 11.9 Å and 10.6 Å respectively, whereas the corresponding distance between Gly residues in the KcsA channel (TVGYG) is 7.9 Å [*210*]. If the M2 helix of the GluN1 is superposed on that of GluN2B, there will be a 4 Å Cα displacement between the Gly residue (NSGIG) of the GluN1 subunit and the corresponding Ser residue (NNSVP) of the GluN2B subunit. Asn residues implicated in voltage-dependent magnesium block [*45*] are situated at the turn between the end of M2 and the beginning of the extended filter sequence, in a position to project their side chains into an aqueous vestibule (Fig. 3.11c, f). Forming the core of the ion channel is the M3 segment, in a similar conformation as the M3 segment in the GluA2 receptor [*138*] (Fig. 3.12a). The extracellular ends of the M3 segments adopt a pyramid-like shape, forming a physical constriction to the ion channel permeation pathway (Fig. 3.11c, d). The M4 segment resides on the periphery of the transmembrane domain, interacting primarily with the M1 and M3

helices of a neighboring subunit and extending for several more turns into the cytoplasmic-space than that seen in the GluA2 receptor.

## Ion channel gate and central vestibule

The solvent accessible pathway through the ion channel pore from the extracellular side of the membrane to the cytoplasm shows an occlusion near the predicted extracellular boundary of the membrane bilayer, a central vestibule, and a second occlusion at the beginning of the selectivity filter, followed by a solvent accessible pathway to the cytoplasm (Fig. 3.11c). We speculate that the physical gate of this closed-blocked state of the NMDA receptor is at the bundle crossing of the M3 helices, in a position similar to that of the shut gate of the antagonist-bound GluA2 receptor [*138*]. The narrowest constriction is defined by Thr 646 of GluN1 and Ala 645 of GluN2B, within the highly conserved SYTANLAAF motif crucial to ion channel gating, near the extracellular boundary of the M3 helices [*211*]. Flanking the constriction is a narrow region too small for ion permeation, spanning Val 642–Leu 653 of GluN1 and Ala 641–Ile 652 of GluN2. Although the arrangement of the M3 helices at the ion channel gate diverges from the approximate fourfold symmetry of the AMPA receptor (Fig. 3.11d) [*138*], we do not yet know if this distinction is inherent to NMDA receptors or is a consequence of their different ligand-bound and functional states.

The pore expands immediately below the M3 bundle crossing to the central vestibule, a cavity flanked by the M3 helices on the sides and the ends of the M2 helices together with the tips of the pore loops on the bottom. A second constriction of the pore is immediately below the central vestibule and is defined by the residues at the beginning of

the pore loop (Fig. 3.11c). Because of the limited resolution of the diffraction data, we are unable to position side-chain groups and to precisely define the location of main chain carbonyl oxygen atoms, and thus are not able to determine if this region of the pore is large enough to conduct ions. Following this constriction, the pore expands to the cytoplasmic space. By contrast with fourfold symmetric potassium channels, the pore loops of this specific ligand-bound state of the NMDA receptor are arranged with approximate twofold symmetry (Fig. 3.11e).

In electron density maps derived separately from data set 1 and 2 and their respective structures (Table 2), we found positive difference electron density within the central vestibule (Fig. 3.11f and Fig. 3.12d–f). Because we crystallized the receptor in the presence of 1 mM MK-801, we suggest this electron density feature could represent a trapped MK-801 molecule that occupies multiple positions or orientations within the central vestibule. Unfortunately, we have been unable to validate MK-801 binding by direct binding assays or by electrophysiology experiments, perhaps because of the very low Po of the receptor construct. Nevertheless, several residues including Ala 643 and Tyr 645 on the GluN1 M3 helix, and Asn 614 (GluN1), Asn 612 (GluN2B) and Asn 613 (GluN2B) on the pore loop 'tips', are near the electron density feature and have been implicated in MK-801 binding [*111*]. We speculate that ion channel blockers, such as MK-801, occupy the central vestibule and block ion conduction by preventing ions from entering the pore loop-lined selectivity filter.

## Coupling of ligand binding and transmembrane domains

The coupling of the LBD to the TMD is similar, in principle, to the AMPA receptor [*138*], with the crucial M3 connections to the LBDs proximal or distal to the overall twofold axis for the GluN1 A–C subunits or the GluN2B B–D subunits, respectively (Fig. 3.13). However, the relative orientation of the NMDA receptor TMD with respect to the LBD is distinct from the GluA2 receptor. Specifically, the LBD layer of the NMDA receptor is rotated by ~35° around an axis that is approximately coincident with the overall twofold axis of the receptor. At this juncture we do not know if this difference is due to inherent differences between NMDA and AMPA receptors or because this specific NMDA receptor complex is trapped in an ATD antagonist-bound, LBD partial-agonist bound, closed-blocked state.

## Conclusion

The GluN1–GluN2B structure harbors an overall twofold symmetry, a layered dimer-of-dimers arrangement of subunits and a positioning of GluN1 and GluN2B subunits in the A–C and B–D positions defined by the full-length GluA2 receptor [*138*]. The rich interdigitations and covalent linkage of the R2 lobes of the ATDs to the LBDs provide molecular routes for transmission of allosteric signals to the glycine and glutamate-binding LBD layer, which is organized as a ring of heterodimeric units above the transmembrane ion channel (Fig. 3.14). Despite closure of the LBD clamshells around partial agonists and an intact ‘non-desensitized’ D1–D1 interface of the LBD heterodimers, the ion channel gate is in a closed-blocked state, providing the first insights into the structural basis for allosteric inactivation of a NMDA receptor and suggesting that plasticity of the LBD layer

may provide a mechanism for modulation of receptor gating. Departing from the fourfold symmetry of the GluA2 transmembrane domain, the pore loops of the NMDA receptor are approximately twofold symmetric. The allosteric antagonist-bound GluN1–GluN2B structure provides a molecular blueprint for the development of new therapeutic agents and a structural framework for biophysical mechanisms of allosteric modulation, gating and ion channel function, as well as a springboard for future studies directed towards determining structures of resting, open and desensitized states and defining locations of ion and blocker binding sites.

## Supplementary discussion: model quality

### GluN1–GluN2B structure 1 at 3.7 Å resolution

Likely due to crystal packing, the overall map qualities of chain A (GluN1) and B (GluN2B) are better than those of chain C (GluN1) and D (GluN2B) in the ATD layer. In the LBD layer, the electron density is best for chain A (GluN1) and chain D (GluN2B) and we only fit respective LBD ligands to each of these LBDs. In contrast, the densities for the LBD in chain B and C are poor, perhaps caused by a lack of crystal contacts. Nevertheless, some structural features including helices B, J, and K in both chain A and C could be seen in omit LBD maps. In the ATD region we built the complete GluN1 ATD (23–390) and GluN2B ATD (27–385) (Fig. 3.15). For the ATD–LBD linking polypeptides, the linker in chains A and C (GluN1) could be traced whereas the linkers between GluN2B ATDs and LBDs are disordered (391–396 missing) (Fig. 3.15). With respect to the LBD–TMD linkers, the linkers connecting M3 and LBD could be traced in all chains. The LBD–M4 linker could also be traced in chain D. The remaining LBD to TMD linking peptides are only partially defined or are disordered, consistent with the observation that the electron densities for M1, M2 and M4 are weaker than for M3. For the TMD, with the exception of M3, all of the other helices (1, 2, and 4) were modeled basically as polyalanine chains. While amino acid number registry is difficult at this resolution, our best estimate of the register in the TMD is as follows: Chain A (GluN1): M1 (558–581), M2 (601–613), M3 (624–653), M4 (819–840); chain B (GluN2B): M1 (553–573), M2 (601–611), M3 (624–653), M4 (819–840); chain C (GluN1): M1 (558–579), M2 (not built), M3 (626–653), M4 (not built); chain D (GluN2B): M1 (553–569), M2 (596–611), M3 (625-653), M4 (814–841). The register of the majority of residues in all M3 segments could be estimated and

the side chains of large amino acids could be modeled (e.g. M631 and Y637 in chain A, Y629 in chain D). Due to weak density, M2 and M4 are missing in chain C (GluN1). The cytoplasmic loops connecting M1 and M2 are disordered in all chains.

**GluN1–GluN2B structure 2 at 3.9 Å resolution**

The overall quality of the electron density of structure 2 is similar to that of structure 1 with the exception that the electron density of the TMD is much better in structure 2. We do not know if this is simply due to variability from crystal to crystal or because all of the diffraction data for structure 2 was measured from a single crystal. As with structure 1, there is electron density for both Ro25-6981 molecules in the ATD layer, for ACPC in chain A (GluN1), and for t-ACBD in chain D (GluN2B). In the TMD we could clearly see electron density for M2 in all chains and the pore loop in chain D. For other chains, the pore loops have discontinuous electron density and we tentatively built the polypeptide chain based on chain D (Fig. 3.15). With the help of some side-chain features of large amino acids, as well as sequence/structure alignment with GluA2 and KcsA, we were able to identify the register in most parts of the TMD. However, there is still register uncertainty due to limited resolution and we thus decided not to build side chains for most of the residues. With respect to the linkers connecting the LBD and TMD, we could trace the entire LBD–M3 in chains C and D and LBD–M4 linkers in chains A (Fig. 3.15). Other linkers are only partially defined. The cytoplasmic loops connecting M1 and M2 are disordered in all chains. Our best estimate of the register in the TMD is as follows: chain A (GluN1): M1 (558–582), M2 (600–613), pore loop (614–623), M3 (624–653), M4 (815–840); chain B (GluN2B): M1 (553–573), M2 (599–611), pore loop (612–622), M3 (623–

653), M4 (813–842); chain C (GluN1): M1(558–578), M2 (600–613), pore loop (614–623), M3 (624–653), M4 (815–834); chain D (GluN2B): M1 (553–573), M2 (597–611), pore loop (612–622), M3 (623–653), M4 (813–841).

## Figures and legends

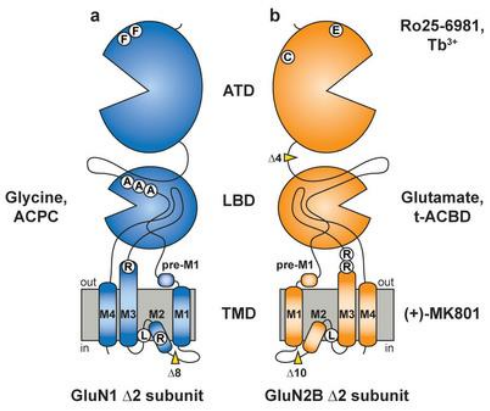


c

```
                22          51          300         350         368         440         469         493
GluN1 Xl  ...RAGCDPK...QANKRHFT...EMENITD...KFANYSI...GIFNGSY...NGPNETI...REMNFTY...NSNKKEWNG...
GluN1 Δ1  ...RAGADPK...QANKRHFT...EMEQITD...KFAQYSI...GIFDGSY...NGPDETI...REMDFTY...NSNAAAWNG...
GluN1 Δ2  ...RAGADPK...QANFFHFT...EMEQITD...KFAQYSI...GIFDGSY...NGPDETI...REMDFTY...NSNAAAWNG...
GluN1 Δ3  ...RAGADPK...QANFFHFT...EMEQITD...KFAQYSI...GIFDGSY...NGPDETI...REMDFTY...NSNAAAWNG...
GluN1 Δ4  ...RAGADPK...QANFFHFT...EMEQITD...KFAQYSI...GIFDGSY...NGPDETI...REMDFTY...NSNAAAWNG...
               588     595         610     617         636         656         741         769         816
GluN1 Xl  ...GRFKVNSEEEEEDA...FSWGVLLNSGIGEG...VWAGFAM...LVLDRPE...ASQKCDL...WKQNVSL...GVFMLVA...
GluN1 Δ1  ...GRFKVNSAAAEEDA...FSWRVLLNSGLGEG...VWALFAM...LVLRRPE...ASQDCDL...WKQEVSL...GVFYLVA...
GluN1 Δ2  ...GRF--------EDA...FSWRVLLNSGLGEG...VWAGFAM...LVLRRPE...ASQKCDL...WKQEVSL...GVFMLVA...
GluN1 Δ3  ...GRFKVNSAAAEEDA...FSWRVLLNSGLGEG...VWAGFAM...LVLRRPE...ASQKCDL...WKQEVSL...GVFMLVA...
GluN1 Δ4  ...GRFKVNSAAAEEDA...FSWRBLLNSGLGEG...VWALFAM...LVLRRPE...ASQDCDL...WKQEVSL...GVFMLVA...
               834
GluN1 Xl  ...EIAYK---------...
GluN1 Δ1  ...EIAYKSRAEARKMK...
GluN1 Δ2  ...EIAYKSRAEAKRMK...
GluN1 Δ3  ...EIAYKSRAEAKRMK...
GluN1 Δ4  ...EIAYKSRAEAKRMK...
```

d

```
                20          64  69          216         343         382           490
GluN2B Xl ...LFYMGCYAQ...PRVALVTMNEDM...NQLKKLQ...EGRNLSF...LKMKYYVWPV...INGTWNG...
GluN2B Δ1 ...LFYSRAYAQ...PRVELVTMQEDM...NQLKKLQ...EGRDLSF...LKM----WPV...INGVWNG...
GluN2B Δ2 ...LFYSRAYAQ...PRVELVTMQEDM...NQLCKLQ...EGRDLSF...LKM----WPV...INGVWNG...
GluN2B Δ3 ...LFYSRAYAQ...PRVELVTMQEDM...NQLCKLQ...EGRDLSF...LKM----WPV...INGVWNG...
               584       593         615         654         839
GluN2B Xl ...GYNRCLADGREPGGPS...NNSVPVQ...MIQEEYVD...HLF----------...
GluN2B Δ1 ...GYNRALADGREPGGPS...NNSLPVQ...MIQRRYVD...HLFYKSRAEARKMK...
GluN2B Δ2 ...GYN----------GPS...NNSLPVQ...MIQRRYVD...HLFYKSRAEARKMK...
GluN2B Δ3 ...GYNRALADGREPGGPS...NNSLPVQ...MIQRRYVD...HLFYKSRAEARKMK...
```

**Figure 3.1: Summary of *Xenopus laevis* NMDA crystallization constructs.**

**a**, **b**, Cartoon representation of amino-terminal domain (ATD), ligand binding domain (LBD) and transmembrane domain (TMD) for GluN1 Δ2 and GluN2B Δ2 subunit

constructs. Location of point mutations are highlighted in white circles. Location of deletions are highlighted with a yellow wedge. Mutated glycosylation sites are not shown and are listed in Table 1. **c**, **d**, Select amino acid sequences of constructs used in these studies compared to wild-type sequence to highlight mutations in GluN1 and GluN2B. Mutations are numbered and the purpose of each is detailed in Data Table 1.

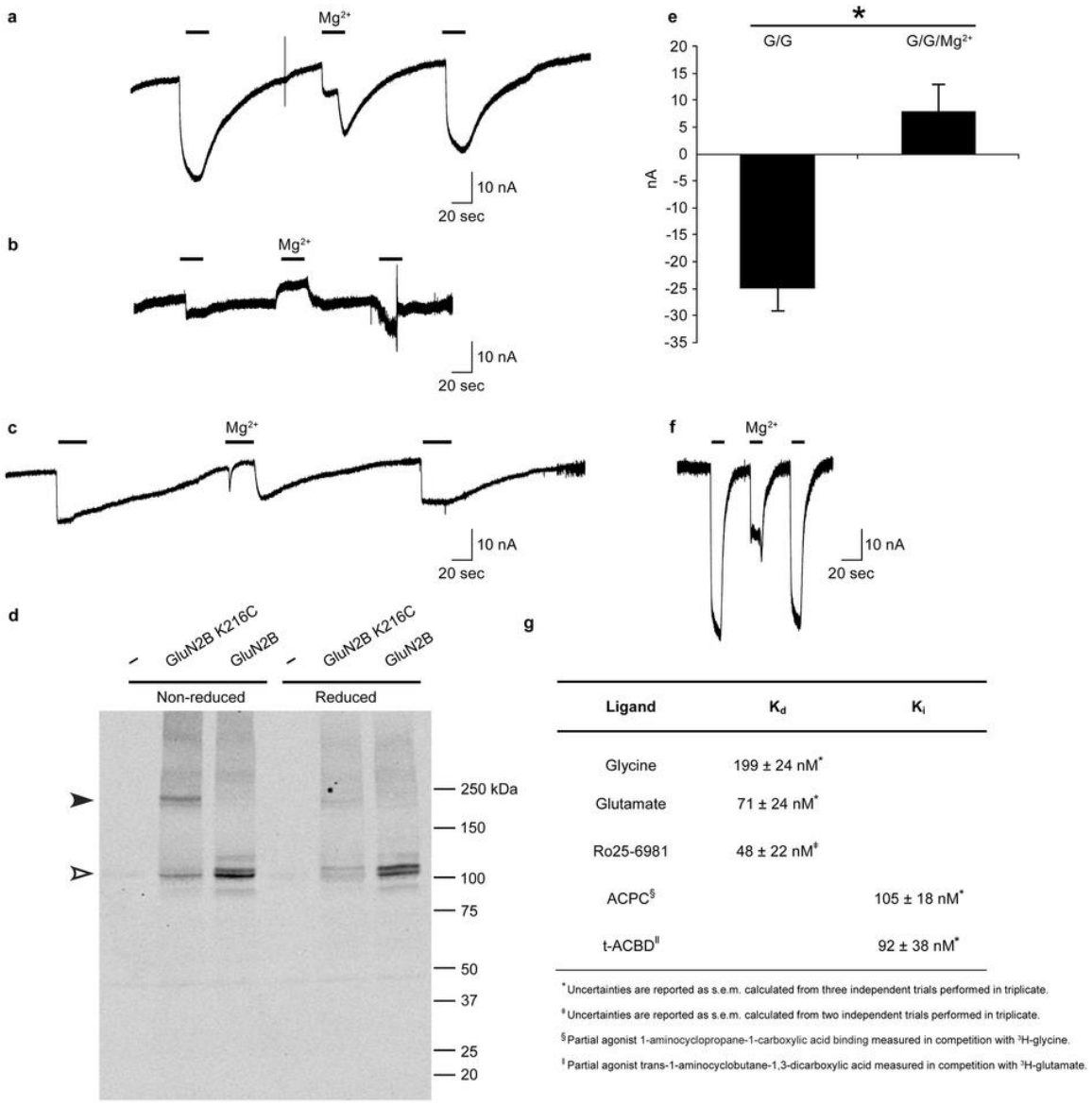


**Figure 3.2: Electrophysiology and western blot analysis of GluN1–GluN2B receptor combinations.**

**a–c**, Representative TEVC currents recorded for oocytes expressing GluN1 Δ4 and GluN2B Δ1 (**a**) or GluN2B Δ3 (**b**, **c**) receptors in response to agonist (100 μM glycine and 100 μM glutamate; bars, 20 s) or agonist plus 1 mM $MgCl_2$ (indicated) after soaking

oocytes in the absence (**a**, **b**) or presence (**c**) of 5 mM DTT. **d**, Western blot analysis of oocytes demonstrating spontaneously crosslinking cysteines (Lys216Cys) introduced at the GluN2B Δ3 intersubunit interface. Oocytes were soaked in the absence (left lanes) or presence of 5 mM DTT (right lanes) before processing for western analysis using an anti-GluN2B antibody. Filled and open triangles indicate positions of crosslinked and monomeric GluN2B, respectively. **e**, Graph of mean agonist-induced inward currents from four reduced oocytes expressing GluN1 Δ4 and GluN2B Δ3 in the absence (G/G, −25 ± −4 nA) or presence of 1 mM $MgCl_2$ (G/G/$Mg^{2+}$, 8 ± 5 nA). Error bars represent s.e.m. The *P* value is <0.001 for the paired *t*-test (asterisk). **f**, Representative TEVC currents recorded in response to agonist (100 μM glycine and 100 μM glutamate; bars, 10 s) or agonist plus 1 mM $MgCl_2$ for oocytes expressing constructs similar to the (GluN1 Δ2)–(GluN2B Δ2) receptor combination with the following exceptions: GluN1 subunit, Asp 656 (wild type), Gly636Leu and Lys741Asp; and GluN2B subunit, Glu 654 (wild type), Glu 655 (wild type), and Lys 216 (wild type). **g**, Binding constants for the (GluN1 Δ2)–(GluN2B Δ2) construct.

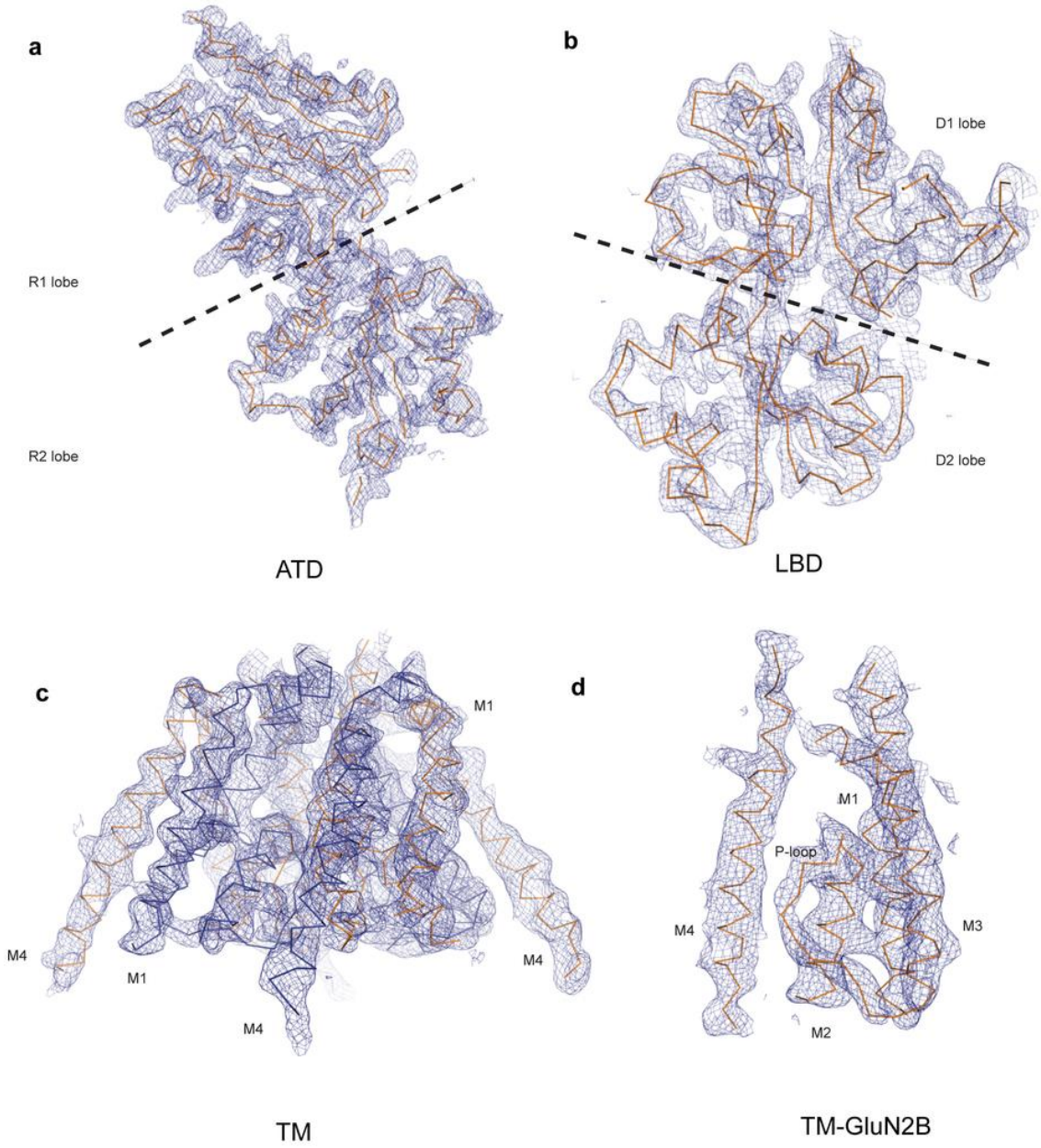


**Figure 3.3: $2F_o$-$F_c$ electron density maps of the GluN1–GluN2B NMDA structure.**

**a**–**d**, The electron densities associated with the GluN1 ATD (chain A) contoured at 1.7 σ (**a**), the GluN1 LBD (chain A) contoured at 1.6 σ (**b**), the TMD of the entire tetrameric

receptor contoured at 1.0 σ (**c**) and the TMD of a single GluN2B subunit (chain D), showing the pore loop, also contoured at 1.0 σ (**d**). Electron density maps and structures were derived from data set 1/structure 1 for panels **a** and **b** and from data set 2/structure 2 for panels **c** and **d** (see Table 2).

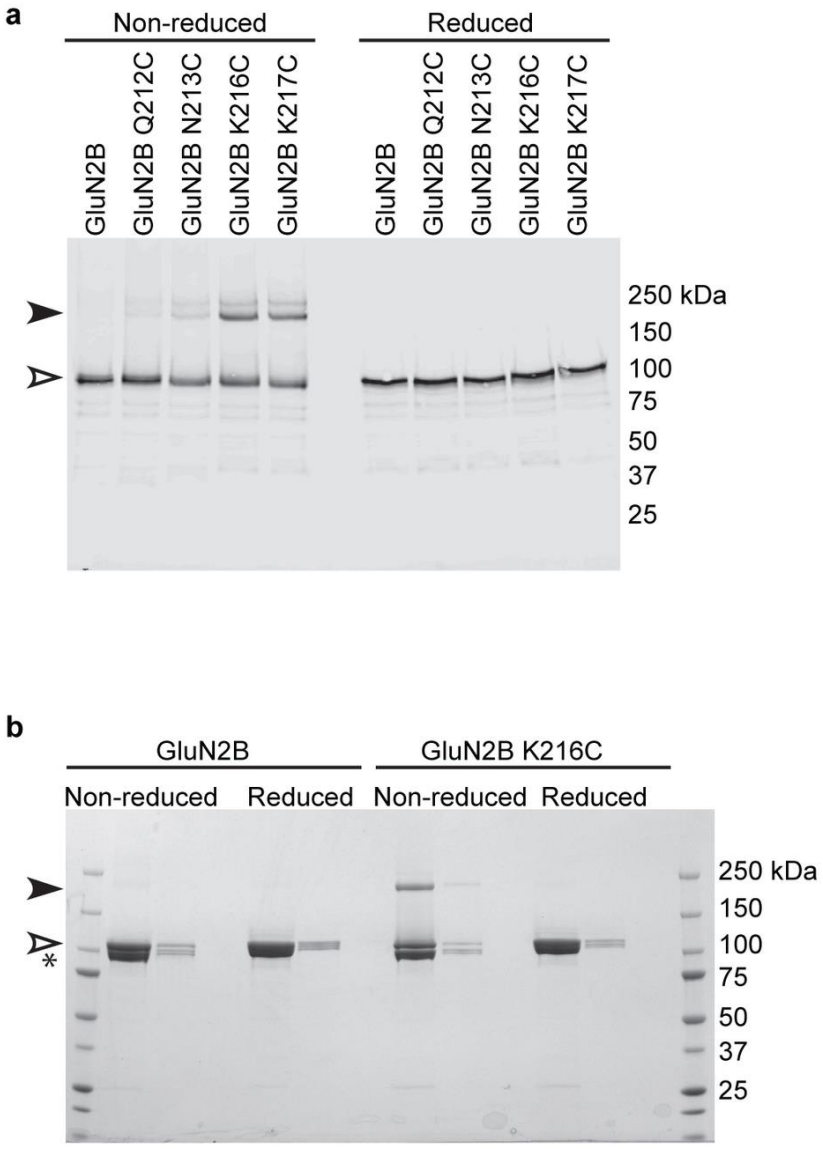


**Figure 3.4: Analysis of spontaneous crosslinking of single cysteine point mutants introduced in the GluN2B ATD of the GluN1–GluN2B receptor complex.**

**a**, Western blot analysis of single cysteine mutants in the α5 helix of the GluN2B subunit. Solubilized extracts of HEK293S GnTI$^{-}$ cells expressing a C-terminal GFP-StrepII tag GluN2B construct (GluN2B Δ1) containing mutants as indicated with untagged GluN1 (GluN1 Δ1) were analyzed by western blot using an anti-GFP polyclonal antibody. The

open and filled arrows correspond to monomeric and dimeric GluN2B bands, respectively. **b**, Coomassie stained SDS–PAGE analysis of spontaneous crosslinking of GluN2B K216C containing receptor. Left and right lanes illustrate samples with different concentrations of protein for GluN1–GluN2B and GluN1–GluN2B K216C receptors. The asterisk indicates GluN1 monomer and the open and filled arrows correspond to monomeric and dimeric GluN2B bands, respectively.

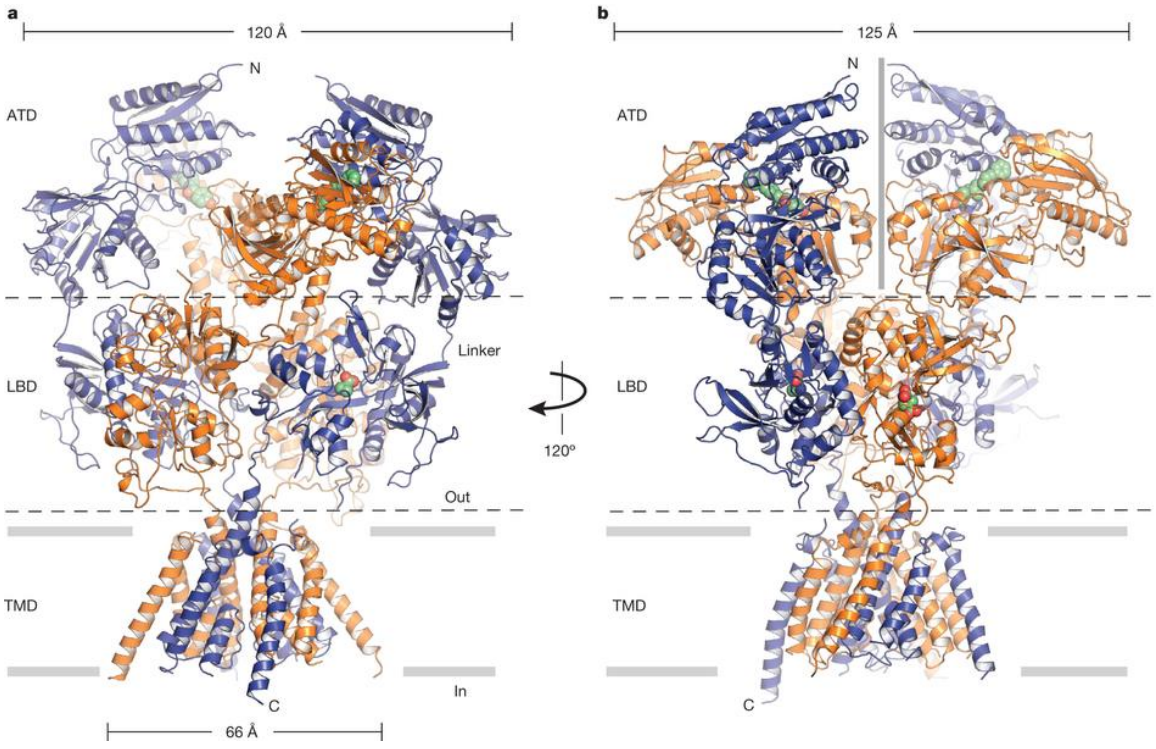


**Figure 3.5: Architecture, symmetry and domain organization of the GluN1–GluN2B NMDA receptor.**

**a**, View of the receptor complex, parallel to the membrane, with the GluN1 subunits in blue and the GluN2B subunits in orange. The ligands Ro25-6981, ACPC and t-ACBD are in space-filling representation. **b**, View of the complex rotated by ~120° around the overall twofold axis of the receptor. The approximate position of the overall twofold axis is shown by a vertical grey bar in the center of the ATD layer. Structure 2 is shown.

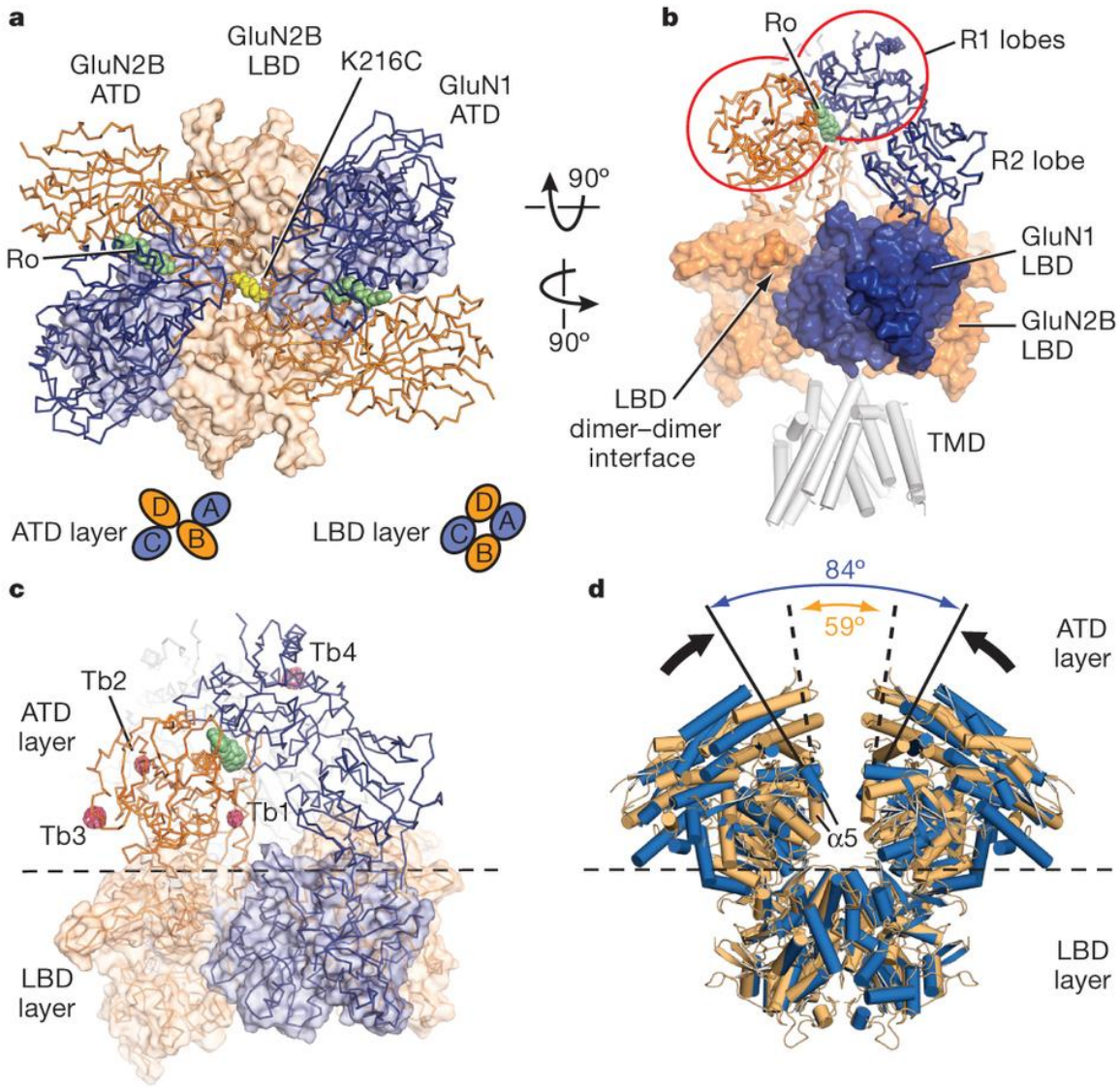


**Figure 3.6: ATD arrangement, cation binding sites and conformational mobility.**

**a**, View of the ATD layer along the overall twofold axis, from the extracellular side of the membrane, centered on the overall twofold axis, and showing the relative location of the underlying LBD layer. Ro25-6981 (Ro) is green and the K216C disulfide is yellow. The arrangements of subunits for ATD and LBD layers are shown as insets. **b**, The inverted ATD heterodimeric 'V' straddles GluN1 and GluN2B LBD subunits on different local

LBD heterodimers. The ATD R2 lobes interact with the LBDs and the R1 lobes cradle bound Ro25-6981 at an ATD subunit interface. Structure 1 is shown in panels **a** and **b**. **c**, $Tb^{3+}$ binding sites. An anomalous difference electron density map is shown contoured at 3.5 σ (pink mesh). Sites Tb1 and Tb2 are located at the 'hinge' between the R1 and R2 lobes, whereas sites Tb3 and Tb4 are at receptor–receptor contacts in the crystal lattice. **d**, The ATD and LBD extracellular domains derived from the two low-resolution GluN1–GluN2B receptor structures (Table 2; data set 4/structure 4) where the GluN2B subunits do not harbor the K216C disulfide bridge, illustrating the conformational mobility of the ATD layer. The angles between the α5 helices of the GluN2B subunits for each of the two independent receptor complexes in the asymmetric unit illustrate the conformational mobility of the ATD layer.

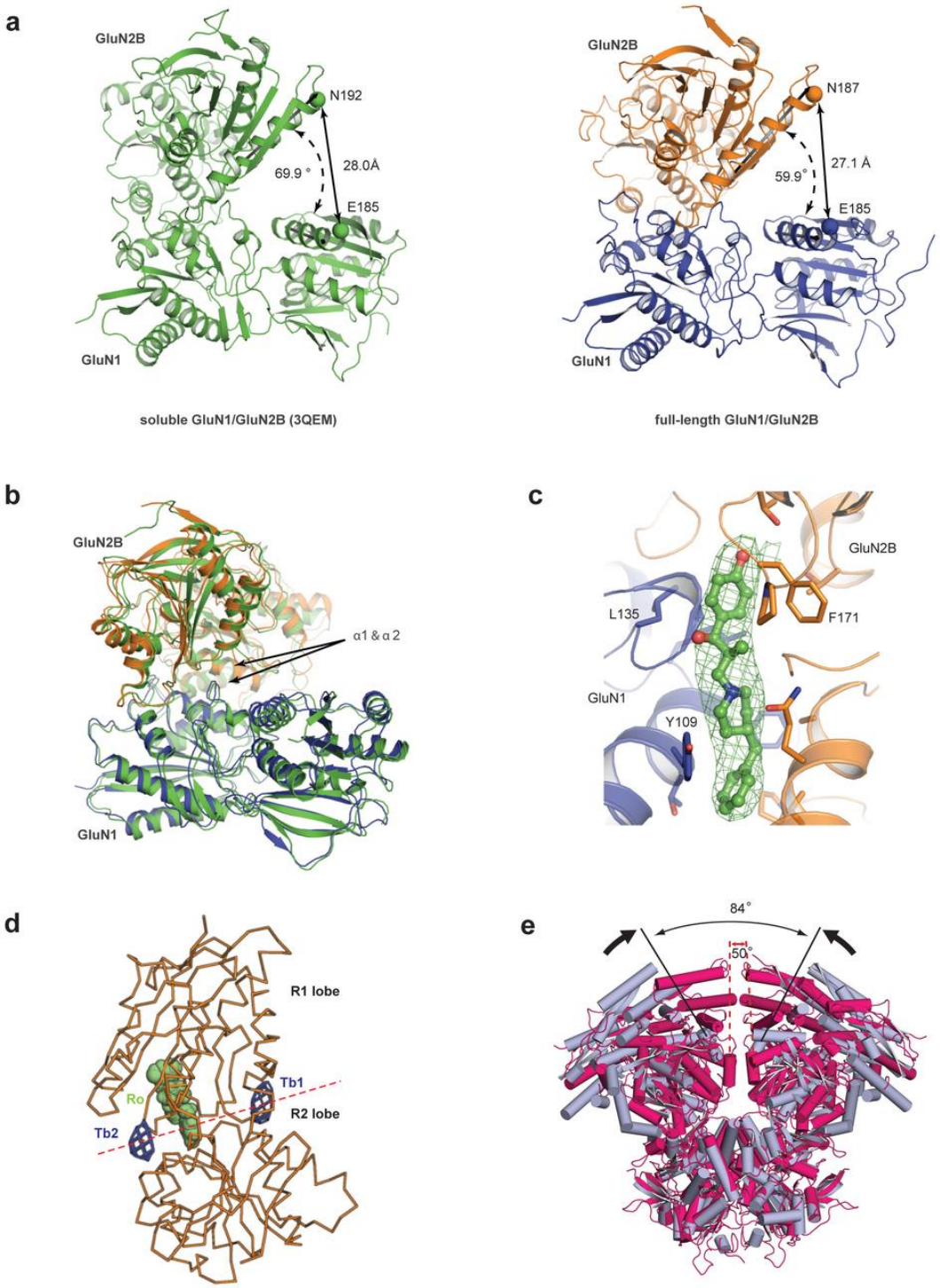


**Figure 3.7: Structural analyses and electron density maps of GluN1–GluN2B ATD heterodimer in the full-length NMDA structure.**

**a**, Intersubunit distance between the indicated marker atoms and angle of domain closure in the soluble ATD structure (PDB code: 3QEM, left panel) or full-length ATD structure (right panel, data set 1/structure 1). **b**, Superposition of the full-length GluN1 (blue)–GluN2B (orange) ATD heterodimer onto the soluble heterodimer structure (PDB code: 3QEM, light grey) by aligning the indicated helices (green) in the R1 lobe of GluN2B. **c**, $F_o$-$F_c$ omit electron density map for Ro25-6981 bound at the GluN1–GluN2B ATD heterodimer interface (chains A and B), contoured at 3 σ (data set 1/structure 1). **d**, Anomalous difference electron density of $Tb^{3+}$ (blue mesh) near the R1–R2 hinge of a single GluN2B ATD (chain B, data set 3/structure 3), contoured at 3.5 σ. **e**, Superposition of the LBD layer of the low resolution GluN1–GluN2B receptor (light blue, data set 4/structure 4) onto the LBD layer of the high resolution K216C receptor (magenta, data set 1/structure 1) illustrates the relative difference in ATD conformations between the two receptor structures (see Table 2). Shown is the most open conformation of the ATDs derived from one of the two independent receptors in the asymmetric unit of data set 4/structure 4.

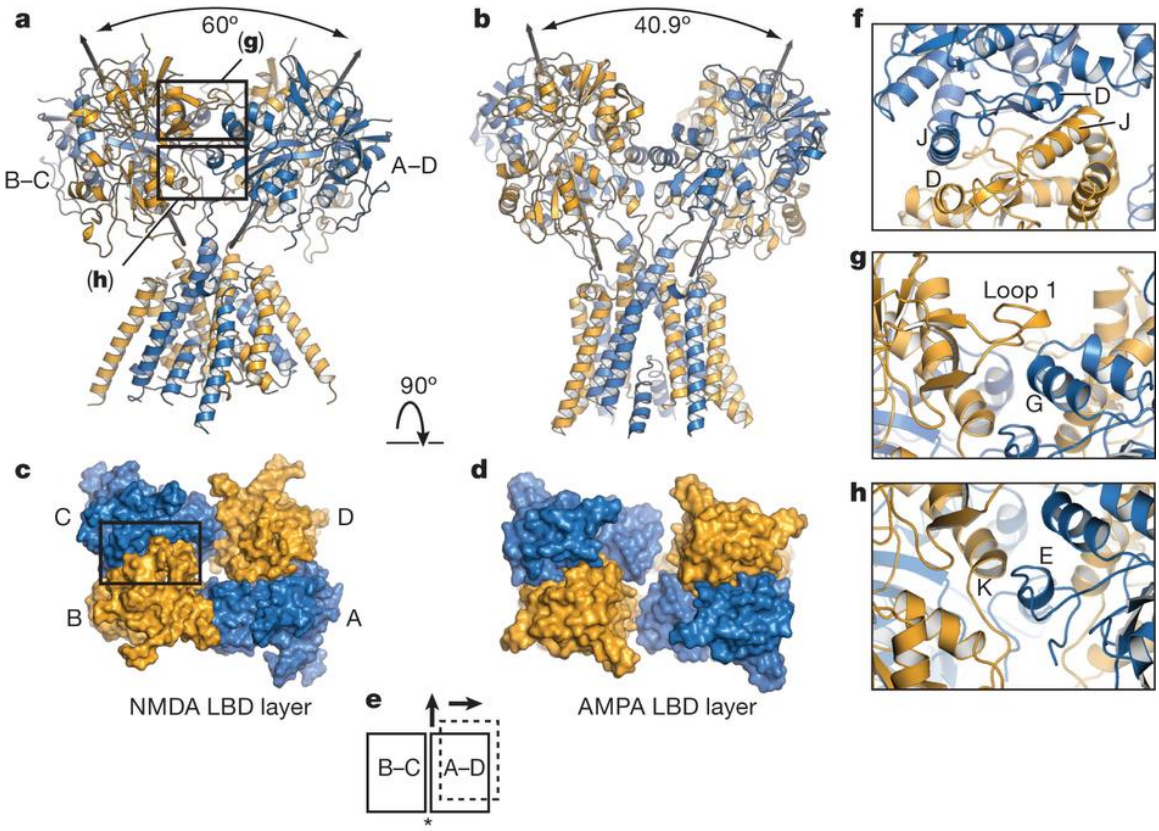


**Figure 3.8: LBD layer forms a ring-like structure.**

**a**, The GluN1–GluN2B LBD and TMD, showing that the pseudo twofold axes of the B–C and A–D LBD heterodimers diverge with an angle of 60°. The boxed areas define regions of LBD dimer–dimer contacts shown in panels **g** and **h**. **b**, View of the antagonist-bound state of the GluA2 AMPA receptor, which shows that the twofold axes of the LBD dimers diverge by an angle of 40.9°. **c**, View from the extracellular side of the membrane, along the overall twofold axis of the receptor, showing the LBDs of the GluN1 and GluN2B subunits, with the LBD heterodimer interface of the B–C subunits emphasized by a box. **d**, GluA2 LBD layer, illustrating how the interface between the B–C and A–D subunits has increased in comparison to the NMDA receptor LBD layer. **e**, Schematic of the LBD layer,

showing the NMDA receptor B–C and A–D heterodimers as rectangles (solid lines) and illustrating the translational shift of the A–D subunits in the AMPA receptor (dotted lines). The asterisk indicates the dimer–dimer interface. **f–h**, Close-up view of the canonical D1–D1 intradimer interface, together with views of the interactions at the interdimer interfaces in panels **g** and **h**. The domains from structure 2 are shown, with GluN1 subunits in blue and GluN2B subunits in orange.

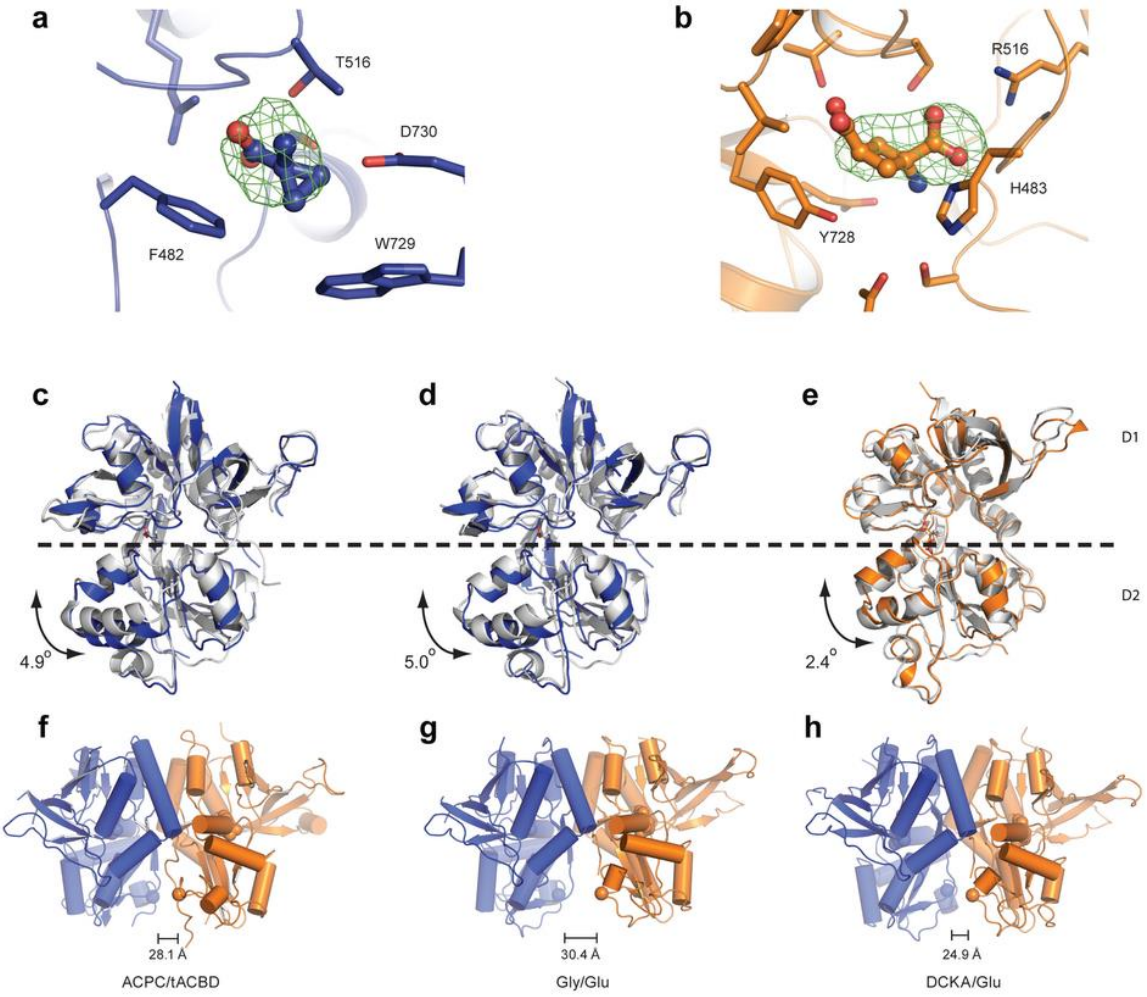


**Figure 3.9: LBD ligand electron densities and conformations.**

**a**, **b**, $F_o$-$F_c$ omit electron density maps for ACPC bound to GluN1 LBD (chain A) (**a**) and t-ACBD bound to GluN2B LBD (chain D) (**b**), contoured at 3 σ and 2.5 σ, respectively (data set 1/structure 1). **c**–**e**, Comparison of LBDs in the full-length GluN1–GluN2B structure to isolated structures by aligning the D1 lobe. The angle difference of beta strand 10 is indicated for each. **c**, The ACPC-bound GluN1 LBD of the full-length structure (structure 1 chain A, blue) is more open than the ACPC-bound isolated GluN1 LBD structure (PDB code: 1Y20, grey). **d**, The ACPC-bound GluN1 LBD of the full-length

receptor (structure 1 chain A, blue) is more open than the glycine-bound isolated GluN1 LBD structure (PDB code: 2A5T, chain A, grey). **e**, The t-ACBD-bound GluN2B LBD of the full-length structure (structure 1 chain D, orange) has a similar domain closure to the glutamate-bound isolated GluN2B LBD (PDB code: 2A5T, chain B, grey). **f**, GluN1–GluN2B LBD heterodimer (structure 1 chain A and D) from the full-length receptor showing the separation of the D2 lobes, measured using the α-carbon atoms of residues $Gly^{664}$ and $Gly^{662}$, respectively. **g**, **h**, Similar measurements as in **f** but using the equivalent residues in the context of the rat glycine/glutamate-bound isolated GluN1–GluN2A LBDs (PDB code: 2A5T) (**g**) or the rat DCKA/glutamate-bound isolated GluN1–GluN2A LBDs (PDB code: 4NF4) (**h**).

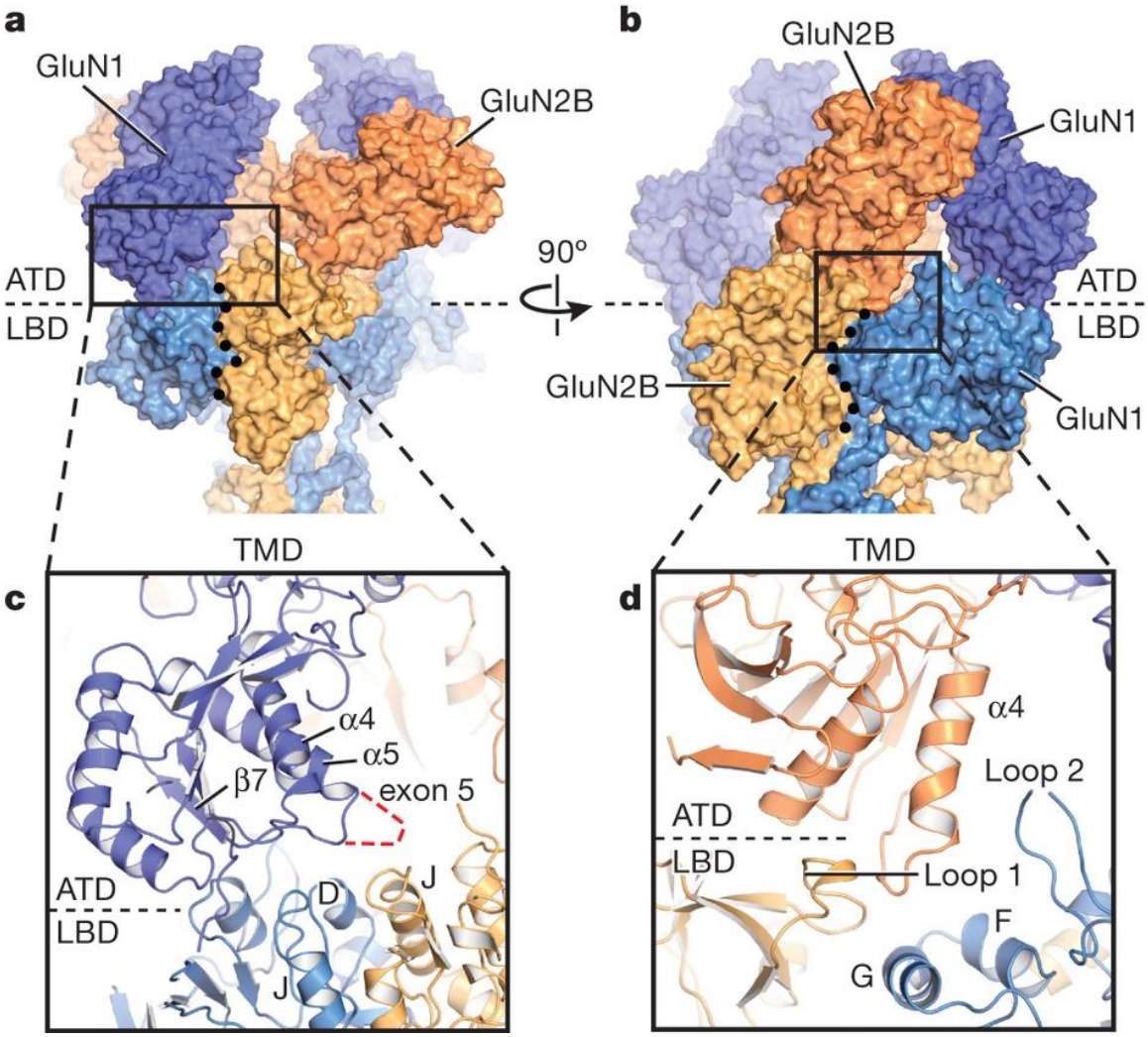


**Figure 3.10: The ATDs participate in extensive contacts with the LBD layer.**

**a**, **b**, Surface representation of the ATD and LBD domains, illustrating how the R2 lobe of the GluN1 subunit is poised above its cognate GluN1 LBD and also near the D1–D1 LBD dimer interface (**a**) and how the R2 lobe of the GluN2B subunit participates in contacts with its cognate GluN2B LBD, near an inter LBD dimer interface (**b**). **c**, **d**, Close-up views of potential interactions between the GluN1 R2 lobe and the GluN1 LBD (**c**) and between the GluN2B R2 lobe with regions on its GluN2B LBD (**d**). The GluN2B R2 lobe is also

near helices G and F and loop 2 of the GluN1 LBD. In **a** and **b**, the black dots define the approximate intra- and interdimer LBD interfaces, respectively. Structure 1 is shown in all panels.

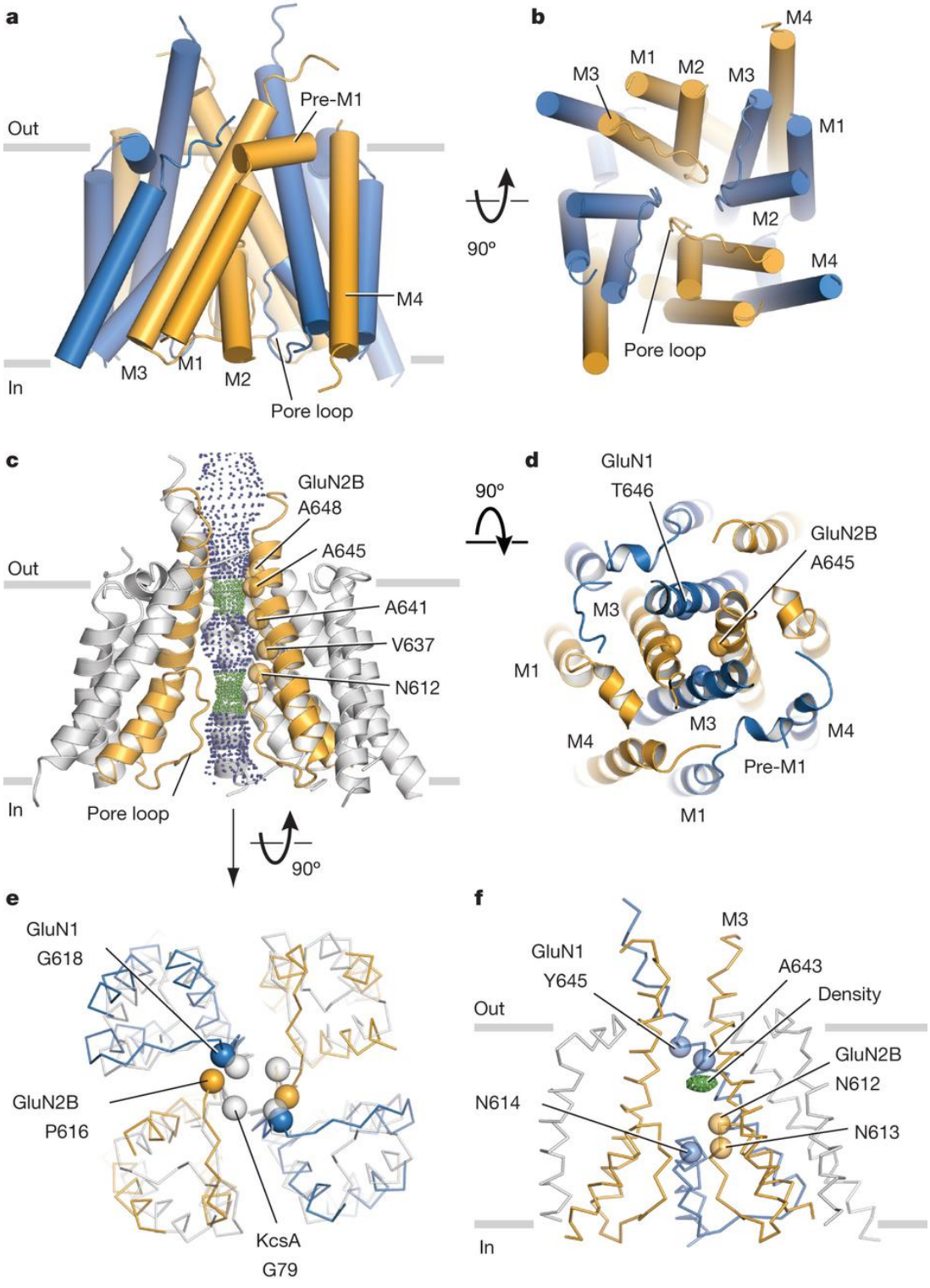


**Figure 3.11: Transmembrane domain architecture, symmetry and coupling to LBD.**

**a**, View of the TMD parallel to the membrane. GluN1 subunits are blue and the GluN2B subunits are orange. **b**, View of the TMD, along the pore axis, from the cytoplasmic side of the membrane. **c**, View of a solvent accessible surface carved along the pore axis using the computer program HOLE, parallel to the membrane, showing that the M3 bundle crossing near the extracellular side of the membrane and the entry into the selectivity filter region, from the central aqueous vestibule, form constrictions in the pore. Green dots indicate a pore radius of 1.15–2.3 Å and blue dots define a pore radius greater than 2.3 Å. Because a number of side chains are not included in the structure, due to the moderate resolution of the diffraction data, the size of the pore is approximate. **d**, View of the extracellular ends of the M3 helices of the NMDA receptor. We have highlighted as spheres the α-carbon atoms for residues Thr 646 and Ala 645 in the GluN1–GluN2B structure, respectively. The distances between neighboring atoms are 6.2, 8.0, 5.4 and 7.1 Å, starting from the α-carbon of GluN2B on the left and going clockwise. **e**, View of the intracellular ends of the TMD of the NMDA receptor in comparison with KcsA. Here the M2 helices of the NMDA receptor were superimposed on the corresponding helices in KcsA, showing the deviation from fourfold symmetry. **f**, Side view of the TMD showing a positive electron density feature (green mesh; 'density') in the central vestibule, calculated using $F_o$–$F_c$ coefficients and phases from the refined structure. The map is contoured at 2.8 σ. Data set 2 and structure 2 were used in all panels (Table 2).

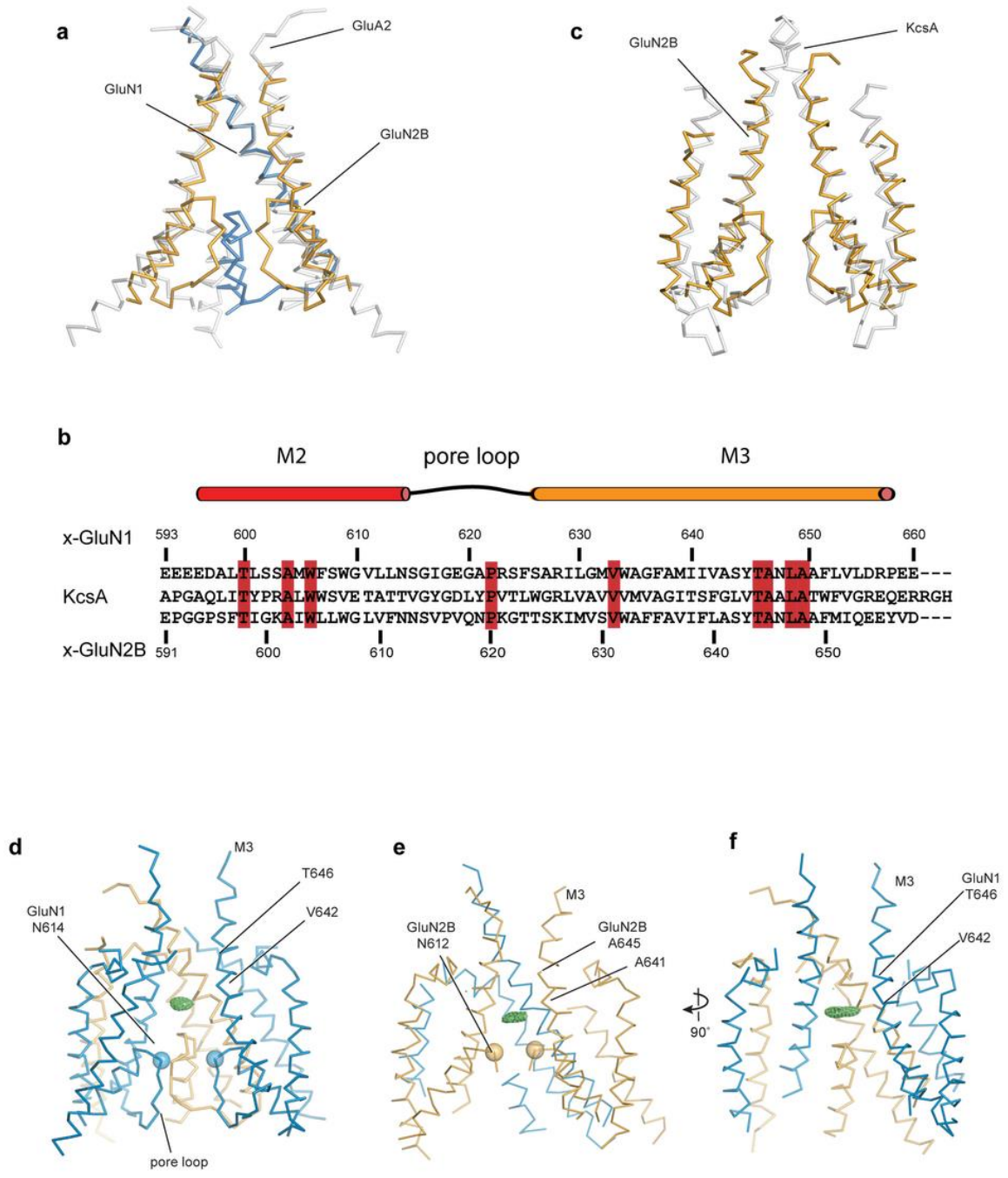


**Figure 3.12: Structural analyses of the transmembrane domain of NMDA receptor.**

**a**, Alpha-carbon superposition of the M3 helices of the GluN1–GluN2B NMDA receptor (structure 2) onto the corresponding M3 regions of GluA2 receptor (PDB code: 3KG2,

grey). The root mean square deviation (r.m.s.d.) is 1.89 Å for 144 aligned α-carbon atoms. The GluN1 subunits are blue and the GluN2B subunits are orange. **b**, Amino acid sequence alignment of the NMDA receptor and the KcsA channel in the M2 and M3 regions using Promals3D (http://prodata.swmed.edu/promals3d/). **c**, Superposition of the four M2 helices of the NMDA receptor onto the corresponding four M2 regions of the KcsA channel (PDB code: 1K4C; residues 61–75) [*210*]. The r.m.s.d. is 1.86 Å. Only chains B and D of the NMDA GluN2B subunits are shown. **d**, Residual electron density in the central vestibule. $F_o$-$F_c$ electron density in the central vestibule is shown for the GluN1–GluN2B receptor from data set 2/structure 2. For clarity, chain C is removed. **e**, $F_o$-$F_c$ electron density map in the central vestibule derived from data set 1/structure 1. For clarity, chain B is removed. **f,** The same electron density map as shown in panel **e** except that the structure has been rotated by ~90° around the pore axis and chain C of the GluN1 subunit has been removed for clarity. All maps are contoured at 2.8 σ.

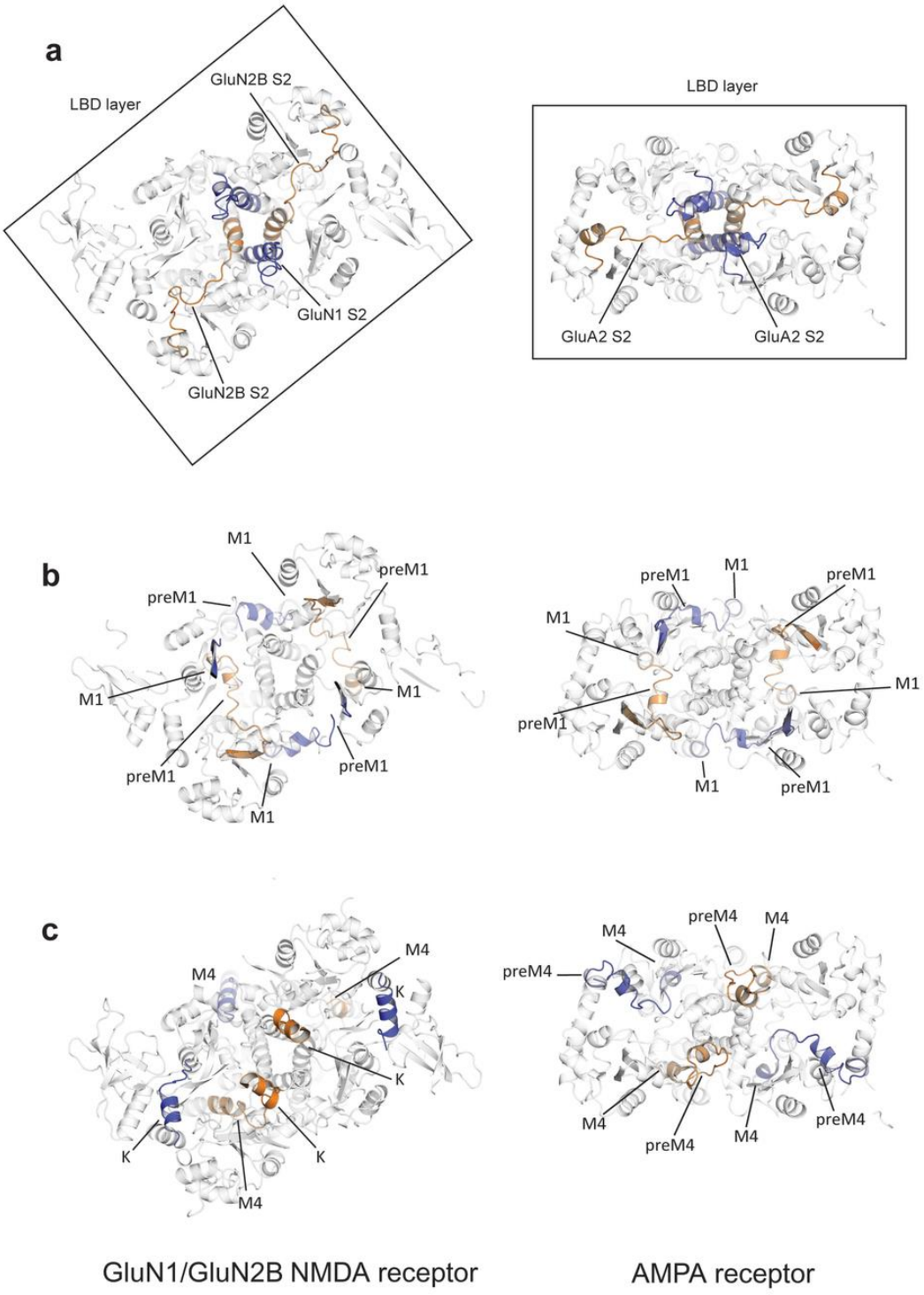


**Figure 3.13: Comparison of LBD layers and LBD–TMD linkers between the NMDA receptor and the GluA2 receptor structures.**

**a**, View from the extracellular side of the membrane of the connections between the TMD and LBD domains of the GluN1–GluN2B structure and of the GluA2 structure (PDB code: 3KG2), showing the relative rotation of GluA2 layer by ~35°. The S2 segment resides within the LBD. The LBD–M3 linkers are highlighted. **b**, The LBD–M1 linkers are highlighted. **c**, The LBD–M4 linkers are highlighted. Structure 1 are used in all panels.

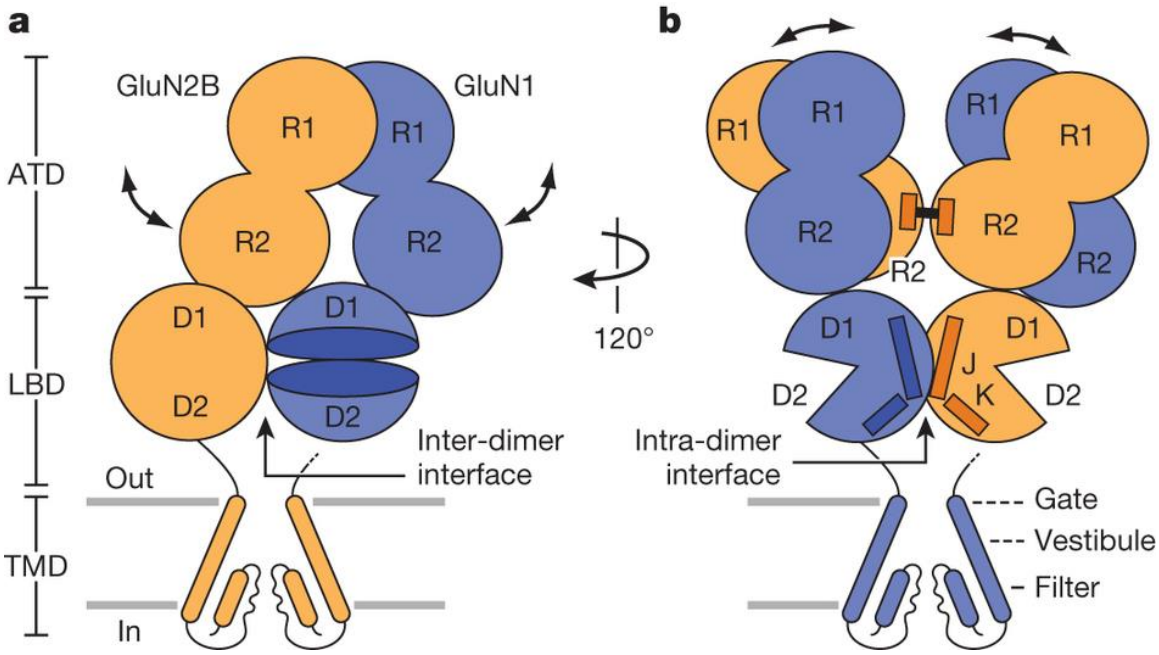


**Figure 3.14: Schematic of the NMDA receptor.**

**a**, Shown is a single ATD heterodimer, two LBD clamshells residing in different LBD heterodimers, and the TMD of GluN2B subunits, emphasizing only the M2, pore loop and M3 elements. The line connecting the M3 helix on the right is 'broken' to illustrate that it is connected to the GluN2B LBD behind the visible GluN1 LBD. Double-headed arrows suggest possible movements of ATDs within an ATD heterodimer. **b**, Rotation of the receptor schematic shown in panel **a** by ~120° showing two ATD heterodimers, a single LBD heterodimer and the TMD of GluN1 subunits. Double-headed arrows show conformational movements between ATD heterodimers observed in the structures described here. The α5 helices, harboring the K216C crosslink, are shown as rectangles at the R2–R2 interface. In both schematics, we emphasize how the R2 lobes of the ATDs are

positioned such they could modulate inter- and intradimer LBD interfaces and, in turn, the ion channel gate.

**a**

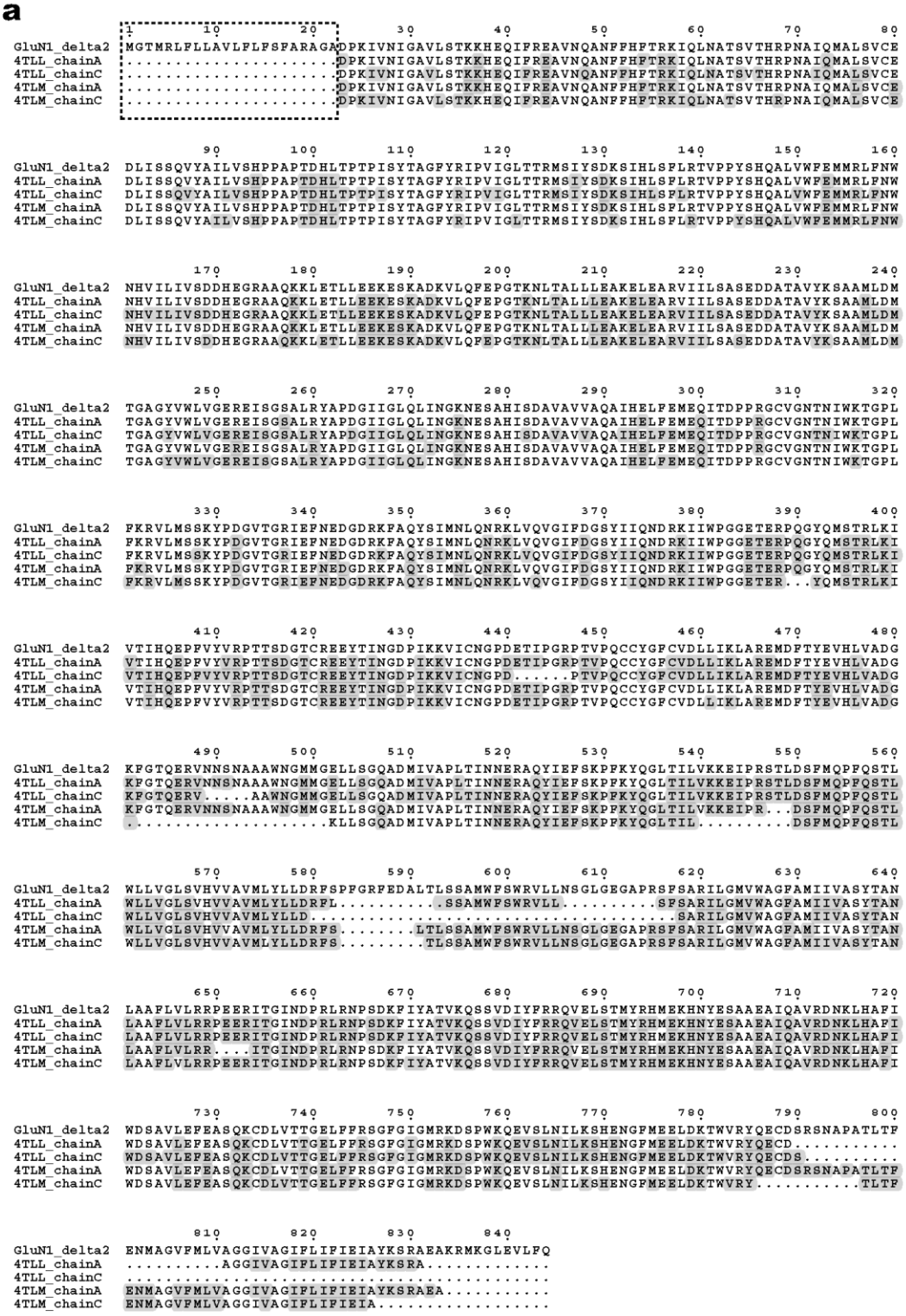
GluN1_delta2
4TLL_chainA
4TLL_chainC
4TLM_chainA
4TLM_chainC

**b**

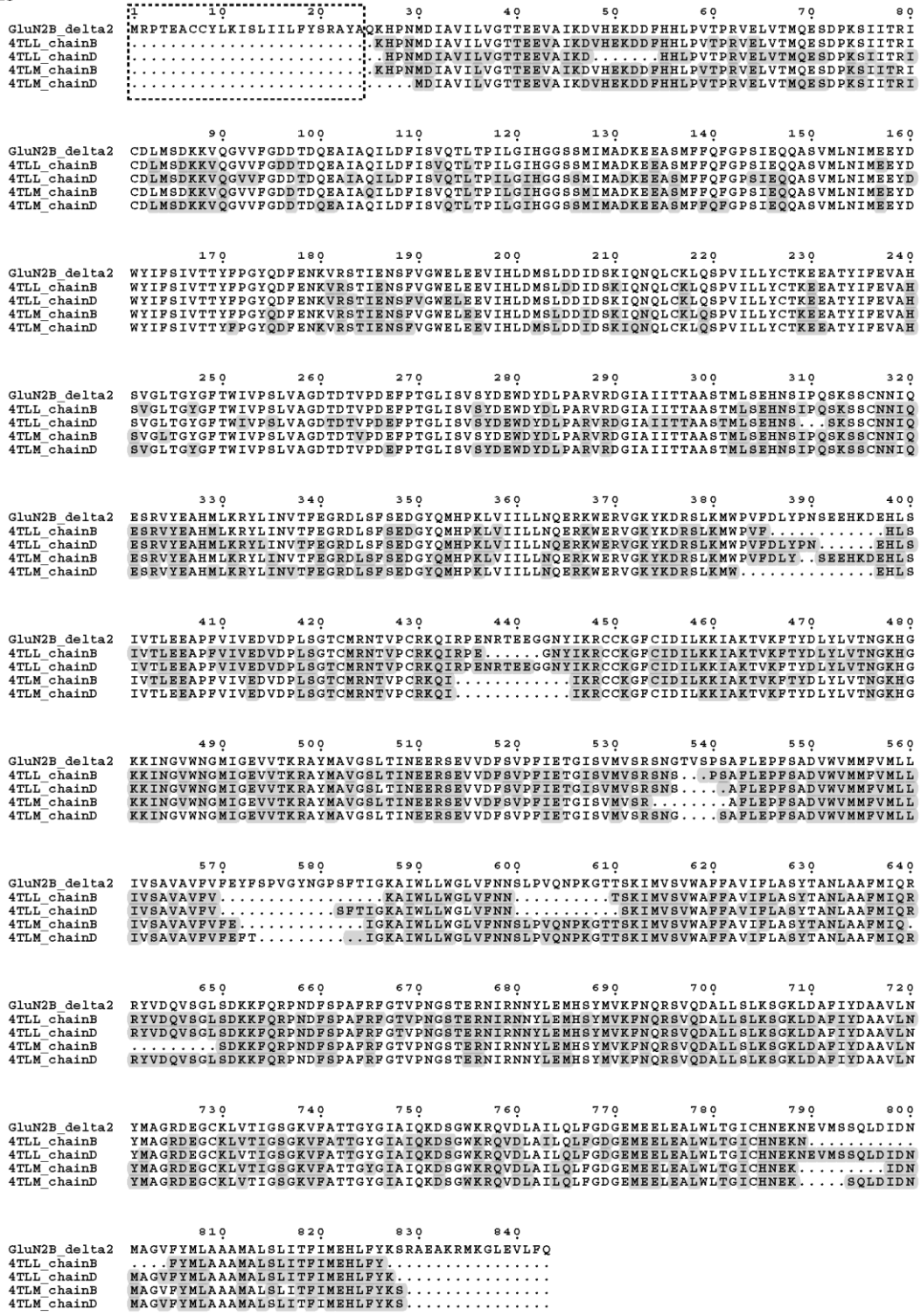
GluN2B_delta2
4TLL_chainB
4TLL_chainD
4TLM_chainB
4TLM_chainD

**Figure 3.15: Completeness of the structural models.**

**a**, The amino acid sequence of GluN1 Δ2 construct and the residues built in the structure 1 and 2. **b**, The amino acid sequence of GluN2B Δ2 construct and the residues built in the structure 1 and 2. The dash boxes highlight the signal peptides predicted by SignalP server (http://www.cbs.dtu.dk/services/SignalP/). The first residues in matured GluN1 and GluN2B are suggested to be Asp 23 and Gln 25, respectively. The LEVLPQ sequences in the C termini of GluN1 and GluN2B are residual residues of the 3C protease recognition site after cleavage. Resides that do not have clear density for their side chains are modeled as Ala (gray box).

# Tables

| | Basic GluN1 Δ construct | | Basic GluN2B Δ construct | |
|---|---|---|---|---|
| | **Residue substitutions** | **Purpose of mutation** | **Residue substitutions** | **Purpose of mutation** |
| | C22A | Remove a potentially reactive cysteine | M20S, G21R,C22A | Remove a potentially reactive cysteine and in so doing, change these three residues to their identities in the human GluN2B subunit |
| | K493A, K494A, E495A[‖] | Reduce surface entropy | A64E | Remove potential protease site |
| | G610R, I617L | Improve thermostability | ΔK382-V385 | Remove flexible regions |
| | N300Q, N350Q, N368D, N440D, N469D, N769E[§] | Remove predicted glycosylation sites | V615L | Improve thermostability |
| | D656R* | Promote desensitized conformation, improve thermostability and expression level | N69Q, N343D, T490V[§] | Remove predicted glycosylation sites |
| | residues 837-847 of AMPA (YKSRAEAKRMK; NP_058957) inserted at C-terminus[‡] | Improve thermostability and expression level | E654R, E655R* | Promote desensitized conformation, improve thermostability and expression level |
| | | | residues 837-847 of AMPA (YKSRAEAKRMK) inserted at C-terminus[‡] | Improve thermostability and expression level |
| | | | C585A | Remove a potentially reactive cysteine |

| **K216 (7.5 Å)** | **GluN1 Δ1:** Basic GluN1 Δ construct plus: | | **GluN2B Δ1:** Basic GluN2B Δ construct |
|---|---|---|---|
| | **Residue substitutions** | **Purpose of mutation** | |
| | E592A, E593A, E594A[‖] | Reduce surface entropy | |
| | G636L, M816Y | Improve thermostability and expression level | |
| | K741D | Improve expression level | |

| **K216C (3.7 Å)** | **GluN1 Δ2:** Basic GluN1 Δ construct plus: | | **GluN2B Δ2:** Basic GluN2B Δ construct plus: | |
|---|---|---|---|---|
| | **Residue substitutions** | **Purpose of mutation** | **Residue substitutions** | **Purpose of mutation** |
| | K51F, K52F | Improve crystal packing | K216C | Decrease flexibility |
| | ΔK588-E595 | Remove flexible regions | ΔR584-G593 | Remove flexible regions |

| **K216C ($Tb^{3+}$ complex 6.5 Å)** | **GluN1 Δ3:** Basic GluN1 Δ construct plus: | | **GluN2B Δ3:** Basic GluN1 Δ construct plus: | |
|---|---|---|---|---|
| | **Residue substitutions** | **Purpose of mutation** | **Residue substitutions** | **Purpose of mutation** |
| | K51F, K52F | Improve crystal packing | K216C | Decrease flexibility |
| | E592A, E593A, E594A[‖] | Reduce surface entropy | | |

| **TEVC** | **GluN1 Δ4:** Basic GluN1 Δ construct plus: | |
|---|---|---|
| | **Residue substitutions** | **Purpose of mutation** |
| | K51F, K52F | Improve crystal packing |
| | E592A, E593A, E594A[‖] | Reduce surface entropy |
| | G636L | Improve thermostability and expression level |
| | K741D | Improve expression level |

**Table 1: Constructs and mutations.**

*See ref. [*208*].

‡See ref. [*138*].

§Potential glycosylation sites predicted using the NetNGlyc 1.0 server (http://www.cbs.dtu.dk/services/NetNGlyc/).

‖ Sites identified for Surface Entropy Reduction approach using the SERp Server (http://services.mbi.ucla.edu/SER/).

| | Data set 1<br>GluN1 Δ2/GluN2B Δ2<br>Structure 1<br>ACPC/t-ACBD | Data set 2<br>GluN1 Δ2/GluN2B Δ2<br>Structure 2<br>ACPC/t-ACBD | Data set 3<br>GluN1 Δ3/GluN2B Δ3<br>Structure 3<br>Gly/Glu | Data set 4<br>GluN1 Δ1/GluN2B Δ1<br>Structure 4<br>ACPC/t-ACBD |
|---|---|---|---|---|
| **Data collection** | ALS 8.2.1 | ALS 8.2.1 | ALS 5.0.2 | ALS 5.0.2 |
| Space group | *C*2 | *C*2 | *C*2 | *C*222 |
| Cell dimensions a, b, c (Å) | 201.5, 117.3, 218.8 | 203.5, 118.4, 226.6 | 203.4, 118.2, 232.9 | 128.0, 616.2,152.3 |
| Cell angles α, β, γ (°) | 90.0, 106.7, 90.0 | 90.0, 103.8, 90.0 | 90.0, 104.3, 90.0 | 90.0, 90, 90.0 |
| Wavelength (Å) | 1.00 | 1.00 | 1.2 | 1 |
| Resolution (Å)* | 48.1-3.70 (3.80-3.70) | 48.7-3.90 (4.00-3.90) | 49.3 (6.67-6.50) | 50 (7.63-7.50) |
| Completeness* | 97.0 (94.5) | 97.4 (95.0) | 90.5 (80.1) | 99 (96.5) |
| Multiplicity* | 5.62 (3.36) | 3.44 (2.74) | 1.87 (1.53) | 6.2 (5.8) |
| I/σI* | 6.69 (2.13) | 7.46 (2.22) | 5.1 (1.27) | 31 (1.79) |
| $R_{meas}$ (%)* | 14.4 (48.6) | 11.0 (49.9) | 13.6 (55.8) | 14.0 (>100)† |
| $CC_{1/2}$ (%)* | 99.5 (48.9) | 99.7 (62.6) | 99.6 (16.7) | |
| Anisotropy (Å: a*/b*/c*)# | 3.5 / 3.5 / 3.9 | 3.5 / 3.5 / 4.8 | | |
| **Refinement** | | | | |
| Resolution (Å)‖ | 48.1-3.59 (3.66-3.59) | 30.0-3.77 (3.85-3.77) | | |
| Completeness (%) | 93.1 (56.4) | 83.2 (43.2) | | |
| No. of reflections | 53380 | 44017 | | |
| $R_{work}/R_{free}$ (%) | 28.2 (35.7) / 32.0 (39.6) | 26.8 (41.9) /31.0 (48.6) | | |
| No. of atoms total | 19991 | 20704 | | |
| Ligand | 124 | 124 | | |
| **Average *B*-factor (Å$^2$)** | | | | |
| Protein | 183 | 199 | | |
| Ligand | 133 | 113 | | |
| **R.m.s. deviations** | | | | |
| Bond lengths (Å) | 0.002 | 0.006 | | |
| Bond angles (°) | 0.636 | 1.384 | | |
| **Ramachandran plot** | | | | |
| Favored (%) | 95.1 | 94.2 | | |
| Allowed (%) | 4.8 | 5.6 | | |
| Disallowed (%) | 0.1 | 0.2 | | |

**Table 2: Crystallographic and structure refinement statistics.**

Data set 1 corresponds to the (GluN1 Δ2)–(GluN2B Δ2) structure at ~3.7 Å resolution. Data set 2 corresponds to the (GluN1 Δ2)–(GluN2B Δ2) structure at ~3.9 Å resolution. Data set 3 is derived from the $Tb^{3+}$-soaked crystals of the (GluN1 Δ3)–(GluN2B Δ3) construct. Data set 4 is corresponds to the low resolution (GluN1 Δ1)–(GluN2B Δ1) molecular replacement solution at 7.5 Å resolution. The LBD ligands are shown under the column headings. All crystallizations included Ro25-6981 and MK-801.

*Highest resolution shell in parentheses.

#Estimates of anisotropy calculated using the anisotropy server (http://services.mbi.ucla.edu/anisoscale/).

†$R_{sym}$ is reported.

‖ We scaled our diffraction data to 3.5 Å resolution for both data sets. However, due to crystal anisotropy and incompleteness at higher resolution, in the data collection section we reported the structures to be determined at 3.7 Å for the data set 1 and 3.9 Å for the data set 2, based on a cutoff of I/σI above 2. We used diffraction data to higher resolution (3.59 Å and 3.77 Å for the refinements against data set 1 and 2, respectively) because there was meaningful signal in the diffraction data used, as judged by map quality.

5% of reflections were used for calculation of $R_{free}$.

| ATD‡ | | sGluN1 (chain A; 3QEM) | sGluN2 (chain B; 3QEM) | GluN1 (chain A) | GluN1 (chain C) | GluN2B (chain B) | GluN2B (chain D) |
|---|---|---|---|---|---|---|---|
| | GluN1 (chain A) | 0.8 | 3.1 | - | 0.7 | 2.9 | 3.0 |
| | GluN1 (chain C) | 0.9 | 3.2 | 0.7 | - | 3.0 | 3.1 |
| | GluN2B (chain B) | 2.9 | 1.2 | 2.9 | 3.0 | - | 0.9 |
| | GluN2B (chain D) | 3.0 | 1.3 | 3.0 | 3.1 | 0.9 | - |

| | | sGluN1/sGluNB (dimer AB; 3QEM) | GluN1/N2B (dimer AB) | GluN1/N2B (dimer CD) |
|---|---|---|---|---|
| | GluN1/N2B (dimer AB) | 1.1 | - | 0.9 |
| | GluN1/N2B (dimer CD) | 1.2 | 0.9 | - |

| LBD§ | | GluN1+ACPC (chainC) | sGluN1+gly (chain A; 2A5T) | sGluN1+ACPC (1Y20) |
|---|---|---|---|---|
| | GluN1+ ACPC (chainA) | 0.98 | 1.2 | 1.3 |
| | GluN1+ ACPC (chainC) | - | 1.3 | 1.2 |
| | sGluN1+ gly (chain A; 2A5T) | 1.3 | - | 0.7 |
| | sGluN1+ ACPC (1Y20) | 1.2 | N.D.[‖] | - |

| | | GluN2B+tACBD (chainD) | sGluN2A+Glu (chain B; 2A5T) |
|---|---|---|---|
| | GluN2B+ tACBD (chainB) | 1.0 | 1.3 |
| | GluN2B+ tACBD (chainD) | - | 1.3 |
| | sGluN2A+ Glu (chain B; 2A5T) | 1.3 | - |

**Table 3: ATDs and LBDs r.m.s.d.**

The r.m.s.d. were calculated using coot SSM superpose function, unit is Å .

‡r.m.s.d. values were determined from superpositions of indicated ATD of the full-length structure 1 (GluN1, GluN2B) and of soluble ATDs (sGluN1 or sGluN2B) onto full-length structure ATDs. PDB codes for the soluble domains as indicated.

§r.m.s.d. values determined from superpositions of indicated LBDs of the full-length structure 1 (GluN1, GluN2B) and of soluble LBDs (sGluN1 or sGluN2B) onto full-length structure LBDs. PDB codes for the soluble domains as indicated.

‖ N.D., not determined.

# Chapter 4

## Concluding remarks

The GluN1–GluN2B receptor structures (**chapter 3**) agree well with the biochemical data from the ATD crosslinking experiments (**chapter 2**). The GluN1 Cys 79, GluN1 Cys 308 and GluN2B Lys 74 (Lys 79 of rat GluN2B) are in close proximity around the R1–R1 interface (Fig. 4.1), in tune with the notion that rat GluN2B K79C could crosslink with either rat GluN1 Cys 79 or Cys 308 [*133*].

In this chapter, on the basis of the full-length GluN1–GluN2B receptor crystal structures, I will discuss allosteric modulation and gating mechanisms of the NMDA receptor. Information from the most recent studies of iGluRs, including new structures of the GluA2, GluK2, and GluN1–GluN2B receptors, are incorporated into the discussion [*212–215*]. I will also suggest future directions for research that may advance our knowledge of not only the NMDA receptor but also the iGluR family in general.

## Comparison of the available NMDA receptor structure

While our manuscript was in press, Karakas and Furukawa reported a crystal structure of rat GluN1–GluN2B NMDA receptor in complex with ifenprodil, glycine and glutamate at 4 Å resolution [*215*]. Similar to our approach, Karakas and Furukawa also introduced disulfide crosslinks to stabilize the receptor and to improve the crystal diffraction quality. In their structure, three pairs of cysteines were engineered. The first pair lies between the ATDs of two GluN2B subunits, in a region close to the K216C of our crystallization constructs. The second and third pairs are between GluN1 M1–GluN2B M4 helices and between GluN2 M4–GluN2B M1 helices, respectively. Consistent with our result, Karakas

and Furukawa also found that crosslinks in the ATD appear to lock the receptor in an inhibited state [*215*].

The structure presented by Karakas and Furukawa is generally in agreement with our structures. By comparing Karakas and Furukawa's structure (PDB code: 4PE5) and our structures (PDB code: 4TLL and 4TLM), the root mean square deviations of Cα atoms for the structures of the GluN1–GluN2B ATD heterodimer, the GluN1–GluN2B LBD heterodimer, and the TMD tetramer are estimated to be 1.4 Å , 1.6 Å and 2.5 Å , respectively. The higher deviation in the TMDs may be due to the two additional engineered crosslinks in Karakas and Furukawa's structure or the intrinsic uncertainty of model building for structures determined at 3.7–4 Å resolution. It is also possible that the subtle differences in the TMD conformation reflect the different ligands used in the two studies.

Despite the overall similarity, our structures provide a more comprehensive description of the pore loops of the TMD. Likely due to the higher resolution of our data, we were able to trace the polypeptide chain for most of the pore loops. Pore loops form the selectivity filter of the NMDA receptor and define the region governing ion permeation and magnesium block. We showed that the asparagine residues (NSGIG in GluN1; NNSVP in GluN2B) are located in the entrance of the selectivity filter, a plausible position to interact with permeant ions and channel blockers [*216*]. Consistent with our structure, previous studies indicated that these asparagine residues are crucial for calcium flux and the sensitivities to $Mg^{2+}$ and the pore blocker MK-801 [*110, 111, 45, 46*]. Although the detailed side chain orientations cannot be pinpointed due to the limitation in resolution, as an approximate estimate the GluN1 asparagine (NSGIG) and the second GluN2B asparagine (NNSVP) of the pore loop perhaps form the narrowest region of the filter, a

conclusion that has also been reached by researchers using electrophysiological experiments coupled with site-directed mutagenesis [*217*, *218*]. Our structures thus provide the first structural glimpse into mechanisms of ion conduction and channel blockers in the iGluR family, even though structures with higher resolution are inevitably required to understand the basis of ion transport.

GluN2B Ser 616 (Ser 633 of rat GluN2B) is an important determinant of $Mg^{2+}$ block, $Ca^{2+}$ permeability, and single-channel conductance of the NMDA receptor [*66*]. Siegler Retchless *et al.* used the structural information of the NaK channel to derive a homology model of the NMDA receptor pore, which suggested that Ser 616 of the GluN2B M3 helix is in the proximity of two tryptophan residues, Trp 598 and Trp 601, of the GluN1 M2 helix. Mutant cycle analyses from the same study showed that GluN2B Ser 616 interacts with GluN1 Trp 598, but not GluN1 Trp 601 [*66*]. The X-ray structure presented here indicates that GluN2B Ser 616, GluN1 Trp 598, and GluN1 Trp 601 are indeed near each other, although we found that GluN2B Ser 616 may be closer to GluN1 Trp 601 than to Trp 598 (structure 2; $C_\beta$ distances: ~4.7 and ~8.8 Å , respectively).

## Implications for the gating mechanism

### Subunit non-equivalence

Several lines of evidence suggest that the GluN1 and GluN2B subunits do not contribute equivalently to gating. First, putting constraints on the GluN1 LBD–TMD linkers by cysteine crosslinks only decreased the open probability by 2-fold, whereas similar constraints on the linkers of the GluN2 subunit reduced the open probability by 62-

fold [*219*]. Second, based on single-channel recordings, the rate constants estimated from a proposed kinetic scheme suggest that constraints on either GluN1 or GluN2 LBD–TMD linkers slowed down the channel opening rate, but constraints on the GluN2 had a notably more pronounced effect. The same scheme also suggested that, after agonist binding, the gating machinery of GluN1 and GluN2 move asynchronously [*219*]. Third, the time course of current decay, caused by washing off both GluN1 and GluN2B agonists, resembles the course of GluN2B ligand unbinding rather than that of GluN1 ligand unbinding [*220*]. Fourth, mutations in the SYTANLAAF motif of GluN1 result in a receptor that can be opened with just the GluN2 agonist, bypassing the requirement of a co-agonist. However, a receptor bearing equivalent GluN2 mutations still requires both GluN1 and GluN2 agonists for channel opening [*220*]. Fifth, mutations in the SYTANLAAF motif of GluN1 and GluN2 seem to preferentially affect different closed states [*221*]. Finally, single glycine insertions into either the GluN1 or GluN2 M3–S2 linker, a region responsible for direct mechanical coupling between ligand binding and channel opening, attenuate activation of the receptor and reduce the open probability [*127*], but insertion into the GluN2 subunit displays a 4.5-fold greater reduction. Kazi *et al.* concluded that the GluN2 subunit moves earlier and transduces more energy than the GluN1 subunit [*127*].

Our structures support the notion that GluN1 and GluN2 are non-equivalent. We showed that GluN1 and GluN2B subunits adopt very different conformations, especially with respect to the orientation of ATDs and LBDs (Fig. 4.2), even though GluN1 and GluN2B share a sequence similarity of ~53 %. Moreover, there are notable differences in the GluN1 and GluN2 LBD–TMD linker, an element essential for the mechanical coupling between agonist binding and channel opening. Although the structures we presented are

snapshots along the gating pathway, given the large conformational distinction observed, it seems plausible to infer that, during activation, GluN1 and GluN2 subunits undergo divergent movements to open the ion channel pore. In harmony with this idea, Sobolevsky *et al.* hypothesized that upon agonist binding in the GluA2 AMPA receptor, the movement in B–D subunits (analogous to GluN2 subunits in the NMDA receptor) is greater than those in A–C subunits (analogous to GluN1 subunits) [*138*]. By comparison of the $GluA2_{cryst}$ and isolated GluA2 LBD structures, Pro 632 on the LBD–TMD linker of the B–D subunit is predicted to move ~7 Å but the equivalent residue of the A–C subunit moves only ~4 Å. Chen *et al.* recently also proposed that for channel activation of the GluA2 receptor, conformational changes in the M3 helices of the B–D subunits play a more prominent role than those in the A–C subunits [*213*]. Furthermore, Meyerson *et al.* analyzed the activation and desensitization states of the GluA2 receptor, and compared them with the desensitization state of the GluK2 kainate receptor [*214*]. These cryo-electron microscopy (cryo-EM) structures showed that the D1 lobes of the LBD move downward by ~10 Å in A–C subunits but only ~4 Å in B–D subunits during receptor activation. For desensitization, the LBDs of B–D subunits undergo a larger rearrangement than that of A–C subunits in the GluK2 kainate receptor [*214*, *222*]. Thus, structural and functional non-equivalences of subunits are a common and essential characteristic of the iGluR family.

**Dynamics of the extracellular domains**

Previous studies have highlighted the significance of structural rearrangements within LBDs and ATDs during the gating cycle. In the LBD layer, agonists induce closure of the

LBD clamshells and remodeling of intradimer interfaces [*124*, *128*, *223*], which leads to channel activation. In the ATD layer, spontaneous hinge-bending motions and/or lobe rotations of GluN1 and GluN2 ATDs impact receptor gating as well as pharmacological properties [*64*, *164*, *203*].

In contrast, global movements "between" domains have not been studied extensively, most likely because the questions surrounding the arrangements of the domains hinder experimental designs. We found that the ATDs are very flexible in the full-length receptor. The ATD dimer can rotate and the two ATD dimer assemblies could move "close" to each other (Fig. 4.3a). If the two pairs of ATD dimers are "glued" together by disulfide-crosslinks and thus restricted in their mobility, the channel activity is significantly reduced [*215*, *216*], suggesting this "inter-dimer" movement is functionally relevant for receptor activation. A similar phenomenon has also been observed in the kainate receptor [*160*]. But how does this ATD motion affect the ion channel pore? We found that in response to the ATD motion, the LBD dimers also move relative to each other, resulting in the rearrangement of the LBD ring (Fig. 4.3b). Therefore the conformational changes in ATDs are coupled to the reorganization of LBDs and the signal could, in turn, propagate to LBD–TMD linkers and the pore.

When the ATD dimers are crosslinked, the dimer-dimer interactions between the LBDs are stronger and the LBD ring is more compact. The detailed correlation between the interdimer movement in LBDs and channel gating is not yet fully understood, but since the ATD-crosslinked mutant locks the NMDA receptor in a low activity state, we speculate that when LBD ring is tightly packed, the pore cannot open. Similarly, Dürr *et al.* showed that in the AMPA receptor, the transition from the apo to the active state is accompanied

by an "expansion" of the LBD ring [*212*]. Meyerson *et al.* observed an expansion of the LBD ring when comparing the antagonist-bound and agonist-bound states of the GluA2 receptor [*214*]. Chen *et al.* also found that the cone snail toxin con-ikot-ikot potentiates the AMPA receptor by stabilizing the LBD ring in an expanded conformation [*213*]. Interestingly, desensitization in AMPA and kainate receptors involves a corkscrew motion of the LBDs, shifting the two-fold symmetric LBD ring towards a quasi-four-fold arrangement [*212, 214, 222*]. Whether a similar mechanism exists in the NMDA receptor is an open question.

## Putative $Ca^{2+}$ modulation sites on the NMDA receptor

The NMDA receptor is subject to modulation by heavy metal ions. Cations bind to the channel pore and block the current in a voltage-dependent manner. Furthermore, magnesium, calcium, nickel, copper, zinc, cadmium, lead and lanthanum ions also interact voltage-independently with the NMDA receptor [*83, 201, 224–228*]. The voltage-independence suggests that, in addition to the pore, these ions also bind to modulatory sites located in the extracellular domains of the NMDA receptor. The binding site of $Zn^{2+}$ has been studied in atomic detail using the isolated GluN2B ATD, but whether a full-length, intact NMDA receptor possesses additional $Zn^{2+}$ sites is unknown. The binding sites of other ions also have not been mapped to specific residues of the receptor.

We have used $Tb^{3+}$ to probe potential ion binding sites in the NMDA receptors. Because of its comparable ionic radius and coordination properties to those of $Ca^{2+}$, $Tb^{3+}$ has been widely used to probe calcium binding [*229*]. We were able to locate two sites

(Tb1 and Tb2) in the ATD that may serve as $Ca^{2+}$ binding pockets. Recent experiments showed that physiological concentrations of $Ca^{2+}$ can alter the NMDA receptor gating and reduce the channel open probability [*228*]. The possibility that $Ca^{2+}$ interacts with the ATD to allosterically influence the receptor is reminiscent of the effect of $Zn^{2+}$ on the NMDA receptor. This finding also reinforces the importance of the ATD as a modulatory domain under physiological conditions. Additionally, Karakas and Furukawa have identified another potential $Ca^{2+}$ binding site in the LBD–TMD linker by using holmium and gadolinium ions [*215*]. Further experiments are necessary to understand the relative contributions of these sites to $Ca^{2+}$ modulation.

## Perspectives

The ~3.7 Å crystal structures of NMDA receptors provide unprecedented views of the subunit arrangement, pore architecture and a dynamic picture of the intact receptor. Future structures based on higher resolution data, however, are necessary not only to reconstruct a more accurate model of the TMD, but also to define the chemistry of ion coordination and pore blocker recognition. Moreover, the conformational changes during channel activation and desensitization remain to be decrypted. To study the structural mechanism of activation, the inclusion of positive modulators such as polyamines [*230*] and PYD-106-like compounds [*97*] may help to stabilize the activated state. Conformation-specific antibodies that lock the receptor in an activated state could also be used to increase the conformational homogeneity of the receptor. Another strategy is to incorporate mutations into crystallization constructs which increase the channel open probability. Similar

approaches have been applied to GluA2 AMPA receptor to stabilize the activated state, but the structures either maintain a closed ion channel pore [*212*, *213*], or were not determined at sufficient resolutions to define the conformation of the pore [*214*]. While these studies suggest that capturing iGluRs in fully activated states seems to be more difficult than anticipated, it remains to be explored if studies on the NMDA receptor will have the same struggle.

Likewise, ligands, antibodies or mutations can be screened to stabilize the desensitized state to help the structure determination of the NMDA receptor in desensitization. In any case, the construct optimization strategy, purification protocol and structures presented in this thesis will provide a useful guide for future experiments.

Recent advances in cryo-EM single-particle analysis have led to a revolution in structural biology. The development of direct electron detectors and new image processing algorithms aiming to correct beam-induced motions has made it possible to obtain near-atomic resolution structures of relatively small proteins, smaller than 0.5 MDa [*231*]. In 2013, Liao *et al.* determined a 3.4 Å cryo-EM structure of the rat TRPV1 ion channel (~0.3 MDa) [*232*]. After one year, the cryo-EM structures of the human γ-secretase (~0.17 MDa) and the *Escherichia coli* β-galactosidase (~ 0.47 MDa) were solved at 4.5 Å and 3.2 Å, respectively [*233*, *234*]. The glutamate receptors have a suitable size for cryo-EM single-particle analysis and the homogenous protein sample of the GluN1–GluN2B NMDA receptor presents a promising candidate for cryo-EM specimen. By applying cryo-EM to the NMDA receptor, we may be able to capture conformations that are recalcitrant to crystallization, thus filling in the "missing" conformational states. Integrating

crystallography and cryo-EM would therefore help us further push the boundaries of our understanding in the glutamate receptor.

## Figures and legends

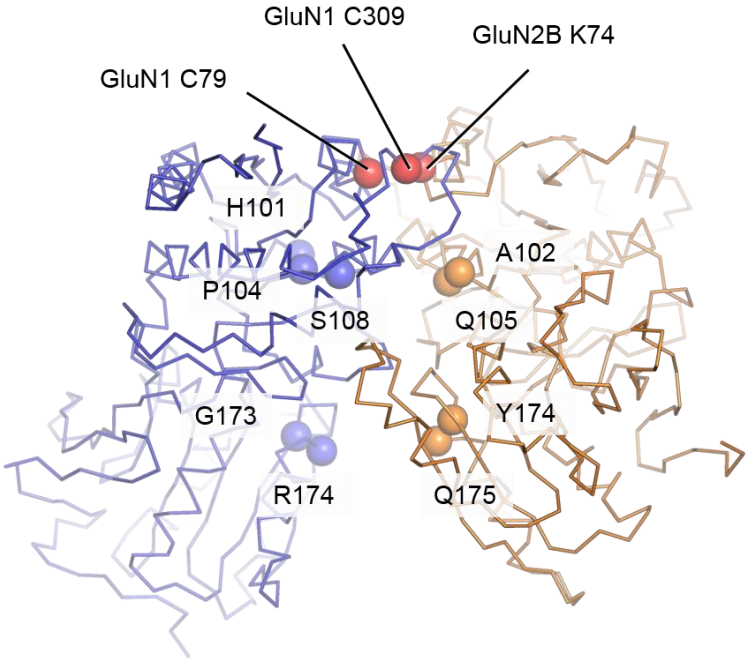


**Figure 4.1: ATD residues studied in chapter 2 map to the structure presented in chapter 3.**

GluN2B K74 (or the equivalent residue in GluN2A), when mutated to Cys, can form crosslinks with either GluN1 C79 or GluN1 C309 (**chapter 2**). Resides studied in chapter 2 are highlighted as spheres. Structure 1 (**chapter 3**) is shown. For clarity, only chain A and C are drawn

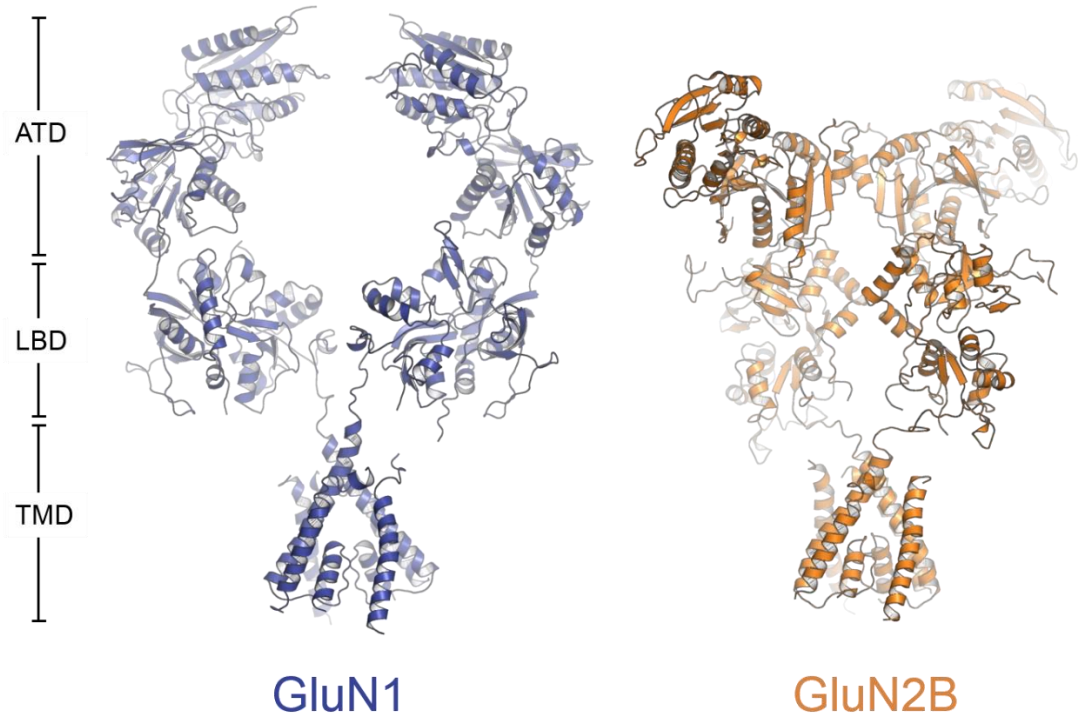


**Figure 4.2: Subunit non-equivalence of the NMDA receptor.**

View of the two subunits, parallel to the membrane, with the GluN1 subunits in blue and the GluN2B subunits in orange. The subunits are aligned so that the TMD of GluN1 and GluN2B subunits are in the same orientation, showing the dramatic difference between GluN1 and GluN2B in the extracellular domains and the LBD–TMD linkers. Structure 2 (**chapter 3**) is shown.

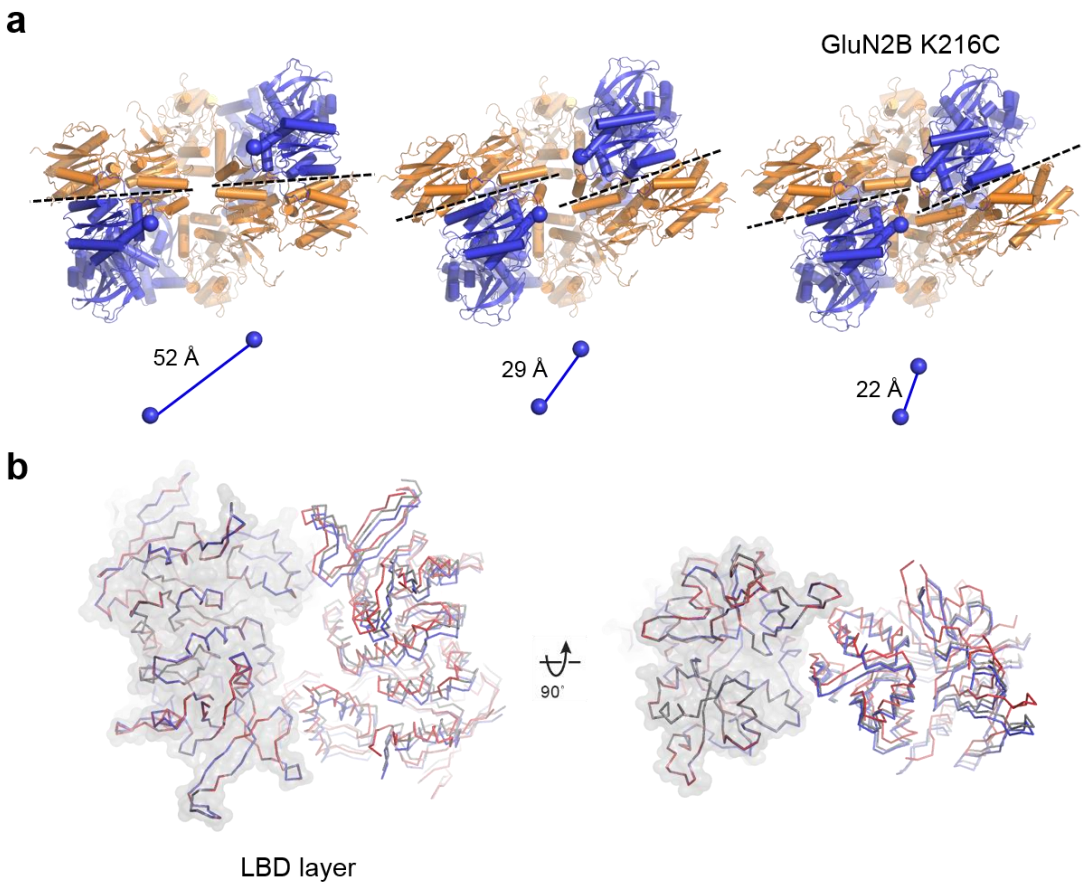


**Figure 4.3: ATD and LBD dynamics of the NMDA receptor.**

**a**, The ATD and LBD layers viewed from the extracellular side of the membrane and showing the relative location of the underlying LBD layer. Left panel, the most "open" conformation of the ATDs derived from structure 4 (see table 1 of **chapter 3**). Middle panel, the other conformation of the ATDs observed in the other tetramer present in structure 4. Right panel, the "closed" conformation of the ATDs observed in structure 1 (**chapter 3**, GluN2B K216C). The dashed line roughly defines the ATD intradimer interface. The α-carbon atoms of Glu 297 in the GluN2B ATDs are highlighted as spheres to illustrate changes in the separation of the ATD dimers. **b**, An overlay of the LBD layers

from the three conformations in **a**. One LBD dimer was used for superposition (surface representation). The motions in the other LBD dimer thus emphasize the conformational changes in the LBD ring. Grey, blue and red ribbons correspond to the left, middle, and right conformation in **a**, respectively.

# References


1. E. M. Tansey, Not committing barbarisms: Sherrington and the synapse, 1897. *Brain Res. Bull.* **44**, 211–212 (1997).

2. E. S. Valenstein, The discovery of chemical neurotransmitters. *Brain Cogn.* **49**, 73–95 (2002).

3. B. S. Meldrum, Glutamate as a Neurotransmitter in the Brain: Review of Physiology and Pathology. *J. Nutr.* **130**, 1007S–1015S (2000).

4. M. Hollmann, S. Heinemann, Cloned glutamate receptors. *Annu. Rev. Neurosci.* **17**, 31–108 (1994).

5. R. Dingledine, K. Borges, D. Bowie, S. F. Traynelis, The glutamate receptor ion channels. *Pharmacol. Rev.* **51**, 7–61 (1999).

6. S. F. Traynelis *et al.*, Glutamate receptor ion channels: structure, regulation, and function. *Pharmacol. Rev.* **62**, 405–496 (2010).

7. P. Paoletti, C. Bellone, Q. Zhou, NMDA receptor subunit diversity: impact on receptor properties, synaptic plasticity and disease. *Nat. Rev. Neurosci.* **14**, 383–400 (2013).

8. H. Furukawa, Structure and function of glutamate receptor amino terminal domains. *J. Physiol.* **590**, 63–72 (2012).

9. J. Kumar, M. L. Mayer, Functional insights from glutamate receptor ion channel structures. *Annu. Rev. Physiol.* **75**, 313–337 (2013).

10. P. J. O'Hara *et al.*, The ligand-binding domain in metabotropic glutamate receptors is related to bacterial periplasmic binding proteins. *Neuron.* **11**, 41–52 (1993).

11. N. Nakanishi, N. A. Shneider, R. Axel, A family of glutamate receptor genes: Evidence for the formation of heteromultimeric receptors with distinct channel properties. *Neuron.* **5**, 569–581 (1990).

12. Y. Stern-Bach *et al.*, Agonist selectivity of glutamate receptors is specified by two domains structurally related to bacterial amino acid-binding proteins. *Neuron.* **13**, 1345–1357 (1994).

13. M. W. Wood, H. M. VanDongen, A. M. VanDongen, Structural conservation of ion conduction pathways in K channels and glutamate receptors. *Proc. Natl. Acad. Sci. U. S. A.* **92**, 4882–4886 (1995).

14. Z. Galen Wo, R. E. Oswald, Unraveling the modular design of glutamate-gated ion channels. *Trends Neurosci.* **18**, 161–168 (1995).

15. G. Q. Chen, C. Cui, M. L. Mayer, E. Gouaux, Functional characterization of a potassium-selective prokaryotic glutamate receptor. *Nature*. **402**, 817–821 (1999).

16. D. R. Curtis, J. W. Phillis, J. C. Watkins, Actions of aminoacids on the isolated hemisected spinal cord of the toad. *Br. J. Pharmacol. Chemother.* **16**, 262–283 (1961).

17. D. R. Curtis, J. C. Watkins, Analogues of glutamic and gamma-amino-n-butyric acids having potent actions on mammalian neurones. *Nature*. **191**, 1010–1011 (1961).

18. G. A. Johnston, D. R. Curtis, J. Davies, R. M. McCulloch, Spinal interneurone excitation by conformationally restricted analogues of L-glutamic acid. *Nature*. **248**, 804–5 (1974).

19. J. C. Watkins, R. H. Evans, Excitatory amino acid transmitters. *Annu. Rev. Pharmacol. Toxicol.* **21**, 165–204 (1981).

20. J. W. Johnson, P. Ascher, Glycine potentiates the NMDA response in cultured mouse brain neurons. *Nature*. **325**, 529–531 (1987).

21. N. W. Kleckner, R. Dingledine, Requirement for glycine in activation of NMDA-receptors expressed in Xenopus oocytes. *Science*. **241**, 835–837 (1988).

22. D. K. Patneau, M. L. Mayer, Structure-activity relationships for amino acid transmitter candidates acting at N-methyl-D-aspartate and quisqualate receptors. *J. Neurosci.* **10**, 2385–2399 (1990).

23. M. Benveniste, M. L. Mayer, Kinetic analysis of antagonist action at N-methyl-D-aspartic acid receptors. Two binding sites each for glutamate and glycine. *Biophys. J.* **59**, 560–573 (1991).

24. J. D. Clements, G. L. Westbrook, Activation kinetics reveal the number of glutamate and glycine binding sites on the N-methyl-d-aspartate receptor. *Neuron*. **7**, 605–613 (1991).

25. A. Kuryatov, Mutational analysis of the glycine-binding site of the NMDA receptor: Structural similarity with bacterial amino acid-binding proteins. *Neuron*. **12**, 1291–1300 (1994).

26. B. Laube, H. Hirai, M. Sturgess, H. Betz, J. Kuhse, Molecular Determinants of Agonist Discrimination by NMDA Receptor Subunits: Analysis of the Glutamate Binding Site on the NR2B Subunit. *Neuron*. **18**, 493–503 (1997).

27. J.-P. Mothet *et al.*, D-Serine is an endogenous ligand for the glycine site of the N-methyl-D-aspartate receptor. *Proc. Natl. Acad. Sci.* **97**, 4926–4931 (2000).

28. T. Papouin *et al.*, Synaptic and extrasynaptic NMDA receptors are gated by different endogenous coagonists. *Cell*. **150**, 633–646 (2012).

29. M. L. Mayer, G. L. Westbrook, The physiology of excitatory amino acids in the vertebrate central nervous system. *Prog. Neurobiol.* **28**, 197–276 (1987).

30. A. B. MacDermott, M. L. Mayer, G. L. Westbrook, S. J. Smith, J. L. Barker, NMDA-receptor activation increases cytoplasmic calcium concentration in cultured spinal cord neurones. *Nature*. **321**, 519–522 (1986).

31. M. L. Mayer, G. L. Westbrook, Permeation and block of N-methyl-D-aspartic acid receptor channels by divalent cations in mouse cultured central neurones. *J. Physiol.* **394**, 501–527 (1987).

32. P. Ascher, L. Nowak, The role of divalent cations in the N-methyl-D-aspartate responses of mouse central neurones in culture. *J. Physiol.* **399**, 247–266 (1988).

33. K. Tsuzuki *et al.*, Ion permeation properties of the cloned mouse ϵ2/ζ1 NMDA receptor channel. *Mol. Brain Res.* **26**, 37–46 (1994).

34. N. Burnashev, Z. Zhou, E. Neher, B. Sakmann, Fractional calcium currents through recombinant GluR channels of the NMDA, AMPA and kainate receptor subtypes. *J. Physiol.* **485**, 403–418 (1995).

35. R. Schneggenburger, Simultaneous measurement of Ca2+ influx and reversal potentials in recombinant N-methyl-D-aspartate receptor channels. *Biophys. J.* **70**, 2165–2174 (1996).

36. M. J. Berridge, Calcium signalling remodelling and disease. *Biochem. Soc. Trans.* **40**, 297–309 (2012).

37. L. Nowak, P. Bregestovski, P. Ascher, A. Herbet, A. Prochiantz, Magnesium gates glutamate-activated channels in mouse central neurones. *Nature*. **307**, 462–465 (1984).

38. M. L. Mayer, G. L. Westbrook, P. B. Guthrie, Voltage-dependent block by Mg2+ of NMDA responses in spinal cord neurones. *Nature*. **309**, 261–263 (1984).

39. R. P. Brewer, A. Parra, C. O. Borel, M. B. Hopkins, J. D. Reynolds, Intravenous magnesium sulfate does not increase ventricular CSF ionized magnesium concentration of patients with intracranial hypertension. *Clin. Neuropharmacol.* **24**, 341–345 (2001).

40. L. Sun *et al.*, Magnesium concentration in the cerebrospinal fluid of mice and its response to changes in serum magnesium concentration. *Magnes. Res.* **22**, 266–272 (2009).

41. M. L. Mayer, G. L. Westbrook, The action of N-methyl-D-aspartic acid on mouse spinal neurones in culture. *J. Physiol.* **361**, 65–90 (1985).

42. S. M. Antonov, J. W. Johnson, Permeant ion regulation of N-methyl-D-aspartate receptor channel block by Mg2+. *Proc. Natl. Acad. Sci.* **96**, 14571–14576 (1999).

43. A. Qian, J. W. Johnson, Permeant ion effects on external Mg2+ block of NR1/2D NMDA receptors. *J. Neurosci.* **26**, 10899–10910 (2006).

44. Y.-C. Yang, C.-H. Lee, C.-C. Kuo, Ionic flow enhances low-affinity binding: a revised mechanistic view into Mg2+ block of NMDA receptors. *J. Physiol.* **588**, 633–650 (2010).

45. N. Burnashev *et al.*, Control by asparagine residues of calcium permeability and magnesium blockade in the NMDA receptor. *Science*. **257**, 1415–1419 (1992).

46. K. Sakurada, M. Masu, S. Nakanishi, Alteration of Ca2+ permeability and sensitivity to Mg2+ and channel blockers by a single amino acid substitution in the N-methyl-D-aspartate receptor. *J. Biol. Chem.* **268**, 410–415 (1993).

47. D. A. Doyle *et al.*, The structure of the potassium channel: molecular basis of K+ conduction and selectivity. *Science*. **280**, 69–77 (1998).

48. M. Watanabe, Y. Inoue, K. Sakimura, M. Mishina, Developmental changes in distribution of NMDA receptor channel subunit mRNAs. *Neuroreport*. **3**, 1138–1140 (1992).

49. H. Monyer, N. Burnashev, D. J. Laurie, B. Sakmann, P. H. Seeburg, Developmental and regional expression in the rat brain and functional properties of four NMDA receptors. *Neuron*. **12**, 529–540 (1994).

50. A. Wenzel, J. M. Fritschy, H. Mohler, D. Benke, NMDA receptor heterogeneity during postnatal development of the rat brain: differential expression of the NR2A, NR2B, and NR2C subunit proteins. *J. Neurochem.* **68**, 469–478 (1997).

51. M. A. Henson, A. C. Roberts, I. Pérez-Otaño, B. D. Philpot, Influence of the NR3A subunit on NMDA receptor functions. *Prog. Neurobiol.* **91**, 23–37 (2010).

52. S. Pachernegg, N. Strutz-Seebohm, M. Hollmann, GluN3 subunit-containing NMDA receptors: not just one-trick ponies. *Trends Neurosci.* **35**, 240–249 (2012).

53. J. A. Gray *et al.*, Distinct modes of AMPA receptor suppression at developing synapses by GluN2A and GluN2B: single-cell NMDA receptor subunit deletion in vivo. *Neuron*. **71**, 1085–1101 (2011).

54. K. R. Tovar, M. J. McGinley, G. L. Westbrook, Triheteromeric NMDA receptors at hippocampal synapses. *J. Neurosci.* **33**, 9150–9160 (2013).

55. C. Rauner, G. Köhr, Triheteromeric NR1/NR2A/NR2B receptors constitute the major N-methyl-D-aspartate receptor population in adult hippocampal synapses. *J. Biol. Chem.* **286**, 7558–7566 (2011).

56. J. E. Chatterton *et al.*, Excitatory glycine receptors containing the NR3 family of NMDA receptor subunits. *Nature*. **415**, 793–798 (2002).

57. Y. Yao, M. L. Mayer, Characterization of a soluble ligand binding domain of the NMDA receptor regulatory subunit NR3A. *J. Neurosci.* **26**, 4559–4566 (2006).

58. G. Rumbaugh, K. Prybylowski, J. F. Wang, S. Vicini, Exon 5 and spermine regulate deactivation of NMDA receptor subtypes. *J. Neurophysiol.* **83**, 1300–1306 (2000).

59. K. M. Vance, K. B. Hansen, S. F. Traynelis, GluN1 splice variant control of GluN1/GluN2D NMDA receptors. *J. Physiol.* **590**, 3857–3875 (2012).

60. G. M. Durand *et al.*, Cloning of an apparent splice variant of the rat N-methyl-D-aspartate receptor NMDAR1 with altered sensitivity to polyamines and activators of protein kinase C. *Proc. Natl. Acad. Sci. U. S. A.* **89**, 9359–9363 (1992).

61. S. F. Traynelis, M. Hartley, S. F. Heinemann, Control of proton sensitivity of the NMDA receptor by RNA splicing and polyamines. *Science*. **268**, 873–876 (1995).

62. D. J. A. Wyllie, M. R. Livesey, G. E. Hardingham, Influence of GluN2 subunit identity on NMDA receptor function. *Neuropharmacology*. **74**, 4–17 (2013).

63. N. G. Glasgow, B. Siegler Retchless, J. W. Johnson, Molecular bases of NMDA receptor subtype-dependent properties. *J. Physiol.* **593**, 83–95 (2015).

64. M. Gielen, B. Siegler Retchless, L. Mony, J. W. Johnson, P. Paoletti, Mechanism of differential control of NMDA receptor activity by NR2 subunits. *Nature*. **459**, 703–707 (2009).

65. H. Yuan, K. B. Hansen, K. M. Vance, K. K. Ogden, S. F. Traynelis, Control of NMDA receptor function by the NR2 subunit amino-terminal domain. *J. Neurosci.* **29**, 12045–12058 (2009).

66. B. Siegler Retchless, W. Gao, J. W. Johnson, A single GluN2 subunit residue controls NMDA receptor channel properties via intersubunit interaction. *Nat. Neurosci.* **15**, 406–413 (2012).

67. T. Kuner, R. Schoepfer, Multiple Structural Elements Determine Subunit Specificity of Mg2+ Block in NMDA Receptor Channels. *J. Neurosci.* **16**, 3549–3558 (1996).

68. G. L. Westbrook, M. L. Mayer, Micromolar concentrations of Zn2+ antagonize NMDA and GABA responses of hippocampal neurons. *Nature*. **328**, 640–643 (1987).

69. S. Peters, J. Koh, D. W. Choi, Zinc selectively blocks the action of N-methyl-D-aspartate on cortical neurons. *Science*. **236**, 589–593 (1987).

70. P. Paoletti, P. Ascher, J. Neyton, High-affinity zinc inhibition of NMDA NR1-NR2A receptors. *J. Neurosci.* **17**, 5711–5725 (1997).

71. J. Rachline, F. Perin-Dureau, A. Le Goff, J. Neyton, P. Paoletti, The micromolar zinc-binding domain on the NMDA receptor subunit NR2B. *J. Neurosci.* **25**, 308–317 (2005).

72. C. M. Low, F. Zheng, P. Lyuboslavsky, S. F. Traynelis, Molecular determinants of coordinated proton and zinc inhibition of N-methyl-D-aspartate NR1/NR2A receptors. *Proc. Natl. Acad. Sci. U. S. A.* **97**, 11062–11067 (2000).

73. A. Fayyazuddin, A. Villarroel, A. Le Goff, J. Lerma, J. Neyton, Four residues of the extracellular N-Terminal domain of the NR2A subunit control high-affinity Zn2+ binding to NMDA receptors. *Neuron*. **25**, 683–694 (2000).

74. E. Karakas, N. Simorowski, H. Furukawa, Structure of the zinc-bound amino-terminal domain of the NMDA receptor NR2B subunit. *EMBO J.* **28**, 3910–3920 (2009).

75. C.-M. Low *et al.*, Molecular determinants of proton-sensitive N-methyl-D-aspartate receptor gating. *Mol. Pharmacol.* **63**, 1212–1222 (2003).

76. K. Williams, A. M. Zappia, D. B. Pritchett, Y. M. Shen, P. B. Molinoff, Sensitivity of the N-methyl-D-aspartate receptor to polyamines is controlled by NR2 subunits. *Mol. Pharmacol.* **45**, 803–809 (1994).

77. K. Williams, K. Kashiwagi, J. Fukuchi, K. Igarashi, An acidic amino acid in the N-methyl-D-aspartate receptor that is important for spermine stimulation. *Mol. Pharmacol.* **48**, 1087–1098 (1995).

78. M. J. Gallagher, H. Huang, E. R. Grant, D. R. Lynch, The NR2B-specific interactions of polyamines and protons with the N-methyl-D-aspartate receptor. *J. Biol. Chem.* **272**, 24971–24979 (1997).

79. T. Masuko *et al.*, A regulatory domain (R1-R2) in the amino terminus of the N-Methyl-D-Aspartate receptor: effects of spermine, protons, and ifenprodil, and structural similarity to bacterial leucine/isoleucine/valine binding protein. *Mol. Pharmacol.* **55**, 957–969 (1999).

80. X. Han *et al.*, Binding of spermine and ifenprodil to a purified, soluble regulatory domain of the N-methyl-D-aspartate receptor. *J. Neurochem.* **107**, 1566–1577 (2008).

81. L. Mony, S. Zhu, S. Carvalho, P. Paoletti, Molecular basis of positive allosteric modulation of GluN2B NMDA receptors by polyamines. *EMBO J.* **30**, 3134–3146 (2011).

82. H. Tomitori *et al.*, Structural changes of regulatory domain heterodimer of N-methyl-D-aspartate receptor subunits GluN1 and GluN2B through the binding of spermine and ifenprodil. *J. Pharmacol. Exp. Ther.* **343**, 82–90 (2012).

83. P. Paoletti, J. Neyton, P. Ascher, Glycine-independent and subunit-specific potentiation of NMDA responses by extracellular Mg2+. *Neuron*. **15**, 1109–1120 (1995).

84. M. Casado, P. Ascher, Opposite modulation of NMDA receptors by lysophospholipids and arachidonic acid: common features with mechanosensitivity. *J. Physiol.* **513**, 317–330 (1998).

85. A. Malayev, T. T. Gibbs, D. H. Farb, Inhibition of the NMDA response by pregnenolone sulphate reveals subtype selective modulation of NMDA receptors by sulphated steroids. *Br. J. Pharmacol.* **135**, 901–909 (2002).

86. N. Burnashev, P. Szepetowski, NMDA receptor subunit mutations in neurodevelopmental disorders. *Curr. Opin. Pharmacol.* **20C**, 73–82 (2014).

87. D. R. Adams *et al.*, Three rare diseases in one Sib pair: RAI1, PCK1, GRIN2B mutations associated with Smith-Magenis Syndrome, cytosolic PEPCK deficiency and NMDA receptor glutamate insensitivity. *Mol. Genet. Metab.* **113**, 161–70 (2014).

88. B. Moghaddam, D. Javitt, From revolution to evolution: the glutamate hypothesis of schizophrenia and its implication for treatment. *Neuropsychopharmacology*. **37**, 4–15 (2012).

89. R. S. Duman, Pathophysiology of depression and innovative treatments: remodeling glutamatergic synaptic connections. *Dialogues Clin. Neurosci.* **16**, 11–27 (2014).

90. S. Endele *et al.*, Mutations in GRIN2A and GRIN2B encoding regulatory subunits of NMDA receptors cause variable neurodevelopmental phenotypes. *Nat. Genet.* **42**, 1021–6 (2010).

91. H. Yuan *et al.*, Functional analysis of a de novo GRIN2A missense mutation associated with early-onset epileptic encephalopathy. *Nat. Commun.* **5**, 3251 (2014).

92. S. Venkateswaran *et al.*, Whole-exome sequencing in an individual with severe global developmental delay and intractable epilepsy identifies a novel, de novo GRIN2A mutation. *Epilepsia*. **55**, e75–9 (2014).

93. A. J. Gleichman, L. A. Spruce, J. Dalmau, S. H. Seeholzer, D. R. Lynch, Anti-NMDA receptor encephalitis antibody binding is dependent on amino acid identity of a small region within the GluN1 amino terminal domain. *J. Neurosci.* **32**, 11082–11094 (2012).

94. K. Williams, Ifenprodil discriminates subtypes of the N-methyl-D-aspartate receptor: selectivity and mechanisms at recombinant heteromeric receptors. *Mol. Pharmacol.* **44**, 851–859 (1993).

95. F. Perin-Dureau, J. Rachline, J. Neyton, P. Paoletti, Mapping the binding aite of the neuroprotectant ifenprodil on NMDA receptors. *J. Neurosci.* **22**, 5955–5965 (2002).

96. E. Karakas, N. Simorowski, H. Furukawa, Subunit arrangement and phenylethanolamine binding in GluN1/GluN2B NMDA receptors. *Nature*. **475**, 249–253 (2011).

97. S. S. Zimmerman *et al.*, Design, synthesis, and structure-activity relationship of a novel series of GluN2C-selective potentiators. *J. Med. Chem.* **57**, 2334–2356 (2014).

98. A. Khatri *et al.*, Structural determinants and mechanism of action of a GluN2C-selective NMDA receptor positive allosteric modulator. *Mol. Pharmacol.* **86**, 548–560 (2014).

99. B. M. Costa *et al.*, A novel family of negative and positive allosteric modulators of NMDA receptors. *J. Pharmacol. Exp. Ther.* **335**, 614–621 (2010).

100. C. A. Mosley *et al.*, Quinazolin-4-one derivatives: A novel class of noncompetitive NR2C/D subunit-selective N-methyl-D-aspartate receptor antagonists. *J. Med. Chem.* **53**, 5476–5490 (2010).

101. K. B. Hansen, K. K. Ogden, S. F. Traynelis, Subunit-selective allosteric inhibition of glycine binding to NMDA receptors. *J. Neurosci.* **32**, 6197–6208 (2012).

102. K. B. Hansen, S. F. Traynelis, Structural and mechanistic determinants of a novel site for noncompetitive inhibition of GluN2D-containing NMDA receptors. *J. Neurosci.* **31**, 3650–3661 (2011).

103. T. M. Acker *et al.*, Mechanism for noncompetitive inhibition by novel GluN2C/D N-methyl-D-aspartate receptor subunit-selective modulators. *Mol. Pharmacol.* **80**, 782–795 (2011).

104. C. R. Honey, Z. Miljkovic, J. F. Macdonald, Ketamine and phencyclidine cause a voltage-dependent block of responses to l-aspartic acid. *Neurosci. Lett.* **61**, 135–139 (1985).

105. J. E. Huettner, B. P. Bean, Block of N-methyl-D-aspartate-activated current by the anticonvulsant MK-801: selective binding to open channels. *Proc. Natl. Acad. Sci. U. S. A.* **85**, 1307–1311 (1988).

106. J. F. MacDonald *et al.*, Actions of ketamine, phencyclidine and MK-801 on NMDA receptor currents in cultured mouse hippocampal neurones. *J. Physiol.* **432**, 483–508 (1991).

107. H. Yuan, K. Erreger, S. M. Dravid, S. F. Traynelis, Conserved structural and functional control of N-methyl-D-aspartate receptor gating by transmembrane domain M3. *J. Biol. Chem.* **280**, 29708–29716 (2005).

108. T. A. Blanpied, R. J. Clarke, J. W. Johnson, Amantadine inhibits NMDA receptors by accelerating channel closure during channel block. *J. Neurosci.* **25**, 3312–3322 (2005).

109. M. Benveniste, M. L. Mayer, Trapping of glutamate and glycine during open channel block of rat hippocampal neuron NMDA receptors by 9-aminoacridine. *J. Physiol.* **483**, 367–384 (1995).

110. A. V Ferrer-Montiel, W. Sun, M. Montal, Molecular design of the N-methyl-D-aspartate receptor binding site for phencyclidine and dizolcipine. *Proc. Natl. Acad. Sci. U. S. A.* **92**, 8021–8025 (1995).

111. K. Kashiwagi *et al.*, Channel blockers acting at N-methyl-D-aspartate receptors: differential effects of mutations in the vestibule and ion channel pore. *Mol. Pharmacol.* **61**, 533–545 (2002).

112. S. E. Kotermanski, J. T. Wood, J. W. Johnson, Memantine binding to a superficial site on NMDA receptors contributes to partial trapping. *J. Physiol.* **587**, 4589–4604 (2009).

113. W. Limapichat, W. Y. Yu, E. Branigan, H. A. Lester, D. A. Dougherty, Key binding interactions for memantine in the NMDA receptor. *ACS Chem. Neurosci.* **4**, 255–260 (2013).

114. D. Lo, G. T. Grossberg, Use of memantine for the treatment of dementia. *Expert Rev. Neurother.* **11**, 1359–1370 (2011).

115. R. M. Berman *et al.*, Antidepressant effects of ketamine in depressed patients. *Biol. Psychiatry*. **47**, 351–354 (2000).

116. A. E. Autry *et al.*, NMDA receptor blockade at rest triggers rapid behavioural antidepressant responses. *Nature*. **475**, 91–95 (2011).

117. P. Mullasseril *et al.*, A subunit-selective potentiator of NR2C- and NR2D-containing NMDA receptors. *Nat. Commun.* **1**, 90 (2010).

118. K. K. Ogden, S. F. Traynelis, Contribution of the M1 transmembrane helix and pre-M1 region to positive allosteric modulation and gating of N-methyl-D-aspartate receptors. *Mol. Pharmacol.* **83**, 1045–1056 (2013).

119. M. Park-Chung, F. Wu, D. Farb, 3 alpha-Hydroxy-5 beta-pregnan-20-one sulfate: a negative modulator of the NMDA-induced current in cultured neurons. *Mol. Pharmacol.* **46**, 146–150 (1994).

120. M. Petrovic, M. Sedlacek, M. Horak, H. Chodounska, L. Vyklický, 20-oxo-5beta-pregnan-3alpha-yl sulfate is a use-dependent NMDA receptor inhibitor. *J. Neurosci.* **25**, 8439–8450 (2005).

121. C. L. Kussius, N. Kaur, G. K. Popescu, Pregnanolone sulfate promotes desensitization of activated NMDA receptors. *J. Neurosci.* **29**, 6819–6827 (2009).

122. J. Borovska *et al.*, Access of inhibitory neurosteroids to the NMDA receptor. *Br. J. Pharmacol.* **166**, 1069–1083 (2012).

123. N. Armstrong, Y. Sun, G. Q. Chen, E. Gouaux, Structure of a glutamate-receptor ligand-binding core in complex with kainate. *Nature*. **395**, 913–917 (1998).

124. H. Furukawa, E. Gouaux, Mechanisms of activation, inhibition and specificity: crystal structures of the NMDA receptor NR1 ligand-binding core. *EMBO J.* **22**, 2873–2885 (2003).

125. Y. Yao, J. Belcher, A. J. Berger, M. L. Mayer, A. Y. Lau, Conformational analysis of NMDA receptor GluN1, GluN2, and GluN3 ligand-binding domains reveals subtype-specific characteristics. *Structure*. **21**, 1788–1799 (2013).

126. N. Armstrong, E. Gouaux, Mechanisms for activation and antagonism of an AMPA-sensitive glutamate receptor. *Neuron*. **28**, 165–181 (2000).

127. R. Kazi, J. Dai, C. Sweeney, H.-X. Zhou, L. P. Wollmuth, Mechanical coupling maintains the fidelity of NMDA receptor-mediated currents. *Nat. Neurosci.* **17**, 914–922 (2014).

128. H. Furukawa, S. K. Singh, R. Mancusso, E. Gouaux, Subunit arrangement and function in NMDA receptors. *Nature*. **438**, 185–192 (2005).

129. A. Jespersen, N. Tajima, G. Fernandez-Cuervo, E. C. Garnier-Amblard, H. Furukawa, Structural insights into competitive antagonism in NMDA receptors. *Neuron*. **81**, 366–378 (2014).

130. R. Jin *et al.*, Crystal structure and association behaviour of the GluR2 amino-terminal domain. *EMBO J.* **28**, 1812–1823 (2009).

131. A. Clayton *et al.*, Crystal structure of the GluR2 amino-terminal domain provides insights into the architecture and assembly of ionotropic glutamate receptors. *J. Mol. Biol.* **392**, 1125–1132 (2009).

132. J. Kumar, P. Schuck, R. Jin, M. L. Mayer, The N-terminal domain of GluR6-subtype glutamate receptor ion channels. *Nat. Struct. Mol. Biol.* **16**, 631–638 (2009).

133. C.-H. Lee, E. Gouaux, Amino terminal domains of the NMDA receptor are organized as local heterodimers. *PLoS One*. **6**, e19180 (2011).

134. A. N. Farina *et al.*, Separation of domain contacts is required for heterotetrameric assembly of functional NMDA receptors. *J. Neurosci.* **31**, 3565–3579 (2011).

135. J. Kumar, P. Schuck, M. L. Mayer, Structure and assembly mechanism for heteromeric kainate receptors. *Neuron*. **71**, 319–331 (2011).

136. T. Kuner, L. P. Wollmuth, A. Karlin, P. H. Seeburg, B. Sakmann, Structure of the NMDA receptor channel M2 segment inferred from the accessibility of substituted cysteines. *Neuron*. **17**, 343–352 (1996).

137. C. Beck, L. P. Wollmuth, P. H. Seeburg, B. Sakmann, T. Kuner, NMDAR channel segments forming the extracellular vestibule inferred from the accessibility of substituted cysteines. *Neuron*. **22**, 559–570 (1999).

138. A. I. Sobolevsky, M. P. Rosconi, E. Gouaux, X-ray structure, symmetry and mechanism of an AMPA-subtype glutamate receptor. *Nature*. **462**, 745–756 (2009).

139. S. Schorge, D. Colquhoun, Studies of NMDA receptor function and stoichiometry with truncated and tandem subunits. *J. Neurosci.* **23**, 1151–1158 (2003).

140. D. Balasuriya *et al.*, α-Amino-3-hydroxy-5-methyl-4-isoxazole propionic acid (AMPA) and N-methyl-D-aspartate (NMDA) receptors adopt different subunit arrangements. *J. Biol. Chem.* **288**, 21987–21998 (2013).

141. A. Rambhadran, J. Gonzalez, V. Jayaraman, Subunit arrangement in N-methyl-D-aspartate (NMDA) receptors. *J. Biol. Chem.* **285**, 15296–15301 (2010).

142. C. L. Salussolia, M. L. Prodromou, P. Borker, L. P. Wollmuth, Arrangement of subunits in functional NMDA receptors. *J. Neurosci.* **31**, 11295–11304 (2011).

143. M. Riou, D. Stroebel, J. M. Edwardson, P. Paoletti, An alternating GluN1-2-1-2 subunit arrangement in mature NMDA receptors. *PLoS One*. **7**, e35134 (2012).

144. P. Paoletti, J. Neyton, NMDA receptor subunits: function and pharmacology. *Curr. Opin. Pharmacol.* **7**, 39–47 (2007).

145. G. L. Collingridge, R. W. Olsen, J. Peters, M. Spedding, A nomenclature for ligand-gated ion channels. *Neuropharmacology*. **56**, 2–5 (2009).

146. M. Papadakis, L. M. Hawkins, F. A. Stephenson, Appropriate NR1-NR1 disulfide-linked homodimer formation is requisite for efficient expression of functional, cell surface N-methyl-D-aspartate NR1/NR2 receptors. *J. Biol. Chem.* **279**, 14703–14712 (2004).

147. S. Qiu, Y.-L. Hua, F. Yang, Y.-Z. Chen, J.-H. Luo, Subunit assembly of N-methyl-d-aspartate receptors analyzed by fluorescence resonance energy transfer. *J. Biol. Chem.* **280**, 24923–24930 (2005).

148. T. Schüler, I. Mesic, C. Madry, I. Bartholomäus, B. Laube, Formation of NR1/NR2 and NR1/NR3 heterodimers constitutes the initial step in N-methyl-D-aspartate receptor assembly. *J. Biol. Chem.* **283**, 37–46 (2008).

149. N. Kunishima *et al.*, Structural basis of glutamate recognition by a dimeric metabotropic glutamate receptor. *Nature*. **407**, 971–977 (2000).

150. K. B. Hansen, H. Furukawa, S. F. Traynelis, Control of assembly and function of glutamate receptors by the amino-terminal domain. *Mol. Pharmacol.* **78**, 535–549 (2010).

151. K. Moriyoshi *et al.*, Molecular cloning and characterization of the rat NMDA receptor. *Nature*. **354**, 31–37 (1991).

152. H. Monyer *et al.*, Heteromeric NMDA receptors: molecular and functional distinction of subtypes. *Science*. **256**, 1217–1221 (1992).

153. L. M. Hawkins *et al.*, Export from the endoplasmic reticulum of assembled N-methyl-d-aspartic acid receptors is controlled by a motif in the c terminus of the NR2 subunit. *J. Biol. Chem.* **279**, 28903–28910 (2004).

154. M. Horak, K. Chang, R. J. Wenthold, Masking of the endoplasmic reticulum retention signals during assembly of the NMDA receptor. *J. Neurosci.* **28**, 3500–3509 (2008).

155. M. Horak, R. J. Wenthold, Different roles of C-terminal cassettes in the trafficking of full-length NR1 subunits to the cell surface. *J. Biol. Chem.* **284**, 9683–9691 (2009).

156. C. A. Puddifoot, P. E. Chen, R. Schoepfer, D. J. A. Wyllie, Pharmacological characterization of recombinant NR1/NR2A NMDA receptors with truncated and deleted carboxy termini expressed in Xenopus laevis oocytes. *Br. J. Pharmacol.* **156**, 509–518 (2009).

157. W. Yang *et al.*, A three amino acid tail following the TM4 region of the N-methyl-D-aspartate receptor (NR) 2 subunits is sufficient to overcome endoplasmic reticulum retention of NR1-1a subunit. *J. Biol. Chem.* **282**, 9269–9278 (2007).

158. T. Kawate, E. Gouaux, Fluorescence-detection size-exclusion chromatography for precrystallization screening of integral membrane proteins. *Structure*. **14**, 673–681 (2006).

159. E. Layne, [73] Spectrophotometric and turbidimetric methods for measuring proteins. *Methods Enzymol.* **3**, 447–454 (1957).

160. U. Das, J. Kumar, M. L. Mayer, A. J. R. Plested, Domain organization and function in GluK2 subtype kainate receptors. *Proc. Natl. Acad. Sci. U. S. A.* **107**, 8463–8468 (2010).

161. R. B. Bass, S. L. Butler, S. A. Chervitz, S. L. Gloor, J. J. Falke, Use of site-directed cysteine and disulfide chemistry to probe protein structure and dynamics: applications to soluble and transmembrane receptors of bacterial chemotaxis. *Methods Enzymol.* **423**, 25–51 (2007).

162. C. L. Careaga, J. J. Falke, Structure and dynamics of Escherichia coli chemosensory receptors. Engineered sulfhydryl studies. *Biophys. J.* **62**, 209–216 (1992).

163. Y. Choi, H. V Chen, S. A. Lipton, Three pairs of cysteine residues mediate both redox and zn2+ modulation of the nmda receptor. *J. Neurosci.* **21**, 392–400 (2001).

164. D. Stroebel, S. Carvalho, P. Paoletti, Functional evidence for a twisted conformation of the NMDA receptor GluN2A subunit N-terminal domain. *Neuropharmacology*. **60**, 151–158 (2011).

165. S. Qiu *et al.*, An endoplasmic reticulum retention signal located in the extracellular amino-terminal domain of the NR2A subunit of N-Methyl-D-aspartate receptors. *J. Biol. Chem.* **284**, 20285–20298 (2009).

166. P. T. Atlason, M. L. Garside, E. Meddows, P. Whiting, R. A. J. McIlhinney, N-Methyl-D-aspartate (NMDA) receptor subunit NR1 forms the substrate for oligomeric assembly of the NMDA receptor. *J. Biol. Chem.* **282**, 25299–25307 (2007).

167. A. Inanobe, H. Furukawa, E. Gouaux, Mechanism of partial agonist action at the NR1 subunit of NMDA receptors. *Neuron*. **47**, 71–84 (2005).

168. A. Ivanovic, H. Reiländer, B. Laube, J. Kuhse, Expression and initial characterization of a soluble glycine binding domain of the N-methyl-D-aspartate receptor NR1 subunit. *J. Biol. Chem.* **273**, 19933–19937 (1998).

169. E. Meddows *et al.*, Identification of molecular determinants that are important in the assembly of N-methyl-D-aspartate receptors. *J. Biol. Chem.* **276**, 18795–18803 (2001).

170. T. V Bliss, G. L. Collingridge, A synaptic model of memory: long-term potentiation in the hippocampus. *Nature*. **361**, 31–39 (1993).

171. D. Soto, X. Altafaj, C. Sindreu, A. Bayés, Glutamate receptor mutations in psychiatric and neurodevelopmental disorders. *Commun. Integr. Biol.* **7**, e27887 (2014).

172. H. E. Peery *et al.*, Anti-NMDA receptor encephalitis. The disorder, the diagnosis and the immunobiology. *Autoimmun. Rev.* **11**, 863–872 (2012).

173. K. Keinänen *et al.*, A family of AMPA-selective glutamate receptors. *Science*. **249**, 556–560 (1990).

174. B. Bettler *et al.*, Cloning of a novel glutamate receptor subunit, GluR5: expression in the nervous system during development. *Neuron*. **5**, 583–595 (1990).

175. P. Werner, M. Voigt, K. Keinänen, W. Wisden, P. H. Seeburg, Cloning of a putative high-affinity kainate receptor expressed predominantly in hippocampal CA3 cells. *Nature*. **351**, 742–744 (1991).

176. Y. Sun *et al.*, Mechanism of glutamate receptor desensitization. *Nature*. **417**, 245–253 (2002).

177. M. L. Mayer, Emerging models of glutamate receptor ion channel structure and function. *Structure*. **19**, 1370–1380 (2011).

178. J. Pøhlsgaard, K. Frydenvang, U. Madsen, J. S. Kastrup, Lessons from more than 80 structures of the GluA2 ligand-binding domain in complex with agonists, antagonists and allosteric modulators. *Neuropharmacology*. **60**, 135–150 (2011).

179. G. Fischer *et al.*, Ro 25-6981, a highly potent and selective blocker of N-methyl-D-aspartate receptors containing the NR2B subunit. Characterization in vitro. *J. Pharmacol. Exp. Ther.* **283**, 1285–1292 (1997).

180. G. B. Watson, T. H. Lanthorn, Pharmacological characteristics of cyclic homologues of glycine at the N-methyl-D-aspartate receptor-associated glycine site. *Neuropharmacology*. **29**, 727–730 (1990).

181. R. D. Allan *et al.*, Synthesis and activity of a potent N-methyl-D-aspartic acid agonist, trans-1-aminocyclobutane-1,3-dicarboxylic acid, and related phosphonic and carboxylic acids. *J. Med. Chem.* **33**, 2905–2915 (1990).

182. A. Dukkipati, H. H. Park, D. Waghray, S. Fischer, K. C. Garcia, BacMam system for high-level expression of recombinant soluble and membrane glycoproteins for structural studies. *Protein Expr. Purif.* **62**, 160–170 (2008).

183. I. Baconguis, E. Gouaux, Structural plasticity and dynamic selectivity of acid-sensing ion channel-spider toxin complexes. *Nature*. **489**, 400–405 (2012).

184. A. Goehring *et al.*, Screening and large-scale expression of membrane proteins in mammalian cells for structural studies. *Nat. Protoc.* **9**, 2574–2585 (2014).

185. M. Hattori, R. E. Hibbs, E. Gouaux, A fluorescence-detection size-exclusion chromatography-based thermostability assay for membrane protein precrystallization screening. *Structure*. **20**, 1293–1299 (2012).

186. P. J. Reeves, N. Callewaert, R. Contreras, H. G. Khorana, Structure and function in rhodopsin: high-level expression of rhodopsin with restricted and homogeneous N-glycosylation by a tetracycline-inducible N-acetylglucosaminyltransferase I-negative HEK293S stable mammalian cell line. *Proc. Natl. Acad. Sci. U. S. A.* **99**, 13419–13424 (2002).

187. P. Gourdon *et al.*, HiLiDe—Systematic approach to membrane protein crystallization in lipid and detergent. *Cryst. Growth Des.* **11**, 2098–2106 (2011).

188. W. Kabsch, XDS. *Acta Crystallogr. D. Biol. Crystallogr.* **66**, 125–132 (2010).

189. Z. Otwinowski, W. Minor, [20] Processing of X-ray diffraction data collected in oscillation mode. *Methods Enzymol.* **276**, 307–326 (1997).

190. M. A. Hanson *et al.*, Crystal structure of a lipid G protein-coupled receptor. *Science*. **335**, 851–855 (2012).

191. M. Strong *et al.*, Toward the structural genomics of complexes: crystal structure of a PE/PPE protein complex from Mycobacterium tuberculosis. *Proc. Natl. Acad. Sci. U. S. A.* **103**, 8060–8065 (2006).

192. A. J. McCoy, Solving structures of protein complexes by molecular replacement with Phaser. *Acta Crystallogr. D. Biol. Crystallogr.* **63**, 32–41 (2007).

193. E. Potterton, P. Briggs, M. Turkenburg, E. Dodson, A graphical user interface to the CCP4 program suite. *Acta Crystallogr. D. Biol. Crystallogr.* **59**, 1131–1137 (2003).

194. K. Cowtan, Recent developments in classical density modification. *Acta Crystallogr. D. Biol. Crystallogr.* **66**, 470–8 (2010).

195. P. Emsley, K. Cowtan, Coot: model-building tools for molecular graphics. *Acta Crystallogr. D. Biol. Crystallogr.* **60**, 2126–2132 (2004).

196. P. D. Adams *et al.*, PHENIX: building new software for automated crystallographic structure determination. *Acta Crystallogr. D. Biol. Crystallogr.* **58**, 1948–1954 (2002).

197. I. W. Davis *et al.*, MolProbity: all-atom contacts and structure validation for proteins and nucleic acids. *Nucleic Acids Res.* **35**, W375–383 (2007).

198. O. S. Smart, J. G. Neduvelil, X. Wang, B. A. Wallace, M. S. Sansom, HOLE: a program for the analysis of the pore dimensions of ion channel structural models. *J. Mol. Graph.* **14**, 354–360 (1996).

199. Schrodinger LLC, The PyMOL Molecular Graphics System, Version 1.3r1 (2010).

200. H. E. Hart, E. B. Greenwald, Scintillation proximity assay (SPA)--a new method of immunoassay. Direct and inhibition mode detection with human albumin and rabbit antihuman albumin. *Mol. Immunol.* **16**, 265–267 (1979).

201. D. B. Reichling, A. B. MacDermott, Lanthanum actions on excitatory amino acid-gated currents and voltage-gated calcium currents in rat dorsal horn neurons. *J. Physiol.* **441**, 199–218 (1991).

202. A. D. Sherry, A. D. Newman, C. G. Gutz, The activation of concanavalin A by lanthanide ions. *Biochemistry*. **14**, 2191–2196 (1975).

203. S. Zhu, D. Stroebel, C. A. Yao, A. Taly, P. Paoletti, Allosteric signaling and dynamics of the clamshell-like NMDA receptor GluN1 N-terminal domain. *Nat. Struct. Mol. Biol.* **20**, 477–485 (2013).

204. M. C. Weston, P. Schuck, A. Ghosal, C. Rosenmund, M. L. Mayer, Conformational restriction blocks glutamate receptor desensitization. *Nat. Struct. Mol. Biol.* **13**, 1120–1127 (2006).

205. M. Gielen *et al.*, Structural rearrangements of NR1/NR2A NMDA receptors during allosteric inhibition. *Neuron*. **57**, 80–93 (2008).

206. K. Erreger *et al.*, Subunit-specific agonist activity at NR2A-, NR2B-, NR2C-, and NR2D-containing N-methyl-D-aspartate glutamate receptors. *Mol. Pharmacol.* **72**, 907–920 (2007).

207. H. Sugihara, K. Moriyoshi, T. Ishii, M. Masu, S. Nakanishi, Structures and properties of seven isoforms of the NMDA receptor generated by alternative splicing. *Biochem. Biophys. Res. Commun.* **185**, 826–832 (1992).

208. M. V Yelshansky, A. I. Sobolevsky, C. Jatzke, L. P. Wollmuth, Block of AMPA receptor desensitization by a point mutation outside the ligand-binding domain. *J. Neurosci.* **24**, 4728–4736 (2004).

209. K. Erreger, S. M. Dravid, T. G. Banke, D. J. A. Wyllie, S. F. Traynelis, Subunit-specific gating controls rat NR1/NR2A and NR1/NR2B NMDA channel kinetics and synaptic signalling profiles. *J. Physiol.* **563**, 345–358 (2005).

210. Y. Zhou, J. H. Morais-Cabral, A. Kaufman, R. MacKinnon, Chemistry of ion coordination and hydration revealed by a K+ channel-Fab complex at 2.0 A resolution. *Nature*. **414**, 43–48 (2001).

211. T. Kuner, P. H. Seeburg, H. R. Guy, A common architecture for K+ channels and ionotropic glutamate receptors? *Trends Neurosci.* **26**, 27–32 (2003).

212. K. L. Dürr *et al.*, Structure and dynamics of AMPA Receptor GluA2 in resting, pre-Open, and desensitized States. *Cell*. **158**, 778–792 (2014).

213. L. Chen, K. L. Dürr, E. Gouaux, X-ray structures of AMPA receptor-cone snail toxin complexes illuminate activation mechanism. *Science*. **345**, 1021–1026 (2014).

214. J. R. Meyerson *et al.*, Structural mechanism of glutamate receptor activation and desensitization. *Nature*. **514**, 328–334 (2014).

215. E. Karakas, H. Furukawa, Crystal structure of a heterotetrameric NMDA receptor ion channel. *Science*. **344**, 992–997 (2014).

216. C.-H. Lee *et al.*, NMDA receptor structures reveal subunit arrangement and pore architecture. *Nature*. **511**, 191–197 (2014).

217. L. P. Wollmuth, T. Kuner, P. H. Seeburg, B. Sakmann, Differential contribution of the NR1- and NR2A-subunits to the selectivity filter of recombinant NMDA receptor channels. *J. Physiol.* **491**, 779–797 (1996).

218. L. P. Wollmuth, T. Kuner, B. Sakmann, Adjacent asparagines in the NR2-subunit of the NMDA receptor channel control the voltage-dependent block by extracellular Mg2+. *J. Physiol.* **506**, 13–32 (1998).

219. R. Kazi *et al.*, Asynchronous movements prior to pore opening in NMDA receptors. *J. Neurosci.* **33**, 12052–12066 (2013).

220. Y.-C. Tu, C.-C. Kuo, The differential contribution of GluN1 and GluN2 to the gating operation of the NMDA receptor channel. *Pflugers Arch.* (2014), doi:10.1007/s00424-014-1630-z.

221. S. E. Murthy, T. Shogan, J. C. Page, E. M. Kasperek, G. K. Popescu, Probing the activation sequence of NMDA receptors with lurcher mutations. *J. Gen. Physiol.* **140**, 267–277 (2012).

222. D. M. Schauder *et al.*, Glutamate receptor desensitization is mediated by changes in quaternary structure of the ligand binding domain. *Proc. Natl. Acad. Sci. U. S. A.* **110**, 5921–5926 (2013).

223. W. F. Borschel, S. E. Murthy, E. M. Kasperek, G. K. Popescu, NMDA receptor activation requires remodelling of intersubunit contacts within ligand-binding heterodimers. *Nat. Commun.* **2**, 498 (2011).

224. M. L. Mayer, L. Vyklicky, G. L. Westbrook, Modulation of excitatory amino acid receptors by group IIB metal cations in cultured mouse hippocampal neurones. *J. Physiol.* **415**, 329–350 (1989).

225. P. Q. Trombley, G. M. Shepherd, Differential modulation by zinc and copper of amino acid receptors from rat olfactory bulb neurons. *J. Neurophysiol.* **76**, 2536–2546 (1996).

226. P. Gavazzo, A. Gazzoli, M. Mazzolini, C. Marchetti, Lead inhibition of NMDA channels in native and recombinant receptors. *Neuroreport*. **12**, 3121–3125 (2001).

227. C. Marchetti, P. Gavazzo, Subunit-dependent effects of nickel on NMDA receptor channels. *Mol. Brain Res.* **117**, 139–144 (2003).

228. B. A. Maki, G. K. Popescu, Extracellular Ca2+ ions reduce NMDA receptor conductance and gating. *J. Gen. Physiol.* **144**, 379–392 (2014).

229. C. H. Evans, Interesting and useful biochemical properties of lanthanides. *Trends Biochem. Sci.* **8**, 445–449 (1983).

230. K. Williams, V. L. Dawson, C. Romano, M. A. Dichter, P. B. Molinoff, Characterization of polyamines having agonist, antagonist, and inverse agonist effects at the polyamine recognition site of the NMDA receptor. *Neuron*. **5**, 199–208 (1990).

231. X. Bai, G. McMullan, S. H. W. Scheres, How cryo-EM is revolutionizing structural biology. *Trends Biochem. Sci.* **40**, 49–57 (2015).

232. M. Liao, E. Cao, D. Julius, Y. Cheng, Structure of the TRPV1 ion channel determined by electron cryo-microscopy. *Nature*. **504**, 107–112 (2013).

233. P. Lu *et al.*, Three-dimensional structure of human γ-secretase. *Nature*. **512**, 166–170 (2014).

234. A. Bartesaghi, D. Matthies, S. Banerjee, A. Merk, S. Subramaniam, Structure of β-galactosidase at 3.2-A resolution obtained by cryo-electron microscopy. *Proc. Natl. Acad. Sci.* **111**, 11709–11714 (2014).